Single Cell analysis using Atomic Force Microscopy (AFM)

Fahmi B. Samsuri

A thesis presented for the degree of Doctor of Philosophy in

Electrical and Computer Engineering,

University of Canterbury,

Christchurch, New Zealand

November 2010

Acknowledgments

I would like to thank my supervisors for their support throughout this project. To Associate Professor Dr. Maan Alkaisi – thank you for all the knowledge that you have shared with me, the guidance and encouragement during my period here. To Professor John Evans – thank you for your guidance and support; your expertise in biological science has helped me tremendously over these years. To Dr. John Mitchell – for your guidance and technical expertise in the development of the Biopolymer; without your contribution this project would not have reached this far.

Further acknowledgement goes to Dr. Kenny Chitcholtan, James Dann and Dr. Peter Sykes for assistance with cell culture techniques and preparation of materials and reagents. I would also like to thank my teammates in the bionanonetwork group, especially Dr. Volker Nock, Siti Norjannah and Lynn Murray for all your support, knowledge-sharing and useful discussions that we had. Last but not least, I acknowledge the efforts made by R.J. Blaikie, G. Turner, and H. Devereux.

This work was supported by the MacDiarmid Institute for Advanced Materials and Nanotechnology, University of Canterbury, Christchurch, the Canterbury Medical Research Foundation and by The New Zealand Institute for Plant & Food Research Ltd.

To my wife, Niza and

my sons, Syameel and Ammar

with love, Fahmi

Preface

This document discusses research work undertaken at the Electrical and Computer Engineering Department at the University of Canterbury, and the Christchurch School of Medicine and Health Sciences at the University of Otago, in collaboration with The New Zealand Institute for Plant and Food Research Limited, Hamilton, between July 2007 and November 2010.

Aspects of research contained in this dissertation are discussed in the following publications:

Author Journal Articles

1. F. Samsuri, J. S. Mitchell, M. M. Alkaisi, and J. J. Evans, "Formation of Nanoscale Bioimprints of Muscle Cells Using UV-Cured Spin-coated Polymers", *Journal of Nanotechnology*, Vol. 2009, 2009.

2. F. Samsuri, M. M. Alkaisi, J. S. Mitchell, and J. J. Evans, "Replication of cancer cells using soft lithography Bioimprint technique", *Microelectronics Engineering*, Vol. 87, pp. 699-703, 2010.

3. V. Nock, L. Murray, F. Samsuri, M.M. Alkaisi and J.J. Evans, "Microfluidics-assisted photo nanoimprint lithography for the formation of cellular bioimprints", *J. Vac. Sci. Technol. B,* 28, C6K17 (2010).

4. F. Samsuri, Maan M. Alkaisi, John J. Evans, Kenny Chitcholtan, John S. Mitchell, "Detection of changes in cell membrane structures using the Bioimprint technique", *Microelectronic Engineering, In Press, Corrected Proof,* available online 29 December 2010.

5. Volker Nock, Lynn Murray, F. Samsuri, Maan M. Alkaisi, John J. Evans, "Microfluidic arrays for bioimprint of cancer cells", *Microelectronic Engineering, In Press, Corrected Proof,* available online 24 December 2010.

Conference Proceedings

1. Fahmi Samsuri, John S. Mitchell, Maan M. Alkaisi, and John J. Evans, "Replication of Muscle Cell Using Bioimprint," AIP Conf. Proc., July 23, 2009, Vol. 1151, pp. 71-74. Advanced Materials and Nanotechnology: Proceedings of the International Conference (AMN-4).

2. Samsuri, F., Alkaisi, M.M., Mitchell, J.S. and Evans, J.J. "Replication of cancer cells using soft lithography Bioimprint technique", *35th International Conference on Micro- and Nano-Engineering (MNE09)*, 28 September to 1 October 2009, Ghent, Belgium (poster presentation). Accepted for publication in *Microelectronic Eng.* (2010).

3. Samsuri, F., Alkaisi, M.M., Evans, J.J., Chitcholtan, K. and Mitchell, J.S. "Atomic Force Microscope study of endometrial cancer cell membranes following replication using UV-Bioimprint technique", *36th International Conference on Micro- and Nano-Engineering (MNE 2010)*, 19 to 22 September 2010, Genoa, Italy (poster presentation).

4. Lynn Murray, Fahmi Samsuri, Volker Nock, John Evans and Maan Alkaisi "Bioimprinted polymers as cell-patterned substrates for cell culture", *36th International Conference on Micro- and Nano-Engineering (MNE 2010)*, 19 to 22 September 2010, Genoa, Italy (poster presentation).

5. Volker Nock, Lynn Murray, Fahmi Samsuri, Maan M. Alkaisi and John J. Evans, "High density microfluidics arrays for Bioimprint", *36th International Conference on Micro- and Nano-Engineering (MNE 2010)*, 19 to 22 September 2010, Genoa, Italy (oral presentation).

6. Volker Nock, Lynn M. Murray, Fahmi Samsuri, Maan M. Alkaisi and John J. Evans, "Microfluidics-assisted photo nanoimprint lithography for the formation of cellular Bioimprints", 54*th International Conference on Electron, Ion and Photon Beam Technology and Nanofabrication (EIPBN 2010)*, Anchorage, USA (poster presentation).

7. Fahmi Samsuri, Maan M. Alkaisi and John J. Evans, "Biochip development using Nanoimprint Lithography (NIL) and metallic thermal evaporation techniques for biological cells manipulation using DEP", *1st International Conference on Electrical, Control and Computer Engineering 2011 (INECCE 2011)*, 21 – 22 June 2011, Kuantan, Malaysia (oral presentation).

Presentations

1. Samsuri, F., Mitchell, John S., Alkaisi, Maan M., Evans, John J., Replication of Muscle Cell Using Bioimprint, *AIP Conference Proceedings*, *AMN-4*, the 4th Advanced Materials and Nanotechnology, Dunedin, NZ, Feb 2009 (Oral presentation).

2. Fahmi Samsuri, Maan M. Alkaisi, John S. Mitchell and John J. Evans, "Cellular replication using soft lithography technique for atomic force microscope (AFM) analysis", 6*th BioNanotechnologyNetwork (BNN) meeting and NZ-Taiwan Symposium on Bio nanotechnologies*, 30th April, 2010, Christchurch, New Zealand.

Table of Contents

Chapter 1: Introduction **1**

Introduction 1

1.1 Cancer cells 12

1.2 Biological events 17

1.3 Research objectives 26

1.4 Thesis outline 28

Chapter 2: Laboratory equipment and experimental techniques **31**

2.1 Micro and Nanofabrication equipment and processes 32

2.2 Mask Writer 33

2.3 Mask Aligner 35

2.4 Evaporator 37

2.5 DekTak 39

2.6 Cell Culture protocols and equipment 41

2.6.1 Cell preparation/dispersion 41

2.6.2 Maintenance of cell culture 42

2.6.3 Splitting confluent cell culture 43

2.6.4 Pituitary cells 45

2.6.5 Rat muscle cells 45

2.6.6 Ishikawa endometrial cancer cells 45

2.6.7 RL95-2 cancer cells 46

2.7 Cell culture plates and chambers 47

2.8 Immunofluorescence 49

2.9 Chemical fixation 52

2.10 ELISA 53

Chapter 3: Atomic Force Microscopy 59

3.1 The cantilever and probe (tip) 61

3.2 Force measurement 64

3.3 Operational modes of AFM 67

3.3.1 Contact mode 67

3.3.2 Non contact mode 69

3.3.3 Tapping mode 70

3.4 Imaging modes of AFM 71

3.5 Biological sample imaging 73

3.6 Advantages/disadvantages of AFM 78

3.7 Experimental setup 81

3.8 Conclusion 87

Chapter 4: Biochip **89**

4.1 Overview 92

4.2 Biochip design 96

4.3 Electrode-cavity design and fabrication 99

4.3.1 Biochip with SU-8 layer 108

4.3.2 Biochip electrode configurations 111

4.4 Polystyrene–beads trapping 113

4.5 Discussion 118

4.6 Conclusion 119

Chapter 5: Bioimprint **121**

5.1 Overview 124

5.2 Materials and methods 127

5.2.1 Materials 129

5.2.2 Methods 133

5.3 Imprints and AFM imaging 135

5.3.1 Polymerization to produce imprints 136

5.3.1.1 Polymerization of muscle cells 137

5.3.1.2 Polymerization of Ishikawa cells 140

5.3.1.3 Replica versus direct cellular imaging 143

5.3.2 AFM imaging of cellular features 145

5.3.2.1 Rat muscle cell imprints 145

5.3.2.2 Endometrial cancer cell imprints 150

5.3.3 Imprints as 3-D scaffolds for tissue culture 153

5.4 Conclusion 156

Chapter 6: Bioimprint of cancer cells **159**

6.1 Cellular features on membrane surfaces 161

6.2 Cell structure during VEGF regulation 165

6.3 VEGF time course expression 168

6.4 Immunofluorescence with microbeads 173

6.5 Conclusions 178

Chapter 7: Summary remarks & conclusions **181**

7.1 Recommendation for future work 189

7.2 Conclusions 190

Appendix **193**

References **223**

List of Figures

1.1	Single cell membrane diagram	3
1.2	Tissue structure of epithelial components	15
1.3	Schematic of exocytosis process	18
1.4	Exocytosis fusion mechanisms	23
2.1	Heidelberg Instruments – Laser pattern generator	34
2.2	Karl Süss MA6 mask aligner	36
2.3	Thermal evaporator	38
2.4	DekTak contact surface profiler	40
2.5	96-well microtitre plate for ELISA	54
2.6	Microplate reader for ELISA	57
3.1	Beam deflection system	61
3.2	A force curve of AFM	65
3.3	Overall DI 3100 system overview	82
3.4	Schematic overview of the piezoelectric head	83
3.5	SEM images of some of the probes	86
4.1	3-D illustration of the Biochip design	97
4.2	Microscope image of cavity and gold electrodes	98

4.3	Three-stage biochip fabrication processes	102
4.4	Two-stage fabrication process	106
4.5	SU-8 layer after exposure showing cracks	109
4.6	Even and smooth film of SU-8 deposition	110
4.7	Cross-section AFM image of single cavity	111
4.8	Electrode pattern configurations	112
4.9	Biochip electrodes – positive DEP	115
4.10	Biochip electrodes – negative DEP	117
5.1	Illustration of Bioimprint replication process	123
5.2	Molecular structure of triglyme	130
5.3	Molecular structure of ethylene glycol dimethacrylate	131
5.4	Molecular structure of methacrylic acid	132
5.5	Schematic of the new Bioimprint process	135
5.6	Microscope images of rat muscle cells	138
5.7	Microscope images of Ishikawa endometrial cancer cells	142
5.8	AFM images of cells under direct cellular imaging	144
5.9	Imprints of rat muscle cells	146
5.10	AFM images of topography and morphology of the cells	147
5.11	AFM images of intrusions and fibres on cell membrane	149

5.12	AFM contour image of muscle cell imprint	150
5.13	AFM images of Ishikawa cells imprint	151
5.14	AFM images showing intrusions or craters of fusion pores	152
5.15	3-D AFM images of Ishikawa cells imprint	155
6.1	AFM images of Ishikawa showing nanopores	162
6.2	ICM image of a live human breast cancer cell	164
6.3	AFM images of control and $CoCl_2$ treated cells imprint	167
6.4	VEGF concentration vs. time for $CoCl_2$ induced samples	169
6.5	Cells induced by $CoCl_2$ and VEGF time course experiment	172
6.6	AFM images of Ishikawa cells with functionalized beads	177

Abstract

Replication of biological cells for the purpose of imaging and analysis under electron and scanning probe microscopy has facilitated the opportunity to study and examine some molecular processes and structures of living cells in a manner that were not possible before. The difficulties faced in direct cellular analysis when using and operating Atomic Force Microscopy (AFM) *in situ* for morphological studies of biological cells have led to the development of a novel method for biological cell studies based on nanoimprint lithography. The realization of the full potential of high resolution AFM imaging has revealed some very important biological events such as exocytosis and endocytosis. In this work, a soft lithography Bioimprint replication technique, which involved simple fabrication steps, was used to form a hard replica of the cell employing a newly developed biocompatible polymer that has fast curing time at room temperature essential for this process. The structure and topography of the rat muscle cell and the endometrial (Ishikawa) cancer cell were investigated in this study. Cells were cultured and incubated in accordance with standard biological culturing procedures and protocols approved by the Human Ethics Committee, University of Otago. An impression of the cell profile was created by applying a layer of the polymer onto the cells attached to a substrate and rapidly cured under UV-light. Fast UV radiation helps to lock cellular processes within seconds after exposure and replicas of the cancer cells exhibit ultra-cellular structures and features down to nanometer scale. Elimination of the AFM tip damping effects due to probing of the soft biological tissue allows imaging with unprecedented resolution. High-

resolution AFM imagery provides the opportunity to examine the structure and topography of the cells closely so that any abnormalities can be identified. Craters that resemble granules and features down to 100 nm were observed. These represent steps on a transitional series of sequential structures that indicate either an endocytotic or exocytotic processes, which were evident on the replicas. These events, together with exocytosis, play a very significant part in the tumorigenesis of these cancer cells. By forming cell replica impressions, not only have they the potential to understand biological cell conditions, but may also benefit in synthesizing three dimensional (3-D) scaffolds for natural growth of biological cells and providing an improvement over standard cell growth conditions. Further examinations by observing the characteristic behaviour of the plasma membrane when the cells were induced by certain compound such as cobalt chloride ($CoCl_2$) under control and stimulated conditions have brought in the opportunity to examine the effect of this stimulant in inducing apoptosis in many different kinds of cells. Numbers of pores formed on the cells membrane were found to increase significantly after the cells where induced with $CoCl_2$ that correlated well with the level of vascular endothelial growth factor (VEGF) receptors expression, which contributed to tumour growth. This indicates $CoCl_2$ has exaggerated the expression of the VEGF growth factor. Investigations were also done to the cells using functionalized nano-particles as bio-markers to establish the connection between exocytosis with nanopores found on the membrane surfaces of the cells. These microbeads were found attached to sites surrounding the nucleus of the cell and higher numbers of visible beads would confirm that there was an up-regulation of the VEGF expression in cells induced by $CoCl_2$. All these can contribute to expanding the knowledge about exocytosis and fundamental physiology of cells, and also assist in understanding diseases especially cancer.

Chapter 1

Introduction

In this multi-disciplinary world of science, engineers and biological scientists have worked together for so long in the development and establishment of new methods, materials and technologies for the purpose of learning and understanding the progression of the basic unit of human nature - the living cells. As mentioned in the title of this thesis, this work represents the contribution that I have made to the development of a method used for biological cell investigations using the Atomic Force Microscopy (AFM). It involved the development and optimization of the Bioimprint™ technique for biological cell replications. The research was intended for studying and investigating the exocytosis process of living cells, and was applied on two different cell types, namely the rat muscle cell line and the Ishikawa endometrial cancer cell line. AFM imaging was taken from the replicated cells and were studied and investigated. Further analyses were conducted to the cancer cells under control and stimulated conditions in order to see their reactions to certain types of stimulants. Investigations were also done to the

cells using functionalized microbeads to establish the connection between exocytosis with nanopores covering the membrane surface of the cells.

For the past few decades, the importance of cellular structure has been increasingly recognized and morphology studies in biological sciences have developed rapidly, as evident by the number of Nobel Prizes awarded in this field. This is because a cell's membrane represents the boundary between the cells and their environment. They play several key functions such as supporting the internal organelles they contain, protecting the cytoplasm from the outer environment, imparting shape to the organism, and acting as a molecular sieve and controlling interfacial interactions (for example, molecular recognition, cell adhesion and aggregation) [1]. In multi-cellular organisms, for instance, humans, appreciating the similarities and differences between cell types and structures are particularly important to the fields of cell and molecular biology as well as to biomedical fields such as cancer research and developmental biology. The functions of the cell membrane are directly related to its structure. Human cells are categorized as eukaryotic cells which are surrounded by double layer phospholipids (lipid bilayer). The exposed heads of the bilayer are hydrophilic, i.e. they are compatible with water both within the cytosol and outside of the cell. However, the hidden tails of the phospholipids are hydrophobic, so the cell membrane acts as a protective barrier to the uncontrolled flow of water. The

membrane is made more complex by the presence of numerous proteins constructed from phosphate group that are crucial to cell activity. These proteins include receptors that allow cells to detect external signalling molecules such as hormones, as well as pores responsible for the controlled entry and exit of ions like sodium (Na+), potassium (K+), calcium (Ca++), and chloride (Cl-). The illustration in Figure 1.1 shows a diagram of a cell membrane with protein / ion channels, pores and phospholipids bilayer structures.

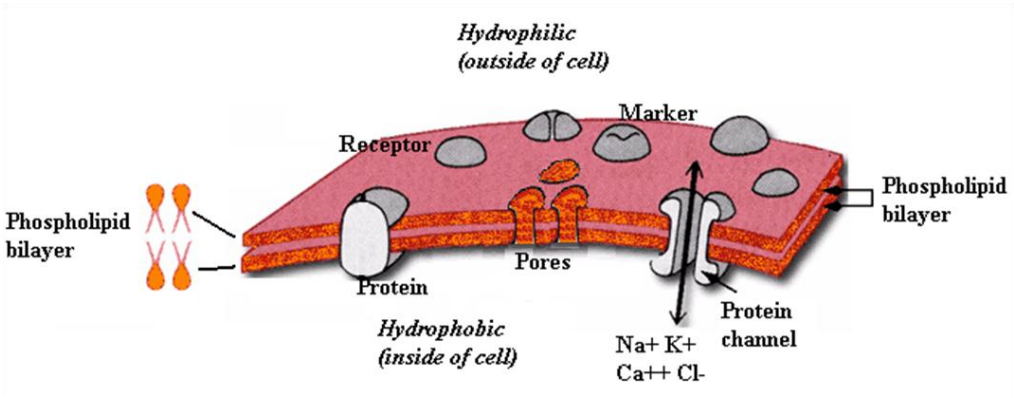

Figure 1.1: Single cell membrane diagram.

The variations in cell surfaces and morphology compared to normal healthy cells can be used as indicatives of diseases and abnormalities such as cancer [2] and if they can be detected at the molecular level, they will offer important means for early diagnosis at the single cell level. This will be an

added advantage to molecular biological studies and cancer treatments. However, accurate determination of such changes by optical microscopy remains a major challenge [3]. For instance, the structure of a single lipid bilayer is around 5 nm thick, which is much smaller than the wavelength of light and is therefore invisible to the eye, even with a standard light optical microscope. Despite that, over the past several decades fundamental work has been done to characterize these layers which consist of several distinct chemical regions across its cross-section using x-ray reflectometry [4], neutron scattering [5], and nuclear magnetic resonance techniques. Other various methods were also reported [6, 7] such as separation and chemical analysis of cell constituents, serological procedures, binding studies (dyes, antibodies and lectins), selective degradation by enzymes, modification of antibiotics, electron microscopy techniques combined with freeze-fracture and surface replica or negative staining, x-ray photoelectron spectroscopy, infrared spectroscopy, and contact-angle and electrophoretic mobility measurements. These methods often require cell manipulation prior to examination (extraction, drying, staining) and in many cases provide averaged information obtained on a large ensemble of cells. This indicates that non-destructive, high resolution tools are needed to probe the molecular surface.

High-resolution microscopic techniques such as atomic force microscopy (AFM) [8] are much better suited to such analyses as they enable three-dimensional (3-D) sub-nanometer resolution under normal ambient conditions. With AFM, high-resolution images of the surface ultra-structure of living cells and the dynamic cellular processes can be captured and conformational changes of individual membrane proteins can be monitored. Nevertheless, AFM is actually much more than a microscope in that it also enables forces to be probed quantitatively. One can measure surface forces and produce spatially resolved maps of the physical properties of the cell surface, including surface hydrophobicity, surface charges, adhesion, and elasticity [1]. It is also possible to measure the elasticity of single surface molecules in relation with function. These measurements provide new insights into the molecular and cellular structure-function relationships of cell surfaces (molecular recognition, protein folding, conformational changes, cell adhesion) [1].

Nevertheless, AFM has the major disadvantage of requiring high scanning tip forces that can damage the sensitive soft biological tissue. Blunter tips have been used to minimize the damage but they result in greatly diminished resolution [9]. Furthermore, scanning using the AFM tipped in an aqueous environment can cause structural movement and loss of resolution due to damping effects [10]. Immobilizing the cells is also a challenge. Some

cells have no tendency to spread over substrates and as a result, the contact area between the cell and substrate is very small, often leading to cell detachment by the scanning tip.

To overcome these problems, several approaches have been proposed, including pre-treatment such as air-drying and chemical fixation to promote cell attachment. However, these treatments may cause significant rearrangement or denaturation of the surface molecules, thereby compromising the biological significance of the results. An interesting substitute is to perform cell immobilization by mechanical trapping in porous membranes [11, 12]. This approach offers two advantages which are fairly simple and uncomplicated, and does not involve drying, coating, or chemical fixation. The only limitation is that this approach can only work for spherical cells. Nevertheless, due to the mobility and softness of these biological tissues, the image quality and resolution were inadequate, stressing the need to use alternative preparation procedures (other than fixation, drying) and imaging modes (non-aqueous and in open-air environment). However, it has been predicted that AFM imaging of cells in liquid should be capable of resolutions of 50-500 nm regardless of whether the cells are living or fixed [13].

Time-consuming preparation procedures when using either air or high vacuum environment associated with transmission electron microscopy (TEM) has been a further limitation which is exacerbated by the need for dehydration and fixation which can deform the cells and introduce artifacts in the imaging process [13]. There was also a report of the use of rapid freezing technique [14] where the cells and tissue samples were high-pressured frozen and cryo-sectioned. To maintain the temperature below phase transition temperature of vitrified water, they needed liquid nitrogen cooled system with ultra-stable cold stages so that the samples can be kept close-to-native state. Besides, without the use of liquid helium to cool down the system, the sample can be damaged by the electron beam [15]. Without the advances in cold stage technology and improvement of TEM vacuum system to inhibit trapping of water or hydrocarbons by the cold sample, such nanoscale imaging tools have therefore not been widely used in life science applications.

Imprint lithography has started to emerge as an alternative to conventional photolithography techniques particularly in nano-patterning technology, which has enabled researchers to fabricate 2-D and 3-D structures with less than 100 nm resolution (1.4 nm minimum features have been reported by nanoimprint lithography (NIL)) [16]. In addition, patterning and modification of functional materials other than typical photoresists have

contributed to the wide spread of this method. Added advantage is that this approach is low cost and high throughput, so the creation of low dost devices with < 100 nm feature sizes can be achieved at a tenth of the cost of traditional photolithography [17-19]. It also has operational ease for use especially in developing devices for biological applications [20]. In imprint lithography, the techniques currently available are categorized as either ‘moulding and embossing’ or ‘transfer printing’ method. Fabrication by moulding and embossing includes techniques such as nanoimprint lithography (NIL), UV-NIL, step and flash imprint lithography (S-FIL), and micro-moulding by elastomeric stamps, while micro- and nano-contact printing are termed transfer printing processes. It is widely known that soft lithography broadly refers to moulding, embossing and printing methods exclusively using an elastomeric mould and/or stamp such as poly (dimethylsiloxane) or PDMS [21] and has been commonly used in applications related to microarrays for genomics, proteomics and tissue engineering.

Whilst polymers have been used in the imprinting of yeasts for quartz crystal microbalance sensors [22, 23], they have only recently been applied to nanoscale imaging. David, Zhang, Palard, Patrick Jr. and Chen [24] have described the UV imprinting on PEGDMA (poly (ethylene glycol dimethacrylate)) by using an optical mask aligner. In their study, the stamps

or moulds were made out of silicon, which required that the imprinted substrates must be transparent to UV. They also reported that the stamps could be made using quartz, thus enabled the imprinting to be carried out on a wider range of materials, such as silicon, quartz, sapphire or polymers. Based on their work, Hydrogen Silsequioxane (HSQ) on quartz substrates were used as stamps and various patterns containing lines and rings from 200 nm to 5 μm sizes were successfully imprinted on the UV sensitive PEG-derivatives. They also found out that the combination of using diluted solution and spin coating technique with certain applied pressure to the stamps would help to reduce the residual imprint layers. However, PEGDMA material has hydrogel properties, which means it will swell when immersed in water. This can be disadvantageous to its use in some applications, but it can also be included as a design feature.

To overcome these imaging challenges, a novel nanoimprint-based approach has been recently developed by a group of researchers from the Department of Electrical and Computer Engineering, Canterbury University whereby the cells are coated with a monomer mixture which is then polymerized over the cell surfaces [25-27] in a positive soft lithography technique [28]. By careful selection of the monomers, it is possible to obtain an imprint of the cellular surface features in the polymer once the cellular material has been washed away from the replica. This imprint replica can

then be imaged using high-resolution techniques such as AFM without the concerns of cellular damage. This approach has come to be known as a "Bioimprint" technique [26]. When combined with AFM imaging, continuous sampling to capture snapshots of biological events and monitoring of cell conditions can be achieved to allow studies of cellular structure and cell response to physiological and noxious stimuli. Furthermore, such techniques have the potential for a biomedical procedure for forming 3-D biocompatible and bioactive scaffolds for tissue culture.

Previous work by a Canterbury University group on obtaining bioimprints has utilized the non-biohazardous poly (dimethylsilxoane) (PDMS) polymer composite [25, 26] and applied this to endometrial cancer cells [29]. This has allowed high-resolution imaging of membrane morphopological structures consistent with exocytosis. This technique utilized thermal setting of the polymer [26] and so had the disadvantage of exposing cells to very high temperatures for some minutes followed by another curing step which took hours to complete. A UV-cured Bioimprint technique was then adopted by photo-curing a siloxane copolymer to visualize pituitary cells [27].

However, there were some significant challenges to overcome with this approach, namely distorted or permeation artifacts resulting from

prolonged curing time, cell dehydration effects, an irradiation time of several minutes which had the potential to induce alterations in cell characteristics and a large number of curing steps that were required to complete the process.

A new polymer has to be developed to resolve these issues. It is known that the use of methacrylic acid / ethylene glycol dimethacrylate copolymer has the advantages that the polymer will set under UV irradiation within seconds [23] if applied at appropriate volumes and polymerize smoothly around surface features making it potentially useful for application in Bio-imprinting of nanoscale features. Furthermore, it can be spin-coated onto immobilized cells to produce polymer layers of various thicknesses.

In this thesis, the development of a new Bioimprint technique that utilizes methacrylic acid / ethylene glycol dimethacrylate copolymer to achieve rapid imprinting of nanoscale features of endometrial cancer cells will be presented. Imprints are formed through aspiration of fluid from immobilized endometrial cells and application of a spin-coated polymer layer. This is followed by peeling-off the UV-cured replicas, and finally cleaning to remove residual cellular material. This negative replica is suitable for imaging by AFM in tapping mode. A number of sub-cellular features are imprinted and the cells remain intact with a minimum of morphological

changes as compared to control sample. This imprinting process can be completed in seconds and opens the way to highly detailed AFM nanoscale imaging of a range of different cell types for the monitoring and the characterization of cellular features that are those associated with disease [30, 31].

1.1 Cancer cells

Cancer is not a new disease that was only discovered in this century, but it was already known since the ancient Egyptians. Most cancers only develop in the latter decades of life and since the expectation of life only began to increase from the middle of the nineteenth century onwards, the number of people that managed to survive the old ages was relatively small compared to those who in fact died because of cancers. Nowadays with better public health and medical care services, infectious diseases which were the major causes of death in the past are manageable and under controlled, but this on the contrary, has caused the proportion of the human population at risk of cancer increased significantly. At least one in three will develop cancer and one in four men and one in five women will die from it [32, 33]. For this reason, cancer detection and prevention are major health issues and to some

extent, cancer research has wider significance to the existence of our generation and the futures to come.

Cancer can affect almost all multicellular organisms, plants as well as animals. Since it involves disturbances in cell proliferation, differentiation, and development, knowledge of the processes underlying this disease will help scientists to understand the very basic mechanisms of life. Johannes Mueller (1801 – 1858), a German physiologist, discovered that cancers were made up of cells. This finding led to the search of the specific differences between normal and cancer cells. During the past few decades, rapid technological progress has allowed us to acquire a huge amount of information about cancer cells in unprecedented detail and by today there seems no limit to the amount of information that can be obtained.

The tissues of the body can be divided into four main groups: the general supporting tissues collectively known as mesenchyme, the tissue-specific cells called epithelium, the ‘defence’ cells known as the haemato-lymphoid system, and the nervous system. The mesenchyme consists of connective tissue such as fibroblasts which make collagen fibres and associated proteins, bone, cartilage, muscle, blood vessels, and lymphatics. The epithelial cells are the specific, specialized cells of the different organs, such as skin, intestine, liver, glands and others. The haemato-lymphoid system consists of

a wide group of cells, mostly derived from precursor cells in the bone marrow which give rise to all the red and white blood cells. In addition, some of these cells (lymphocytes and macrophages) are distributed throughout the body either as free cells or as fixed constituents of other organs, for example, in the liver, or as separate organs such as the spleen and lymph nodes.

The nervous system is made up of the central nervous system (the brain and spinal cord and their coverings) and the peripheral nervous system, which is comprised of nerves leading from these central structures. Thus, each tissue has its own specific cells, usually several different types, which maintain the structure and function of the individual tissue. The specific cells are grouped in organs which have a standard pattern, as can be seen in Figure 1.2. There is a layer of epithelium, the tissue specific cells, separated from the supporting mesenchyme by a semi-permeable basement membrane. The supporting tissues (or stroma) are made up of connective tissues (collagen fibres) and fibroblasts (which make collagen), which may be supported on a layer of muscle and/or bone depending on the organ. Blood vessels, lymphatic vessels, and the nerves pass through the connective tissue and provide nutrients and nervous control among other things for the specific tissue cells. In some instances, for example, the skin and intestinal tract, the epithelium which may be one or more cells thick depending on the tissue, cover surfaces. In others, it may form a system of tubes such as in the lung or

kidney, or solid cords such as liver, but the basic pattern remains the same. Different organs differ in structure only in the nature of the specific cells and the arrangement and distribution of the supporting mesenchyme [32].

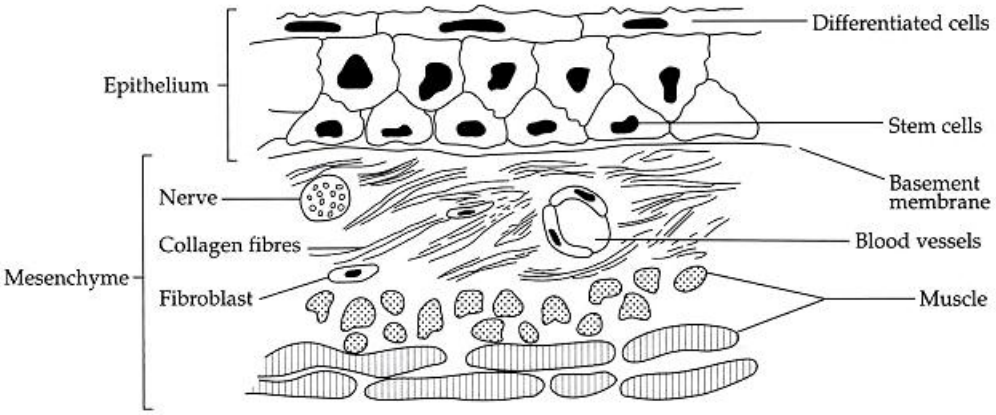

Figure 1.2: Tissue structure showing epithelial and mesenchymal components [32].

As the cell is the basic unit of life, the study of cellular physiology is critical to an understanding of cancer cell structure. With Bioimprint, it allowed us to track cell life within a specific time course. These studies will be especially crucial to discover when cancer cells secreted certain hormones the most and its importance to cancer cell progression. This will be explained

and investigated using functionalized microbeads; see Chapter 6: Bioimprints of cancer cells for more details.

The organization of cells into multicellular organisms depends upon sophisticated communication systems. During development, and in the mature organism, cells need to be able to sense the appropriate time to grow, divide, migrate, differentiate, survive or die. These processes are all controlled by families of growth factors, which bind to specific receptors on the surface of their targets. Once activated, these receptors initiate signalling pathways, which determine the response of the cells. Aberrant activation of one or more of these pathways can lead to unregulated cell division, and the formation of a tumour.

While there are many kinds of growth factor receptors, two families have emerged as promising therapeutic targets in the treatment of cancer: the epidermal growth factor receptor (EGFR) family and the vascular endothelial growth factor (VEGF) receptors. Though EGFR and its relatives are expressed on epithelial cell-derived tumour cells and contribute directly to tumour cell growth, VEGF receptors are expressed on the endothelial cells lining blood vessels, which are normal, untransformed cells. VEGF receptors contribute to tumour growth by triggering vessel growth which is essential to supply nutrients to a growing tumour. For this research work, studies were

concentrated on observing the cell structure during the regulation of VEGF and the effect of using certain organic or inorganic compounds such as cobalt chloride ($CoCl_2$) in exaggerating the expression of the growth factor.

To achieve these objectives in this research a number of different cells obtained either from approved cell lines or patients from Christchurch Hospital were studied. The cells used were the rat muscle cells, rat pituitary glands cells, Ishikawa endometrial cancer cells and RL95-2 epithelial cancer cells. Cells were cultured and incubated in accordance with standard biological culturing procedures and protocols approved by the New Zealand Human Ethics Committee.

1.2 Biological events (Exocytosis mechanism)

Membranes serve diverse functions in cells viability; one of which is to regulate the movement of materials into and out of cells. Exocytosis is the process by which a cell directs the contents of the secretory vesicles out of the cell membrane. These secretory vesicles or also known as secretory granules contain soluble proteins that are to be secreted to the extracellular environment, as well as membrane proteins and lipids that are sent to become

components of the cell membrane. This can be explained by the illustration in Figure 1.3.

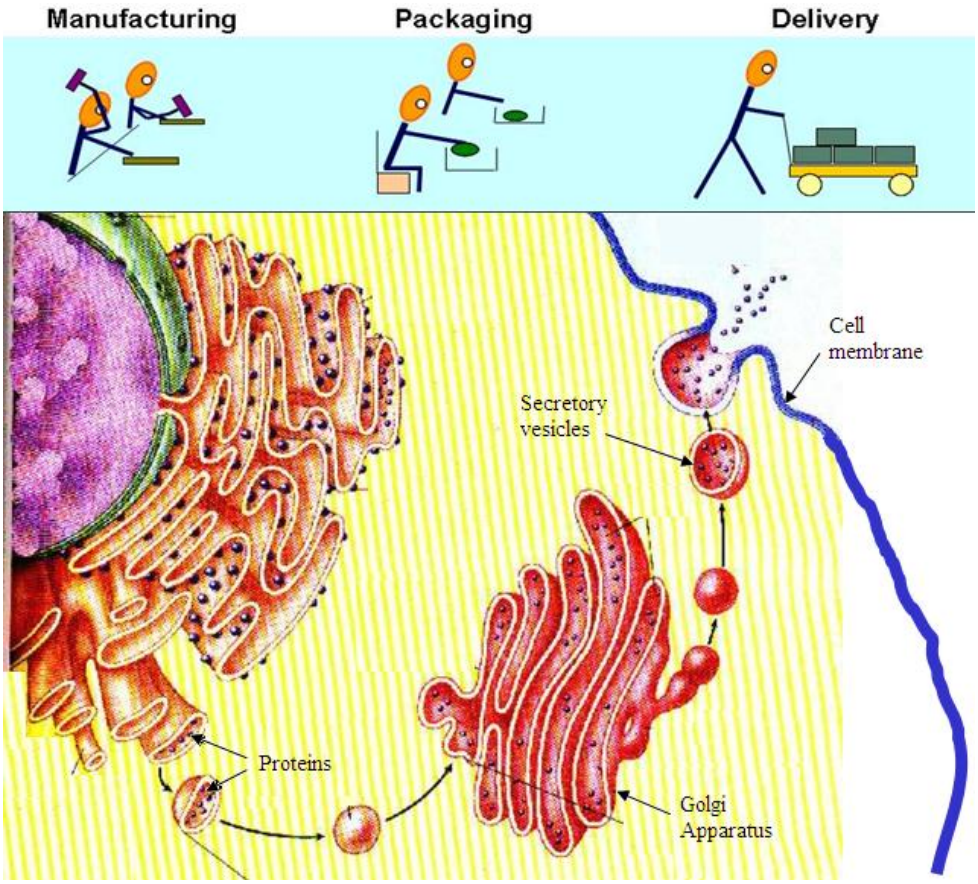

Figure 1.3: Schematic of exocytosis process in the plasma membrane [34].

There are two types of exocytosis in multicellular organisms such as human. The first one is known as Ca^{2+} triggered non-constitutive and the

other is known as non Ca^{2+} triggered constitutive. Constitutive exocytosis is performed by all cells and provides the release of components of the extracellular matrix.

Newly synthesized proteins leave the endoplasmic reticulum and are transported along with lipids to the *cis* Golgi network, from where they both exit via the *trans* Golgi network in transport vesicles destined for the cell surface or other compartments [35]. On the contrary, non-constitutive or regulated exocytosis involving secretory vesicles, in which proteins and other substances are stored for later release, requires an external signal to occur. This signal that triggers the release is controlled by the families of growth factors that bind to specific receptors on the cell surface, and are called the secretagogues.

Membrane fusion events of dynamic exocytosis occur in the range of nano- to milliseconds. There are only a few techniques that have the potential of capturing these events by having a snapshot of the process taken or replicated for a period of time. Bioimprint is one of the methods that have the capability to achieve that purpose.

There are five main steps involved in exocytosis progression which proceed sequentially beginning with:

1. Vesicle Trafficking

It is a mandatory feature for eukaryotic cells. It can be thought as cargo traffic between different cell organelles and between cell and its surroundings. In this first step, the vesicle containing the waste product or chemical transmitter is transported through the cytoplasm towards the part of the cell from which it will be eliminated. For example, the transport of proteins from *trans* Golgi network to cell surface. F-actin forms a cortical actin network under the plasma membrane and the exocytotic vesicles are transported along microtubules to the vicinity of plasma membrane, but are not secreted before the cortical actin network opens locally. Local disassembly of the local cortical F-actin network is required during exocytosis especially in specific-function-cells such as mast cells, chromaffin cells, and pancreatic acinar cells.

2. Vesicle Tethering

In this second step, as the vesicle approaches the cell membrane, it is secured and pulled towards the part of the cell from which it will be eliminated. Tethering involves links over long distances to bring vesicles into the vicinity of the appropriate acceptor membrane and confer additional compartmental specificity [36]. Tethering

interactions are likely to be involved in concentrating synaptic vesicles at the synapse.

3. Vesicle Docking

In this step, the vesicle comes in contact with the cell membrane, where it begins to chemically and physically merge with the proteins in the cell membrane. Docking is the process during which the vesicle and pre-synaptic membrane line up in a fusion-ready state. Stable docking represents several distinct molecular states whereby the interactions underlies the close and rigid association of a vesicle with its target and this may include the molecular rearrangements needed to trigger the bilayer fusion. Tethering and docking of the vesicle at the target membrane pave the way for the formation of a tight core SNARE complex.

4. Vesicle Priming

In those cells where chemical transmitters are being released, this step involves the chemical preparations for the last step of exocytosis. Activation of fusion machinery known as the SNARE proteins by tethering triggers the assembly of protein complexes linking vesicles and plasma membranes together.

5. Vesicle Fusion

In this last step, the proteins forming the walls of the vesicle merge with the cell membrane and breach, pushing the vesicle contents (waste products or chemical transmitters) out of the cell. This step is the primary mechanism for the cell's plasma membrane size increase.

There are various modes in exocytosis mechanism but they can be categorized in three major models, with different secretion activities and fidelities for each model. This can be explained by the illustration in Figure 1.4 [37] which shows the exocytosis models as *'kiss-and-collapse/full collapse'*, *'kiss-and-run'*, and *'kiss-and-stay'*.

'*Kiss-and-collapse*' mechanism has been widely used to describe mechanism completing the total fusion of the vesicle to the plasma membrane with the waste product or chemical transmitter transported being released of the cell to the extra-cellular environment. This would explain how the membrane of the vesicle permits the transport of characteristic cell-surface proteins that need to be expressed on the surface of the cell and how the plasma membrane continuously redevelops its structure.

However, without a reverse mechanism to the exocytosis, regeneration of cell membrane would definitely create cells larger in sizes compared to their normal dimensions. To compensate this, cells need to

perform endocytosis, which is the process where cells absorb molecules such as proteins needed for augmentation from outside the cell by engulfing them with their cell membranes into the intra-cellular environment.

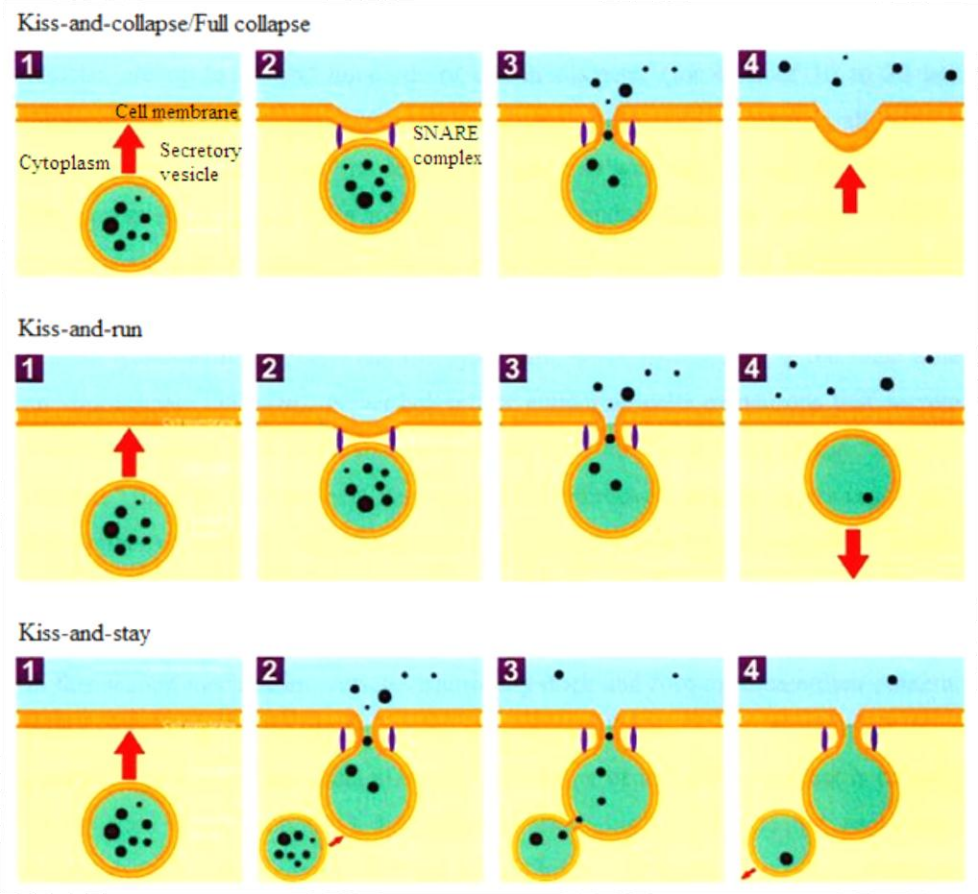

Figure 1.4: Exocytosis fusion mechanisms named '*kiss-and-collapse/full collapse*', '*kiss-and-run*', and '*kiss-and-stay*' [37].

All cells perform endocytosis as most substances important to their growth dynamics are large polar molecules that cannot pass through the hydrophobic plasma or cell membrane. In addition to supporting bidirectional mechanism of transport and communication, endocytosis is seen to act as a regulatory-balancing mechanism to satisfy the cell surface constancy requirement [29].

'*Kiss-and-run*' model suggests that fused vesicles can detach from the cell membrane and be retracted into the cytoplasm with the vesicles able to preserve their integrity during this process [38]. This transient state of vesicle fusion with the plasma membrane is also referred to as 'transient fusion' and has been documented by Schneider [38]. Controversy has been surrounding the interpretation of this process in recent years. As mentioned before, these vesicles fuse with the plasma membrane by forming a transient fusion pore while still maintaining vesicle integrity. After detachment, vesicle can fuse again without any preceding endosomal fusion. Therefore, the advantage of transient fusion is rapid cycling between a fusion state and a non-fusion state. It seems that some cells, such as chromaffin cells, can switch between total and transient fusion by varying the extra-cellular calcium [39]. In recent years, morphological techniques, such as fluorescent microscopy or atomic force microscopy (AFM) have provided evidence for the '*kiss-and-run*' model. Both approaches showed that vesicles release their

contents within seconds [40] to minutes [41]. After the fusion event, the vesicles detach and return into the cytosol while preserving their integrity and morphology.

"*Kiss-and-stay*" is a model of a secretion process that has just emerged in the cell physiology study quite recently, which involves the sequential replenishment mechanism of exocytosis. In this model, it is suggested that the vesicles still follow the same fusion with the plasma membrane as in the "*kiss-and-run*" model, but in this case the exocytosis is differentiated by a much longer fusion pore opening and without any undocking step following thereafter. During this fusion, the vesicles start to reacidify and refill with neurotransmitters from other transport vesicles that fuse onto them.

As shown in Figure 1.4, the first vesicle acts as a channel through which the content of a secondary vesicle can be released after their fusions. In this mechanism, multiple vesicles can fuse to a single granule that has already maintained an opening on the plasma membrane with the vesicles remain in a readily releasable pools. This sequential secretory mechanism thus allows the cell to take advantage of a large supply of fusion-ready granules without needing to transport them to the plasma membrane [42]. With this process, cells are capable of secreting a large amount of

neurotransmitters to the outside environment without any significant alteration to the structural morphology of their membranes.

1.3 Research objectives

Bioimprint replication technique developed earlier by Muys [26] was a novel approach in applying nano-imprint lithography scheme for the use in biological imaging, especially when utilizing the non-destructive, high resolution atomic force microscopy. Current work, however intends to bring improvements to the existing Bioimprint method in terms of better materials used for the replication, which is the use of Biopolymer that is biocompatible and with simpler steps involved in the replication process. Concentration was given on developing the Bioimprint technique for replicating living cell features especially membrane structures at the nanometer scale. The aim was to uncover a new biocompatible polymer that is capable of replicating intricate structures with higher resolution compared to previous works, fast curing time with better membrane topography transfer and able to preserve feature details. It should also able to provide accurate determination of any morphological changes due to the fusion of exocytosis pores on the surface membrane. Nonetheless, concentration was also given in developing and

designing a Biochip platform that would be used to manipulate cells movement and trapping them at certain locations on the micro assays of the Biochip for easy identification and handling.

There are still a lot to learn and explore in relation to secretory vesicle mechanism of cells especially the exocytosis process, which explains how the cells secrete the contents of the vesicle to the extracellular matrix. Further investigation into observing the characteristic behaviour of the plasma membrane when the cells are induced by certain compounds such as cobalt chloride ($CoCl_2$) and cyclohexamide will bring in the opportunity to examine the effect of these agents in inducing apoptosis in many different kinds of cells [43].

Cobalt chloride is a hypoxia mimetic agent in cell cultures and widely used in the treatment of anaemia. During chemical hypoxia induced by cobalt chloride, hypoxia-inducible factor 1-alpha (HIF1- α) mediates the increase induction of a variety of receptors including VEGF [44]. However, cobalt exposure in higher dosage can lead to tissue and cellular toxicity [45]. Cyclohexamide is an antibiotic produced by *Streptomyces griseus* that inhibits protein synthesis in cells. Cells induced with cyclohexamide exhibit decrease in the numbers of VEGF expressions. Nevertheless, it is too toxic and non-selective for common use in clinical practice, though broadly used

in treatment of cancers and management of graft-versus-host reactions following transplantation in a patient [46].

Other than that, cell membrane examination under the influence of these chemical agents were targeted in order to establish the time course during which the VEGF receptors were secreted the most within a 24- hour time frame. Further investigation and analysis using nano-particles as bio-markers conducted at the later stage of the work was essential to prove that the pores found on the membrane surfaces were actually the granules from the exocytosis mechanism. All these can contribute to expanding the knowledge about exocytosis and fundamental physiology of cells, and also assist in understanding diseases especially cancer.

1.4 Thesis outline

The opening of chapter of this thesis is dedicated to the cancer cells, explaining the cell structures, types of cells, and the differentiations between healthy and cancerous cells. This chapter also introduces AFM as the leading tool in investigating the cancer cells by applying a novel technique developed by our laboratory named Bioimprint™. In the following chapter, '*Laboratory equipment and experimental techniques*', a brief background

provides an introduction to the equipment applied in this research and the biological experimental techniques used, with detail descriptions being forwarded in Appendix A.

The following chapter entitled '*Atomic Force Microscopy*' focusing on the current state-of-the-art in AFM imaging, its application to biological systems and a comparison to other metrology tools. The subsequent chapter '*Biochip*' presents a detailed design and fabrication steps for the development of the Biochip. It explains the design of electrode array chip as an electrically controllable method of positioning and trapping biological cells. An electrokinetic force known as DEP is used to position cells within cavities fabricated above and around a series of interdigitated electrodes.

The fifth chapter introduces Bioimprint, which is the core of this research. It describes the issues faced before by the same technique but with different method and materials. In this chapter, a newly developed Biopolymer, designed to overcome some of the inherent difficulties of cellular analysis by AFM and the previous Bioimprint technique. The following chapter continues to explain the detailed analysis of AFM imagery of the cell's imprint and discusses the range of fusion pores imaged in the Ishikawa endometrial cancer cells. The correlation between the number of fusion pores and the expression of human vascular endothelial growth factor

(VEGF) will be presented to show that the number of pores will increased dramatically when the VEGF proteins are induced by certain type of chemical compound. This chapter will highlight the topography and the morphology of cancer cells, obtained through the Bioimprint replication process and how this technique can help us to understand the surface of cancer cells better.

In the chapter '*Summary remarks and conclusion*' the key areas of this research are discussed and summarised with recommendations on future work and project directions. The final chapter comes to an end made by statements that conclude the key findings of this project and current projects that benefited from this research.

Chapter 2

Laboratory equipment and experimental techniques

This chapter introduces semiconductor equipment used at the Nanofabrication Laboratory, Department of Electrical and Computer Engineering, University of Canterbury. The equipments were used for the fabrication of the Biochip and the Bioimprint development. Highlight includes facilities for semiconductor material processing, nanofabrication, and device development. They make up the main fabrication facility for the inter-departmental Nanostructure Engineering, Science and Technology research group, as well as the MacDiarmid Institute for Advanced Materials and Nanotechnology. In addition, this chapter presents the biological protocols and experimental techniques employed for the preparation and culturing of cells from rat pituitary glands, and human endometrial cancer cells (Ishikawa cancer cell line) at the Laboratory for Cell and Protein

Regulation, Department of Obstetrics and Gynaecology, School of Medicine and Health Sciences, University of Otago.

2.1 Micro and Nanofabrication equipment and processes

Photolithography or also known as optical lithography is a process used in micro- and nanofabrication in the semiconductor industry to define patterns by selectively remove parts of a thin material film of a substrate. It uses UV light exposure to transfer a geometric pattern from a photo mask to light-sensitive photo resist on the substrate. A series of chemical developments then engraves the exposure pattern into the material underneath the photo resist. In this work, the photolithography process was extensively used for the fabrication of the Biochip platform.

The equipment in the Nanofabrication Laboratory covers most aspects of semiconductor device fabrication for this research and detail explanation of techniques and devices will be presented hereafter. Some of the principal tools are: Optical lithography mask writer, mask aligner, optical microscopy (Olympus BX30 with digital image capture), thin film deposition (evaporator), Dektak, and the most important equipment of all, the atomic

force microscopy (AFM), which will be discussed in its own separate chapter.

2.2 Mask Writer

The Heidelberg µPG 101 mask writer is a micro laser pattern generator for direct writing of photomasks, suitable for research and development environment with low volume mask making. This device was used in the fabrication of the photomask design, particularly the masks used in the Biochip fabrication. The system is very useful for applications in microfabrication such as MEMs, BioMEMs, integrated optics, micro fluidics or any other device fabrication that requires high resolution and precision of microstructures. Figure 2.1 displays the integrated system comprising of the main laser writer (insert image), an electrical power regulator for self-controlled vacuum and compressed air, and a personal computer for system control.

The system works fundamentally the same as a laser printer but with higher resolution of up to 250 000 dpi compared to the latest desktop laser printer with print resolution only up to 1200 dpi (in black). It is capable of writing features down to 3 µm size on areas of up to 100 x 100 mm^2 or optional even down to 1 µm size on areas of up to 30 x 30 mm^2. The

machine is equipped with diode laser at 405 nm, which can also be used to expose standard photoresist being used in lithography.

Figure 2.1: Heidelberg Instruments µPG – Laser pattern generator.

Vector and raster-scan exposure modes are available for mask writing, which will enable the system to create high resolution 2-D patterns. Multiple data input formats like AutoCAD DXF (Drawing Exchange Format), CIF (Caltech Intermediate Form) mask database, and even BMP (bitmap) can be used to transfer design files to the system. The ease of use

helps to provide a platform for fast prototyping and fabrication of micro-pattern on photomasks with high precision and accuracy in fraction of the cost compared to the ones developed by third party manufacturers elsewhere.

2.3 Mask Aligner

A mask aligner is a top and bottom side contact printer used to contact, align, and transfer features from a patterned mask to a photosensitive material by UV radiation exposure. Karl Süss MA6 (Karl Süss GmbH, Germany) mask aligner was used in this research for precision and accurate alignment and fabrication of Biochip microarrays, and as a UV light source for Bioimprint cancer cell replications. The machine comes with a 350 W Mercury UV lamp as the exposure source, with an intensity of 2.7 mW/cm^2. The MA6 can be used for fine lithography down to 1 micron or better and is ideal for use with I-line (365 nm) resists. Other than that, it can handle regular semiconductor wafers up to 6 inches, with variety of mask holders that can accommodate masks from 4 to 6-inch. Figure 2.2 shows the MA6 aligner in the Nanofabrication Laboratory's film deposition room facility.

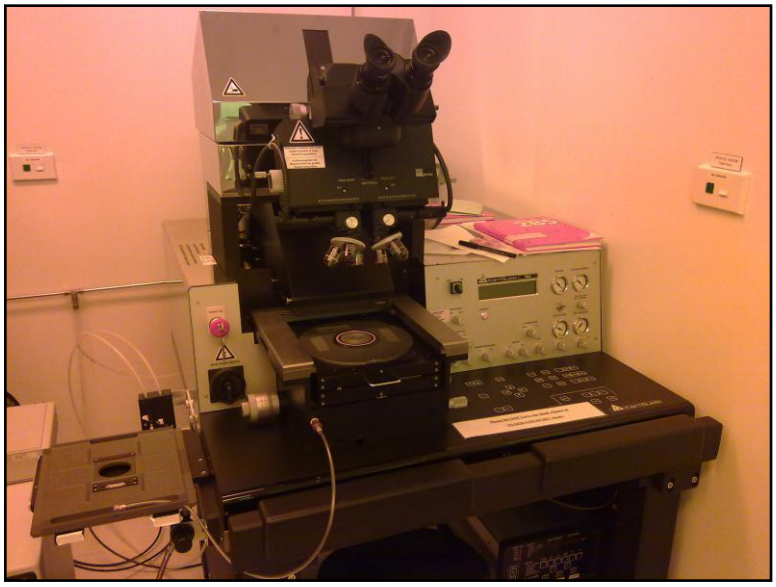

Figure 2.2: Karl Süss MA6 mask aligner.

There are several modes of operation in which the MA6 performs its functions. Exposures can be done in vacuum (vacuum between substrate and mask), low vacuum (vacuum level between substrate and mask can be adjusted), hard (nitrogen pressure under the substrate), or soft (vacuum under the substrate) modes.

Initially, when a substrate has been loaded on the chuck (a platform that holds the underlying substrate), MA6 will perform WEC (Wedge Error Compensation). In this procedure, the chuck is automatically adjusted such that the substrate is perfectly parallel to the mask. WEC can be executed in

two different programs: contact and proximity. Contact WEC relies on the overall flatness of the mask and substrate to produce a parallel pair. On the other hand, Proximity WEC uses a three-point contact (via proximity flags) procedure to achieve parallel adjustment. Proximity WEC is always performed when exposing with a proximity program, while contact programs can choose either one of the WEC options.

MA6 is also equipped with a split field microscope (5x, 10x, 20x objectives) and an automated stage for a high precision alignment. Two separate focus adjustment can be performed for mask and substrate surface, and alignment is accomplished by moving the wafer in such a way that the alignment markers on the mask are well-aligned with those on the substrate.

2.4 Evaporator

Thin film deposition is one of the techniques available in semiconductor fabrication, and thermal evaporation is the common method used for that purpose. The source materials, for instance gold, nickel chromium or zinc oxide that was used for the Biochip platform is evaporated in a vacuum chamber. They were placed on a resistive boat or crucible which was then applied with a certain level of current. Eventually this will cause the

temperature of the material to rise and once the material reached its melting point, it started to evaporate.

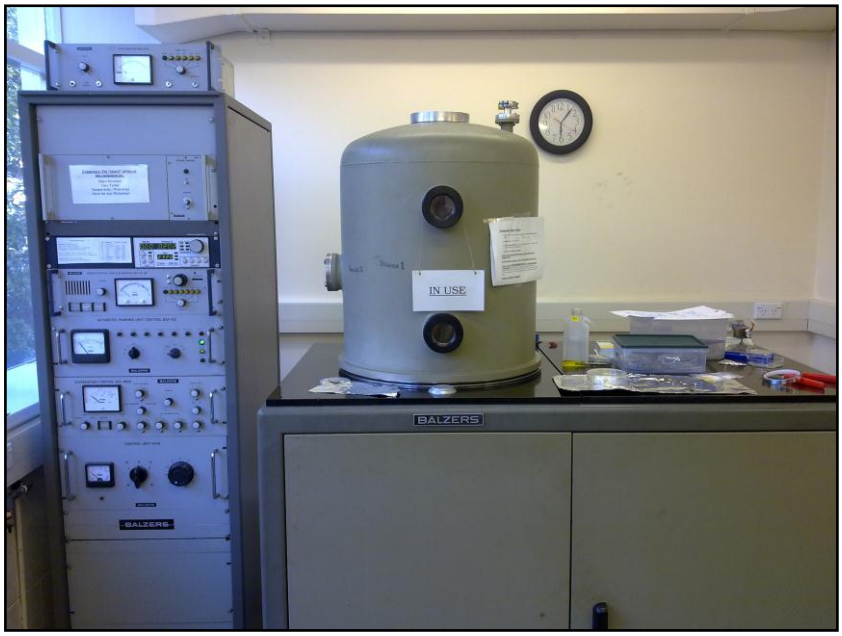

Figure 2.3: Thermal evaporator for thin film deposition.

Vacuum environment in the chamber allowed vapour particles from the material to travel directly to the depositing substrate, which was placed above the boat where they condensed back to a solid state. The thickness of the layer deposited was measured by using a quartz crystal oscillator,

positioned next to the substrate in the chamber. A high vacuum evaporator, named Balzers AG (Fürstentum, Liechtenstein) as shown in Figure 2.3 was used extensively in this work to evaporate layers of gold and nickel chromium as the electrodes for the Biochip fabrication on a silicon nitride wafers.

2.5 Surface Profiler (Dektak 150)

Dektak 150 (Veeco, USA) is a stylus surface profiler used to measure a surface's profile; in this case the Biochip's surface, in order to quantify its roughness. Vertical resolution is usually in the nanometre level, though lateral resolution is usually lesser. The profiler performs by moving its stylus vertically in contact with a sample and then moved laterally across the sample for a specified distance and contact force. It measures small surface variations in vertical stylus displacement as a function of position. The height position of the stylus generates an analog signal which is then converted into a digital signal before being stored, analysed, and displayed.

The radius of the stylus comes in different options ranging from 50 nm to 25 µm, and also available in High Aspect Ratio (HAR) tips (10 µm x 2 µm and 200 µm x 20 µm). The horizontal resolution is controlled by the scan

speed and data signal sampling rate. The stylus tracking force can range from 1 to 15 mg with LIS (Low Inertia-Sensor) 3 sensor, or 0.03 to 15 mg with N-Lite sensor option [47]. Figure 2.4 illustrates the Dektak 150 contact surface profiler on a workbench in the Nanofabrication Laboratory.

Figure 2.4: Dektak 150 contact surface profiler.

2.6 Cell Culture protocols and equipment

Cells were prepared in accordance with institutional guidelines of the Christchurch School of Medicine and Health Sciences, University of Otago. This section will explain in general the protocols for cell culture and equipments. For more details of solutions, media, and rat cell culture protocols see Appendix A.1 – *Rat cell culture protocols*. For more details of media and endometrial cancer cell culture protocols see Appendix A.2 – *Protocol for cancer cell culture and cloning*. For more details on reagents and cell regulation using cobalt chloride ($CoCl_2$)/cyclohexamide ($C_{15}H_{23}NO_4$) refer to Appendix A.3 – *Protocol for cancer cell culture and regulation using cobalt chloride/cyclohexamide*.

2.6.1 Cell preparation/dispersion

Cells were obtained from the cryovials (stored in the freezer cabinet with plastic coloured boxes). The cells must be kept in -80 ºC freezer or in liquid nitrogen. Cell dispersion was carried out under aseptic conditions. They were prepared in a laminar flow cell culture hood (EMAIL Air Handling Biological Safety Cabinet Class II). All glassware used for cell preparation was autoclaved before use and together with all the solutions were sterilized with ethanol.

All cells (in cryovials) and solutions were first pre-warmed to 37 ºC before use. The culture media used is called Minimum Essential Medium alpha-Medium (α-MEM) (Gibco, Auckland, NZ) containing, 2.2 g/L sodium bicarbonate, 1 % penicillin/streptomycin, 0.1 % BSA that has been added with a 10% of Fetal Bovine Serum (Gibco, Auckland, NZ) medium. Once the cells were ready, they were transferred into culture flasks (50 ml with carted neck) and 10 ml of the α-MEM was added in each flask. Then they were stored in the incubator (37 ºC, 0.5% CO_2) for at least 1 – 2 days (to allow the cells to adhere to the surface). Medium should be changed after 1 - 2 days and was replaced with another 10 ml of (α-MEM + FBS 10%).

2.6.2 Maintenance of cell culture

Cell culture media was changed when required, which was generally every second of third day. Media was aspirated using a sterile Pasteur pipette in the cell culture hood. α-MEM with 10% FBS which had been pre-warmed to 37 ºC was then added to the flask, using a sterile 10 ml transfer pipette. The volume of α-MEM added was dependent on the size of the flask: 25 cm^2 – 10 ml; 75 cm^2 – 20 ml; 175 cm^2 – 30 ml.

2.6.3 Splitting confluent cell culture

When cells reached a confluent state, they were split in preparation for further use. Cultures that had become confluent were then placed in the cell culture hood, where the cell culture media was removed by aspiration. 10 ml of Phosphate Buffered Saline (10xPBS pH 7.4) that had been pre-warmed to 37 ºC was then used to wash the cells. The PBS was then removed and the wash step was repeated twice more. Following the final aspiration of the PBS from the flask, 2.5% Trypsin (Gibco, Auckland, NZ) in PBS was added to the cells. Cells were dislodged by light tapping on the side of the flask.

The spilt cells then were transferred into a larger multi-wells or culturing plate for different experiments. 10 ml of α-MEM with 10% FBS was added to the cell suspension in the flask, and the cells and the media were then transferred into a 15 ml Falcon tube. Cells were evenly dispersed through the media by light tapping on the outside of the tube. A small sample of the cell suspension was then removed, and used to perform a cell count with a haemocytometer. Haemocytometer is a device originally designed for the counting of blood cells. It is now used to count other types of cells as well as other microscopic particles. The cell counting formula is:

$$c^s = DFc = DF\left(\frac{n}{v}\right)/sq$$

c^s = concentration of sample, cell/ml

c = concentration of the solution on haemocytometer

DF = Dilution factor of sample

n = number of cells per 1 mm^2

v = volume under the coverslip (i.e. $1x10^{-4}$ ml)

sq = number of 1 mm^2 squares

Cells were then centrifuged at 1500 rpm for 5 minutes at room temperature. After that, the supernatant was aspirated and the media (α-MEM + FBS 10%) was then added with the volume added dependent on the cell count performed earlier, the size of the plate and the concentration of cells required. The plate was then stored in the incubator for 2 – 6 days depending on the type of experiments the cells were going to be used. Incubations were performed on up to four separate occasions in at least duplicate and supernatants were assayed in duplicate. Supernatant medium was transferred to tubes, frozen immediately and stored at -20 ºC until assayed by ELISA (Bachem AG, Bubendorf, Switzerland and R&D Systems, Minneapolis, MN, USA) for VEGF.

2.6.4 Pituitary cells

Cells from the rat pituitary gland were collected according to protocols approved by the Animal Ethics Committee. Pituitary cells were prepared at the Laboratory for Cell and Protein Regulation, Department of Obstetrics and Gynaecology, Christchurch School of Medicine and Health Sciences and dispersed according to protocols prepared by Prof. John J. Evans.

Adult female Sprague-Dawley rats were used for this experiment and they are housed in conditions of controlled humidity, temperature (22 °C) and lightning (14 hours of light, 10 hours of dark). Pellet food and fresh water should be available ad libitum.

2.6.5 Rat muscle cells

Rat muscle cells were obtained and handled by The New Zealand Institute for Plant and Food Research Limited. Cell culturing and replication using Bioimprint were prepared and carried out at the Laboratory of Functional Foods and Health according to protocol proposed by Dr. John S. Mitchell.

2.6.6 Ishikawa endometrial cancer cells

Ishikawa endometrial cancer tissues (human cancer cell line) were obtained from RIKEN BioResource Centre (RIKEN BRC), Japan and were derived from ovarian cancer malignant of a 30-year-old Asian woman patient. The

cells have epithelial-like morphology and can be anchoraged to culture plates. Cell were stored in cryovials and kept either in -80 °C freezer or in liquid nitrogen container at an extremely low temperature (~77 K / -196 °C).

2.6.7 RL95-2 cancer cells

RL95-2 tissues were obtained from a tumour-derived human uterine. They are a new human endometrial cell line, derived from a Grade 2 moderately differentiated adenosquamous carcinoma of the endometrium [48]. Protocols for handling the tissue culturing of these cancer cells were prepared by Dr. Kenny Chitcholtan and James Dann.

During the course of this work, some experiments were also done using endometrial cancer tissues (JDS-8 cells) that were collected from consenting women under Ethics Approval CTB/04/02/005. Tumour cells were obtained from patients undergoing hysterectomy operation to remove the uterus and sample of the tumour was collected by the duty pathologist. This was done at the Christchurch Women Hospital and performed by a gynaecological oncology specialist, Dr. Peter Sykes.

2.7 Cell culture plates and chambers

Cells can be grown in plates with various formats, such as 96-well, 24-well or 6-well plates. For rat pituitary gland cells, they were grown in 6-well plates (BD Falcon, NJ, USA) on top of glass cover slips (22 mm) that were placed in each of the wells. Plates were placed in the incubator with a lid, and in general the media should not fill the wells more than half-way (i.e. 3.2 ml for a 6-well plate and 1 ml for a 24 well plate). Cover slips need to be dipped and cleaned in a 70% ethanol and leaned against the cultured dish to dry before being used for cell culturing. The cover slips can also be prepared using autoclaved method to achieve optimum uncontaminated conditions.

Growth and differentiation of anchorage dependent cells such as pituitary gland cells are strongly influenced by the glass or plastic culture flasks offered as substrate. Cell growth rates can often be improved by surface coating with attachment factors such as fibronectin, collagen, gelatine or polylysine. Moreover, proper coating may prevent from cell de-differentiation, a common phenomenon seen in many cell lines [49, 50]. For this work, Polylysine (Sigma Aldrich, MI, USA) was used to promote cell immobilisation and adhesion. 50 ml of distilled water were added to 5 mg of polylysine, and the cover slips surfaces were aseptically coated with 120 µl – 500 µl of the solution per 500 mm^2. The solution were removed by aspiration

after 5 minutes and the surface was thoroughly rinsed with distilled water and let dry for at least two hours before being introduced to cells and medium. If the cover slips must be sterilised after coating with polylysine, γ-irradiation is recommended instead of autoclaving.

Another type of cell culture plate was also used for most part of this research. A 4-wells Permanox™ and 2-wells glass Lab-Tek™ Chamber Slide™ system (Nunc, Denmark) were used extensively for cell culturing and cell replication using Bioimprint. Permanox is a strong, biologically inert material which is highly resistant to nonchlorinated hydrocarbons, acetone, and many other electron microscopy (EM) reagents. It has not been shown to be auto fluorescent, and has a low oxygen solubility which makes it suitable for experiments performed under anoxic conditions [51].

Ishikawa endometrial cancer cells were cultured in these chambers and after 1 - 2 days of incubation, the cells were induced with certain stimuli. Once the supernatant of each chambers were collected for further analysis, the cells were replicated using the Bioimprint monomer mixture without the need to transfer the cells prior to replication. For ease of use, the upper structure of the chamber slide can be removed once cell culturing or replication process has completed.

2.8 Immunofluorescence

Immunofluorescence is a technique allowing the visualization of a specific protein or antigen in cells or tissue sections by binding a specific antibody chemically conjugated with a fluorescent dye such as fluorescein isothiocyanate (FITC). There are two major types of immunofluorescence staining methods; the first method is direct immunofluorescence staining in which the primary antibody is labelled with fluorescence dye; while the second method is indirect immunofluorescence staining in which a secondary antibody labelled with fluorochrome is used to recognize a primary antibody. Immunofluorescence staining can be performed on cells fixed on slides and tissue sections. Immunofluorescence stained samples are examined under a fluorescence microscope or confocal microscope.

In this research, secondary antibody conjugated with Goat anti-rabbit lgG MicroBeads 1 ml with the diameter of 50 nm for each bead were used to identify and isolate granules with possible exocytosis pores on the plasma membrane of the cancer cells. The cells were induced with cobalt chloride ($CoCl_2$) stimulation to monitor whether there was any upregulation or not of the vascular endothelial growth factor (VEGF) expression. For the experiment, four cell samples were prepared. The first sample consists of control cell that was stained only with primary antibody, while the second

sample consists of control cell that was stained only with secondary antibody. The third sample was prepared for cells induced with $cocl_2$ and stained with both primary and secondary antibodies, and in the fourth sample, the cells were incubated under normal condition but with staining from both the primary and secondary antibodies.

Experiments were done using Ishikawa endometrial cancer cells where they were grown on the 4-wells Permanox™ Lab-Tek™ Chamber Slide™ system until they reached 70% confluent. Once they were ready, the culture media was removed and the cells were chemically fixed with 4% paraformaldehyde (diluted in 1xPBS pH 7.4, 0.6 ml – 1 ml) for 45 minutes at room temperature (RT). The supernatants from each well were collected in 1 ml micro Eppendorf test tubes and kept in -80 °C freezer for later use. Next the cells were washed five times with cold (1xPBS pH 7.4), five minutes at a time, while being put on the laboratory shaker with speed up to 20 rpm.

Then the cells were blocked using block solution which consists of 5% w/v Bovine Serum Albumin (BSA) diluted in 1xPBS pH 7.4 (500 µl) for 60 minutes at RT. Next the cells were washed four times with cold (1xPBS pH 7.4) , five minutes at a time, while being put on the laboratory shaker with speed up to 20 rpm. Afterwards, the cells were permeabilised with 0.5% v/v Triton-X100 (prepared in 1xPBS pH 7.4) for 20 minutes at RT; or using

99% methanol (-20 °C, 0.5 ml) at kept at 4 °C for 12 minutes. Then the cells were washed again four times with cold (1xPBS pH 7.4), five minutes at a time, while being put on the laboratory shaker with speed up to 20 rpm.

Later, the cells were incubated with primary antibody (Rabbit α-VEGF 20 µl) which was diluted in $^{1}/_{100}$ to $^{1}/_{200}$ dilution and kept at 4 °C overnight. Antibody diluting solution is 2.5% w/v BSA in 1xPBS pH 7.4 Reagent Diluent. Then the cells were washed four times with cold (1xPBS pH 7.4), five minutes at a time, while being put on the laboratory shaker with speed up to 20 rpm. After that, the cells were incubated with secondary antibody, which was Goat anti-rabbit lgG (MACS No. 120-000-292) ($^{1}/_{500}$ dilution) and kept at 37 °C for 1 hour. Then the cells were washed four times with cold (1xPBS pH 7.4 + 0.05% v/v Tween-20), five minutes at a time, while being put on the laboratory shaker with speed up to 20 rpm. This was followed with the last wash using cold 1xPBS pH 7.4.

To visualize the cells under AFM, they need to be prepared first before any imaging can be done. The cells were washed by immersion in distilled water 2 times, followed by drying through blotting from the corners of the slide and then aspiration of excess fluid from the extreme edges. To get better results, the cells were left to dry at RT overnight.

2.9 Chemical fixation

Chemical fixation is a biological technique that employs agents which permeate tissues and cells and combine covalently with their major biochemical constituents (lipids, proteins and carbohydrates) and fix them into place. There are two types of chemical fixation:

1. ***Coagulative fixatives (ethanol, methanol, Hcl, chromic acid)***

   This technique is used primarily for fixing specimens for light microscopy and precipitate (coagulate) and denature proteins not normally visible at the light microscopy level. Therefore, it is not suitable for Electron Microscope.

2. ***Non-coagulative Fixatives (formaldehyde, glutaraldehyde, acrolein)***

   This fixation method forms intra and intermolecular links and change the *sol* (fluid colloidal solution) from of the cytoplasm into an electron transparent gel. Formaldehyde penetrates tissues rapidly but may be extracted by repeated washing. Glutaraldehyde penetrates tissues slower but due to its bifunctionality, it is able to crosslink proteins into permanent

stasis. Cell membranes are partially permeabilized but cells remain osmotically active.

For this research, cells were fixed in a 2.5% glutaraldehyde (ProSciTech (QLD, Australia) in physiological PBS and incubated for 30 – 60 minutes either at RT or in one instance at 37 °C. A solution comprising 4% formaldehyde was also trialled with no visible or advantage over glutaraldehyde.

2.10 ELISA

Enzyme-linked immunosorbent assay (ELISA), is a biochemical technique widely used in immunology for measuring the concentration of a particular molecule such as hormone or drug in a fluid for example cell culture supernates. The ELISA has been used as a diagnostic tool in medicine as well as a quality control check in various industries. The molecule is detected by antibodies known as the antigen (or capture antibody) and usually monoclonal antibodies are used.

Plate preparation was a necessity for this experiment. The capture antibody was first affixed to a surface and then a specific antibody (or

detection antibody) was applied over the surface so that it could bind to the capture antibody. This antibody was linked to an enzyme, and in the final step a substance was added that the enzyme would convert to detectable signal. Thus in the case of fluorescence ELISA, when light of the appropriate wavelength is shone upon the sample, any antigen/antibody complexes will fluoresce so that the amount of antigen in the sample can be inferred through the magnitude of the fluorescence.

Figure 2.5: A 96-well microtitre plate for ELISA.

Performing an ELISA involved at least one antibody with specificity for a particular capture antibody (in this case mouse anti-human VEGF). The

sample with an unknown amount of human VEGF was immobilized on a solid support (usually a 96-well polystyrene microtitre plate as shown in Figure 2.5) either non-specifically (via adsorption to the surface) or specifically (via capture by another antibody specific to the same antigen, in a "sandwich" ELISA). After the antigen was immobilized the detection antibody was added, forming a complex with the antigen. The detection antibody could be covalently linked to an enzyme, or could itself be detected by a secondary antibody which was linked to an enzyme through bioconjugation. Between each step, the plate was typically washed with a wash buffer solution to remove any proteins or antibodies that were not specifically bound. After the final wash step, the plate was developed by adding an enzymatic substrate to produce a visible signal, which indicated the quantity of antigen in the sample.

A microplate reader (VersaMax – Molecular Devices, USA) shown in Figure 2.6 was used to detect the optical density of each well and was set to 540 nm wavelength. This reader used a grating monochromator to select the exact wavelength needed for every assay. This technique utilized fluorogenic, electrochemiluminescent, and real-time polymerase chain reaction (PCR) detection modes to create quantifiable signals. These new detection modes can have various advantages including higher sensitivities and multiplexing [52, 53]. For more details on reagents and ELISA protocols

refer to Appendix A.4 – *Protocol for DuoSet® ELISA development system to measure human Vascular Endothelial Growth Factor (VEGF).*

Once the results from the microplate reader were obtained, the duplicate readings for each standard, control, and sample were averaged and the average zero standard optical density was subtracted from the results. Next, a standard curve was constructed using computer software such as Microsoft Excel by plotting the mean absorbance for each standard on the y-axis against the concentration on the x-axis and the best fit curve was drawn through the points on the graph. Then the data were linearized by plotting the log of the VEGF concentrations (ng/ml) versus the log of the time course (hour/s). Any dilution to the samples would require the concentration reading from the standard curve be multiplied by the dilution factor.

Figure 2.6: Microplate reader for ELISA development kit to measure natural and recombinant human Vascular Endothelial Growth Factor (VEGF). Insert: 96-well microtitre plate before development.

Chapter 3

Atomic Force Microscopy

Atomic Force Microscopy (AFM) is the main imaging tool used in this thesis. This is because of its very high resolution imaging capability, the ability to image in air and liquid environment, its unique 3-D non-destructive technique that is insensitive to material properties, able to provide extraordinary topographic contrast with direct height measurements and unobscured views of surface features (without any coating and expensive sample preparation needed), and at the same time able to yield far more complete information than other two-dimensional profilers. As to further understand the concept of AFM, a description of the principles of operation will be presented in this chapter.

AFM or also known as scanning force microscope (SFM) was first invented by Binnig, Quate and Gerber [8, 54] in 1986 while working at IBM Research in Zurich. The idea started in the early 1980s when Gerd Binnig and Heinrich Rohrer developed the first scanning tunnelling microscope, the predecessor of AFM. The achievement earned them the Nobel Prize for

Physics in 1986. AFM only became available commercially when it was introduced to the market in 1989.

The main reason why AFM was developed in the first place was to overcome the fundamental problem faced by researchers during those days when using STM, which was only capable of capturing the images of conducting or semiconducting surfaces. Whilst, AFM has the capability to produce images of almost any type of surface, such as polymers, glass, composites, ceramics and even biological samples.

AFM is a very high-resolution type of scanning probe microscopy, with demonstrated resolution on the order of fractions of a nanometer, which is more than 1,000 times better than the optical diffraction limit of a light microscope. Currently, AFM is the forefront in nanoscale imaging, measurement and manipulating instruments compared to other high-resolution tool such as scanning electron microscope (SEM).

AFM works by "feeling" the surface with a mechanical probe, and gathers the data to form useful information such as imaging. To achieve such a well-defined scanning image of a sub-nanometers resolution, AFM uses piezoelectric elements that facilitate tiny but accurate and precise movements on electronic commands.

3.1 The cantilever and probe (tip)

At present, most of AFMs available in the market employ the laser beam deflection system, a novel optical approach to AFM established by Meyer and Amer [55]. In the system, an array of photodiodes detector known as a position sensitive detector monitors the deflection of a laser beam from the back of the reflective AFM cantilever, as illustrated in Figure 3.1. The cantilever is typically microfabricated from silicon (*Si*) or silicon nitride (Si_3N_4) with a sharp tip (probe) radius of curvature on the order of nanometers at its end.

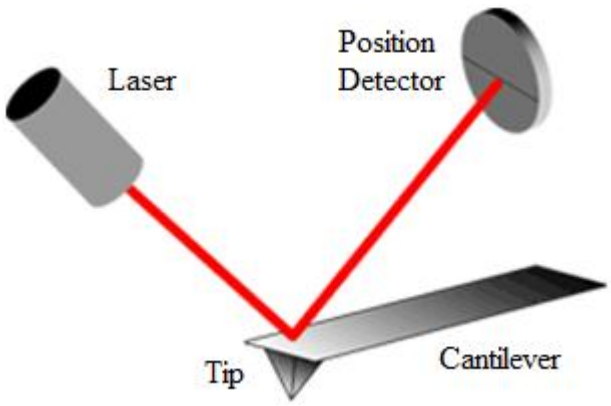

Figure 3.1: Beam deflection system, using a laser and position detector to measure the beam position [56].

During scanning, the tip is brought into proximity of a sample surface, and according to Hooke's Law, forces generated between the tip and the sample lead to a deflection of the cantilever. These forces include:

1. ***Van der Waals forces***

   This force that was named after Dutch scientist Johannes Diderik van der Waals is the attractive or repulsive forces between molecules (or between parts of the same molecule) other than those due to covalent bonds or the electrostatic interaction of ions with one another or with neutral molecules [57].

2. ***Capillary forces***

   Capillary action usually happens in fluid scanning especially that involves the imaging of biological samples. This action refers to the behaviour of liquids such as water that will tend to move up-hill (against the force of gravity) when the tip of the cantilever touches the surface of the liquid.

3. ***Electrostatic forces***

   Electrostatic force is the phenomenon that results from the slow-moving or stationary electrical charges between the tip and surface of the sample. They are present at a height between 0.1 – 1.0 μm and

can be either attractive or repulsive depending on the sample and tip materials.

4. ***Fluid surface tension forces***

   Some materials such as polymers and fixative chemicals used in fixing biological specimens are likely to have condensed water vapour on the surface. This phenomenon causes surface tension effects that can attract the tip downwards at an amplitude 10 – 200 nm from the sample.

5. ***Fluid film damping***

   Fluid film damping is the initial boundary force exclusive to tapping mode, resulting from the dampened air film being squeezed between the oscillating probe and sample at a distance of 10 μm from the surface [27].

The change in directions of the reflected laser beam are measured by the position detector as the tip scans the surface, and these values are used to calculate the deflecting angle which is dependent on the length of the cantilever. Since sample surface is not typically level, to maintain a constant force between the tip and the sample would be very difficult. If the tip was scanned at a constant height, it would probably cause damages to the sample as the risk of collision between the tip and the surface exists. To overcome

this problem, a feedback mechanism is employed to adjust the tip-to-sample distance, which then will enable the system to maintain a constant force between the tip and the sample. Current AFM designs operate with a vertical piezoelectric scanner to hold the cantilever and moves the tip in the *z* direction for maintaining a constant force, while the sample is being scanned in *x* and *y* directions using another piezoelectric block. The resulting map of the area $s = f\{x, y\}$ represents the topography of the sample.

3.2 Forces measurement

For proper imaging, knowing the forces involved is very important because the AFM relies heavily on the forces between the tip and sample. Figure 3.2 highlights the typical force curve illustrating the repulsive and attractive forces in the approach and retraction stages of the free end of the cantilever as the fixed end is brought vertically to, and away from the sample. Initially, the tip is engaged and moves slowly toward the surface of the sample, but at this stage there is still no deflection because the distance between the tip and surface is far apart. Once the tip has reached a proximity distance to the sample, the tip is pulled toward the surface as a result of the attractive surface tension force.

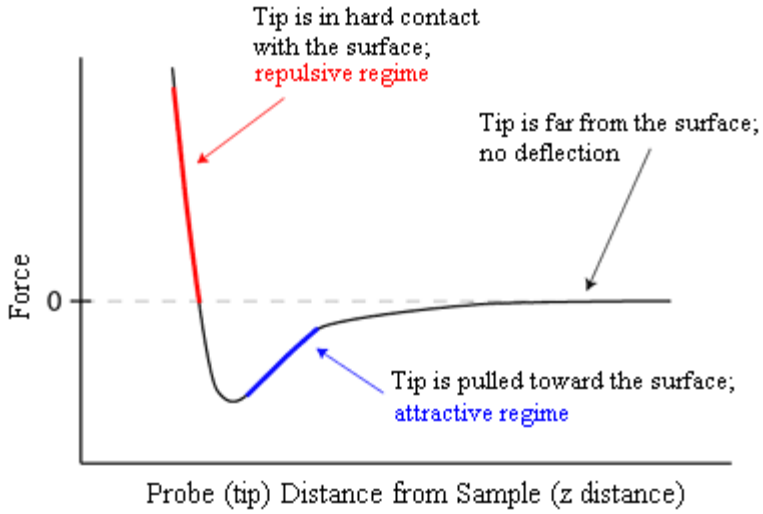

Figure 3.2: A force curve detailing the main regimes during tip approach and retraction [56].

However, when the tip has come to hard contact with the surface, the retraction stage starts due to the repulsive force that is pulling away the tip from the surface and runs clear. Based on Hooke's Law:

$$F = -kx$$

F = applied force

k = force constant (stiffness)

x = cantilever displacement from its equilibrium position

This shows that the force is not measured directly, but is calculated by measuring the deflection of the cantilever, and is directly proportional to the force constant of the cantilever. Probe choice is vital for the acquisition of high-resolution images and depends on the sample type, the environment during scanning and the operation mode. To ensure high sensitivity with respect to the applied force, the cantilever should have a maximum deflection for a given force, and consequently a minimum force constant *k*.

The two main types of cantilevers mentioned previously, the silicon or silicon nitride differ primarily by their force constants: from 1 to 200 N/m for silicon cantilevers and under 2 N/m for those made from silicon nitride. For imaging soft samples, it is better to have as low an interaction force applied on the sample as possible. On the other hand, the cantilever deflection has to be high enough to be readily detected. For this reason softer (lower force constants) cantilevers are much better suited for biological samples as they apply a lower force on the surface and respond more easily to surface fluctuations, whereas higher force constant cantilevers are used for hard surfaces. Other than that, the radius of curvature of the tip is a key component of the cantilever, as it determines the lateral resolution of the image. Optimal resolution becomes possible with very sharp tips but they may very easily damage fragile biological samples [58].

3.3 Operational Modes of AFM

AFM has two main primary modes of operation which can be categorized as static mode and dynamic mode. In the static mode, the cantilever is "dragged" across the surface of the sample and the disposition of the surface are measured directly using the deflection of the cantilever. While in the dynamic mode, the cantilever which is attached to the piezoelectric scanner is oscillated at or close to its fundamental resonance frequency or a harmonic. AFM calculates and modifies the oscillation amplitude, phase and resonance frequency of the cantilever's movement based on inputs from the tip-to-sample interaction forces. These changes in oscillation provide information about the sample's characteristics.

3.3.1 Contact Mode

In static mode operation, which is the primary mode of AFM operation, the static tip deflection is used as a feedback signal. Cantilever tips with low force constant parameters are normally used to boost the deflection signal in such a way to avoid noise and drift that can happen when measuring static signals. As the tip is raster-scanned across the surface, it is deflected as it moves over the surface corrugation. However, close to the surface of the

sample, attractive forces can be quite strong, causing the tip to “snap-in” to the surface. Thus, static mode AFM is almost always done in contact where the overall force is repulsive. As a result, this technique is much better known as the ‘contact mode’.

In this mode the tip is constantly adjusted to maintain a constant deflection, and therefore constant height above the surface. It is this adjustment that is displayed as data. Nevertheless, the ability to track the surface in this manner is limited by the feedback circuit. Sometimes the tip is allowed to scan without this adjustment, but in this case, only the deflection signal can be measured. Nevertheless, this approach is still useful for small, high-speed atomic resolution scans, thus made it better known as variable-deflection mode.

During imaging, the tip is in hard contact with the surface, so the stiffness or the force constant value of the cantilever used need to be less that the effective spring constant which holding the atoms together, and this can be in the order of 1 - 10 nN/nm. Most contact mode cantilevers have a force constant of < 1 N/m.

3.3.2 Non-Contact Mode

Non-contact mode belongs to a family of AC modes, which refers to the use of an oscillating cantilever. A stiff cantilever is oscillated at a frequency slightly above its resonance frequency where the amplitude of oscillation is typically a few nanometers (< 10 nm). In this stage, the tip approaches the surface in the attractive regime, meaning that the tip is quite close to the sample, but not touching it (hence got the name, 'non-contact'). The forces between the tip and sample are quite low, and can be in the order of pN (10^{-12} N). Van der Waals forces act upon this interaction and cause a decreased resonance frequency of the cantilever. This drop, combined with the feedback loop system maintains a constant oscillation amplitude or frequency by adjusting the average tip-to-sample distance. The detection scheme in this approach is based on measuring the changes in tip-to-sample distance at each (x, y) data points, which then allows the scanning software to construct a topographic image of the sample surface.

Non-contact mode AFM has the advantage over contact mode as it does not experience tip or sample degradation effects that sometimes can be observed at the tip after numerous scan runs. That is why non-contact mode is much preferable than contact mode especially for measuring soft samples. Stiff and hard samples may produce images that show the same profiles

when imaged either in contact or non-contact mode. However, in the case of stiff sample that has a few monolayers of adsorbed fluids lying on the surface, the images would look quite different. AFM working in contact mode will penetrate the liquid layer to image the underlying surface, while in non-contact mode AFM will oscillate above the absorbed fluid layer to image both the liquid and surface of the sample.

3.3.3 Tapping Mode

Most samples develop a liquid meniscus layer in ambient conditions. As a result, detecting short-range forces while keeping the tip close enough to the sample, and at the same time preventing the tip from sticking to the surface presents a major problem for non-contact dynamic mode in ambient conditions. Dynamic contact mode (or known as intermittent contact or commonly referred to as tapping mode) was developed to avoid this problem [59]. A stiff cantilever is oscillated up and down at near its resonance frequency and closer to the sample than in non-contact mode. The amplitude of this oscillation is normally greater than 10 nm, between 100 to 200 nm. Part of the oscillation extends into the repulsive regime, so the tip intermittently touches or taps the surface. A piezoelectric actuator is used by the AFM electronic servo to control the height of the cantilever above the

sample's surface. The servo adjusts the height to maintain a specific oscillation amplitude for the cantilever as the tip is scanned over the sample.

The advantage of tapping the surface is improved lateral resolution on soft samples. Lateral forces such as drag, which is common in contact mode, are virtually eliminated. Moreover, although the lateral forces in tapping mode are comparable to those in contact mode, the energy dissipation, that causes sample degradation, is much smaller [9, 60]. It also lessens the damage done to the surface and the tip compared to the amount done in contact mode. Tapping mode is gentle enough even for the visualization of supported lipid bilayers or adsorbed single polymer molecules (for example: 0.4 nm thick chains of synthetic polyelectrolyte) under liquid medium. With proper scanning parameters, the conformation of single molecules can remain unchanged for hours [61].

3.4 Imaging modes of AFM

The main basic application of AFM is as an imaging tool as it can, in principle, perfectly reproduce the sample topography. In the contact mode, resulting height and deflection images are complementary to each other and give a complete mapping of the sample. As the tip-to-sample forces are

constantly maintained, the height image presents variations of the vertical position of the cantilever which correlates with the changes. This provides the image with the real heights of the sample surface topography. Meanwhile, the deflection image reflects instantaneous changes of the cantilever deflection, and thus provides a map of derivatives of height profile lines [62]. In this manner, the edges of the surface are much clearer when compared to the height image, where often the edges look indistinct and less differentiated. Deflection images offer significant information regarding surface steps, crystal boundaries or extracellular structures of fibres such as proteins.

In the tapping mode, height and deflection images exhibit the similar topography information, though the deflection image is replaced by an amplitude image mode. Another type of imaging known as the phase contrast provides compositional mapping when multi-component material is imaged using tapping mode. It is the extension of tapping mode based on the measurement of the cantilever phase lag that well reflects differences in viscoelasticity, friction or adhesion between two materials. This high capacity to differentiate material properties allows for immediate compositional mapping of polymer systems and thus a better understanding of semi-crystalline polymer structure [62].

3.5 Biological Sample Imaging

The microscope is undoubtedly one of the greatest inventions that men have ever made. The use of lenses for spectacles (eyeglasses), distant vision (telescopes), and high magnification (microscopes) required early lens makers accurately to grind lenses with different focal lengths. However, the use of microscope in clinical studies had a slow beginning; only after more than two centuries passed since the first microscope was invented, before the value of microscopes began to be appreciated by clinical and laboratory scientists. Soon thereafter the microscope became an indispensable laboratory tool at medical schools all around the world [63]. Optical microscopes have improved medicine and biological studies in so many different ways. The discoveries of bacterial species, viruses and other microorganisms have proved the exceptional contribution of microscopes in medical diagnosis and many other biomedical fields.

Under these circumstances, alternative techniques to optical microscope such as scanning electron microscopy or AFM has further increased our knowledge about structures of different parts of the body through pathology specimens, biopsies, or even *in situ*, which can be seen under the microscopes, so that any morphological abnormalities can be detected. This contributed tremendously especially in clinical examinations

and together with its high resolution capability; AFM can be an extremely powerful tool in early detection and diagnosis of diseases such as cancers.

AFM has proved to be a very valuable technique and is widely used in the life sciences in providing 3-D topographical images of surface ultra-structure as well as functional-interactive investigations with nanoscale accuracy. From imaging living cells [64, 65], Deoxyribonucleic acid (DNA) [66], membranes [67, 68] or proteins, to measuring adhesion between two cells [69], and detecting micromechanical properties of the cells, AFM allows high resolution images to be captured, without the need to dry or freeze the biological samples. However, the imaging technique is very specific, and requires extreme care during the entire scanning time.

Most of the biological samples suitable for imaging with AFM are subject to artifacts if they are dried. This problem is not unique to the AFM imaging. It has long been a concern in electron microscopy and methods have been developed to minimize its effect with that imaging technique (namely fixation, critical point drying, and environmental EM). The solution to this problem when using AFM is much simpler. Rather than drying the sample, an image can quite successfully be obtained with AFM in fluid [70].

Biological samples can best be imaged in fluid, either in two of the imaging modes: contact mode or tapping mode. Biological materials are often both delicate and tenuously immobilized on a surface, even more so in fluid than in air. As a result, the vertical and shear forces exerted on the sample via the tip in contact mode can damage the sample by compressing, tearing, or removing it from the surface. Imaging with tapping mode however, particularly in fluid, presents the advantage of greatly reducing shear forces [71], allowing delicate samples to be imaged more easily [72]. The use of cantilevers with very low force constants and blunter tips made from silicon-nitride is recommended for imaging soft tissues such as living cells as sharp tips may have destructive effects on the cell membranes and can tear them apart.

However, there is another problem in biological material imaging using AFM which hinders the prospect of acquiring high resolution and accurate determinations of cellular ultra-structures. Immobilization of biological samples on a substrate is a major issue that needs to be tackled beforehand. Scanning especially in contact mode has the potential to drag or push the samples away from their exact locations; which would lead to a decrease in image resolution. To overcome this problem, several approaches have been proposed and the common practice is to coat the substrate's

surface with biological adhesion coatings such as poly-l-lysine, collagen, or Cell Tak (BD Biosciences, USA) to promote cell adhesion. Poly-l-lysine is a highly positively charged amino acid chain and with 0.5 – 5 mg/ml concentration generally allows good binding [64, 68, 73].

Collagen is a group of naturally occurring proteins and it is the main component of connective tissue in mammals. Most collagen is derived from young beef cattle from certified BSE (bovine spongiform encephalopathy) free animals and is used for promotion and maintenance of a differentiated phenotype in a variety of cell cultures [74]. While Cell Tak is a cell and tissue adhesive made from polyphenolic proteins secreted by *Mytilus edulis* which can be used to attach cells or tissue sections to many types of surfaces, including plastic, glass, metal, FEP polymer and biological materials [41].

Even if the biological samples are able to be anchored to the substrate's surface, there is still a challenge to image them in fluid. The presence of glycocalyx and hydrocarbons on the surface of the cells and the substrate used for coatings will modify the sample absorption and the AFM imaging resolution. Glycocalyx refers to extracellular polymeric material (glycoprotein) such as polysaccharide matrix that is excreted by the epithelial cells to form a coating on the surface of the epithelial tissue. This poorly defined coat covering the membrane is responsible for cell adhesion. While

hydrocarbons are organic contamination that can form on the surface of the substrate when it is exposed to air and they can absorb onto the tip during scanning. This build-up of molecules and cell debris on the tip will create aggregates that can deteriorate the quality of image captured over time. These organic contaminations can be simply eliminated by treating the cells with enzymes and exposed them to a short UV light radiation prior imaging to enhance resolution [75]. Hydrocarbons can also be reduced by using water that has been filtered with the Millipore system for the preparation of the biological samples.

AFM temporal resolution is another technical difficulty when dealing with monitoring cellular dynamic processes in real time. An average scanning time of a minimum of 60 seconds per image and increased up to 20 minutes (for a scan rate of 0.3 Hz) is required, whereas a lot of cellular dynamic events happen typically within milliseconds. Given that full scan captures last minutes, at this rate there will be inconsistent and varying results across the image [9]. A temporary solution for getting higher temporal resolution is to increase scan rate but would involve sample damage and very poor resolution.

Problems involving biological samples imaging do not only occur during image scanning, but the cells also are subjected to other destructive

effects. They are usually imaged in balanced salt buffer at room temperature, which is totally different to their normal physiological environment such as in the human body. This condition may drastically affect the cells and can lead to apoptosis, but it has been reported that cells are found to remain viable for up to 48 hours under the AFM imaging [76].

Based on the facts presented, AFM is known to have some weaknesses in biological sample imaging, but it still remains a very powerful tool to observe nanoscale structure never can be seen by other means of equipments. However, this is subjected to constant evolutions and improvements. These problems have led us to adopt Bioimprint technique to capture cell membrane topography. Snapshots can be imaged to capture events at different time scale. The details of the Bioimprint technique and the materials used will be explained in full in chapter 5.

3.6 Advantages/Disadvantages of AFM

AFM has several advantages compared to other high-resolution imaging techniques such as the scanning electron microscope (SEM). The electron microscope can only provide a two-dimensional projection or a two-dimensional image of a sample, whereas AFM is able to provide a true three-

dimensional surface profile. In addition, samples viewed by AFM do not need any particular handling, such as metal or carbon coatings that would permanently alter or damage the sample. Even more, the electron microscope needs an expensive vacuum environment for proper operation, and takes more time to setup the equipment before it is ready for imaging.

On the contrary, AFM in most of its modes can work perfectly well in ambient air or in liquid environment. This makes AFM better suited for biological macromolecules study and even examining living organisms. In theory, AFM can provide higher image resolution than SEM and it has been shown to give true atomic resolution in ultra-high vacuum (UHV) [77] and more recently, in liquid environments [78]. High resolution AFM images are comparable in resolution to other methods such as scanning tunnelling microscopy (STM) and transmission electron microscopy (TEM). Another advantage of this tool is the ability to integrate AFM with other microscopy techniques such as optical microscopy, confocal microscopy, Raman spectroscopy imaging, scanning electrochemical microscopy (SECM), and other complementary microscopical techniques.

Another aspect of AFM that contributes to its advantage over other tools lies with the further development of the AFM tips and cantilevers. A large variety of AFM tips are available in the market to cater every special

need of AFM studies. One example of this type of tip is the functionalized AFM probes. The AFM (silicon or silicon nitride) tip is functionalised by applying chemical or biological coatings to the probes or off-the-shelf tipped AFM cantilevers. Applications include mapping the functional group microstructure in polymers and binding or recognition interactions in biological systems. At the same time, a large number of research groups around the world are attempting to develop cantilever arrays as biosensors for medical diagnostic applications.

Even though AFM seems to be superior to other techniques in terms of atomic resolution images, it does have certain disadvantages when compared to tools like SEM. This is especially true in the area of single scan image size. In one pass, SEM can image an area with the size of a few square millimeters and a field depth of a few millimeters. However, AFM can only image a maximum height of < 10 μm and a maximum scanning area of about 150 x 150 μm. AFM is also much slower in terms of scan speed when compared to SEM. The relatively slow rate of scanning during AFM imaging often leads to thermal drift in the image [79, 80], making AFM less suited for measuring accurate distances between topographical features on the sample.

Another limitation of AFM is the inability to measure steep walls or overhangs, which is caused by the nature of the AFM tips. For SEM, a

common method to image the dimension of these high aspect ratio structures is by imaging the cross-sectional end of the cleaved sample. Whereas in AFM, special shape tips are used to scan sideways as well as up and down (either both contact and non-contact modes) to measure the sidewalls. However, a higher cost is involved in producing the special cantilevers and a bit of trade-off is observed when attaining lower lateral resolution and the introduction of additional artifacts.

3.7 Experimental Setup

The atomic force microscopy used in this research is a Digital Instruments (DI) 3100 Nanoscope III from Veeco Instruments Inc. (Santa Barbara, CA). It is a highly versatile scanning probe microscopy system with a 90 x 90 μm piezo scanner that allows standard AFM imaging as well as tapping mode operation. With the TUNA module included, STM-like tunnelling mode imaging and scanning conductive microscopy becomes possible. Figure 3.3 exhibits the DI 3100 AFM system illustrating the microscope mounted on a vibration and noise protection table which is connected to a pressurized air supply. The microscope is placed inside an insulating box for three stages of vibration isolation and sound proofing.

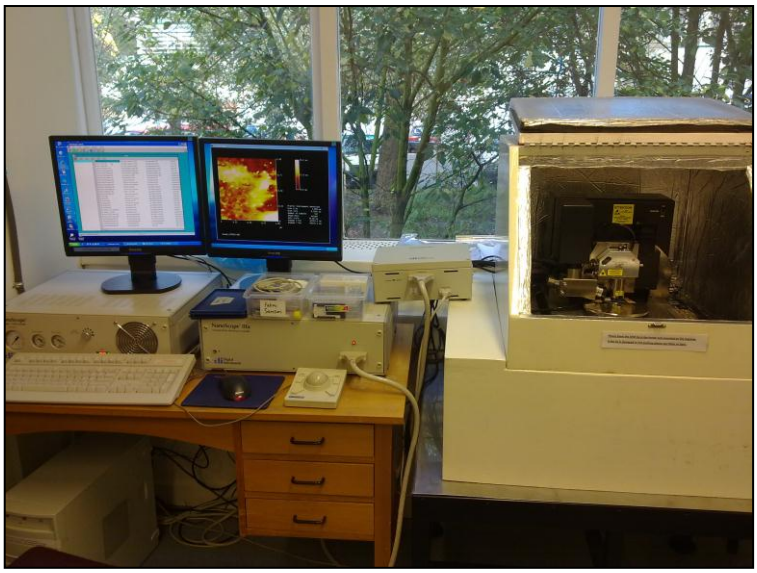

(a)

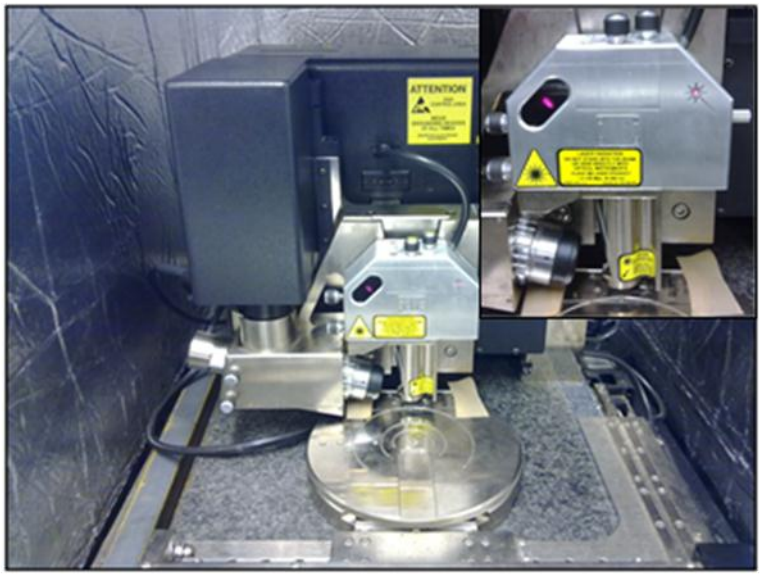

(b)

Figure 3.3: (a) Overall DI 3100 system overview and the (b) AFM platform.

Insert: The piezoelectric scanner head.

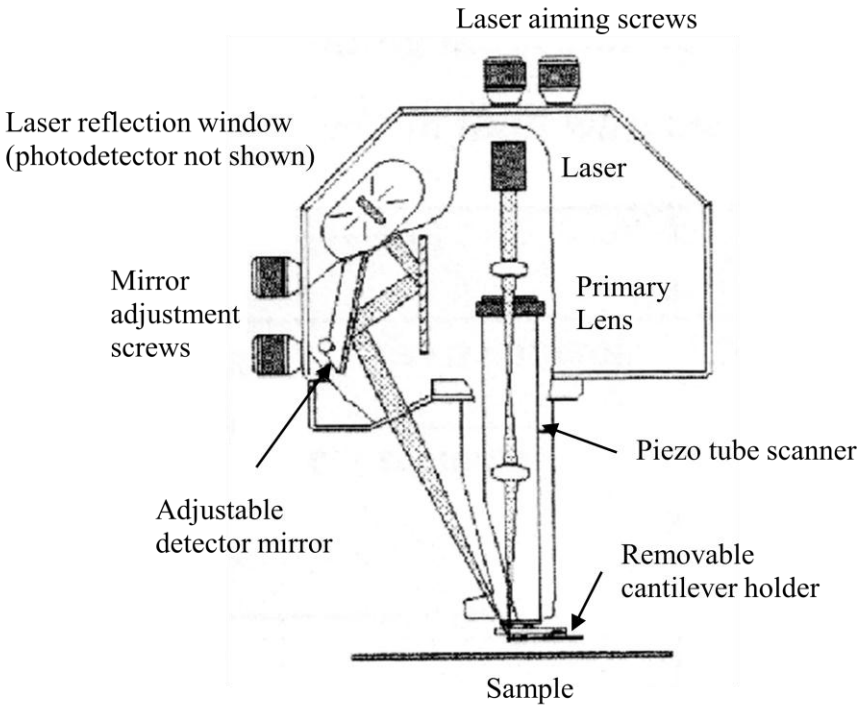

Figure 3.4: Schematic overview of the piezoelectric scanner head.

The samples are placed on a motorized translation stage with a range of 100 x 120 mm, and the sample chucks will accept various sizes of silicon wafers. Stage control is integrated into the Nanoscope III v. 5.31r1 application software. The microscope head is connected to a Nanoscope III controller. A breakout box installed in the wiring between the controller and the microscope allows a direct access to all analog signals of the setup, e.g. piezo scan signals and tip feedback. The controller box, together with the

original DI control PC, two TFT displays, trackball, keyboard and a fibre light source / vacuum pump is mounted in a DI electronics console. The piezoelectric AFM scanner head is designed to scan overhead while keeping the sample stationary. The cross-section diagram of the scanner head can be referred to Figure 3.4. With X/Y and Z-axial limits of ~ 110 µm and 6.23 µm, respectively, AFM is suitable to scan cell samples in size range of 12 µm to height < 6 µm. A video microscope installed in close proximity to the AFM head provides the opportunity for live observations of the tip and sample.

All imagery presented in this research has been achieved by either imaging living cells in semi-fluid condition or imaging the replicated cells on the Bioimprint polymer using tapping mode in air environment at room temperature. The type of cantilevers and tips chosen for this work is shown and described in Table 3.1. A few examples of the SEM images of the AFM probes used are illustrated in Figure 3.5.

The preferred AFM probe which was used extensively for this work is the HI'RES/DP14 (Mikromasch, Estonia) as it provides enhanced resolution imaging. It features a typical tip radius as small as 5 nm and a higher aspect ratio near the apex of the tip. Sometimes this probe is nicknamed as the "sting tip" due to its sharpness. However, because of its

very high cost, this probe was only used when high resolution images were needed; while for general AFM scanning, less expensive probes such as Tap300-G (BudgetSensors, Bulgaria) were used.

Part No.	***Type***	***Tip Radius (nm)***	***Force Constant (N/m)***	***Resonant Frequency (kHz)***
DP14/ HI'RES-C[a]	Rectangular	< 5 nm	5.0, 1.8-12.5	160, 110-220
NSC11[a]	Triangular	< 10 nm	3.0, 1.5-5.0	60, 45-75
Tap300-G[b]	Rectangular	< 10 nm	40, 20-75	300, 200-400
ACT-10[c]	Rectangular	< 6 nm	40, 25-75	300, 200-400

Table 3.1: Cantilever and tip properties used for AFM imaging.

[a] (Mikromasch, Estonia)
[b] (BudgetSensors, Innovative Solutions Bulgaria Ltd. – with alignment grooves cantilevers)
[c] (Nanoscience Instruments, Inc. – short cantilever with aluminium coating on the back side)

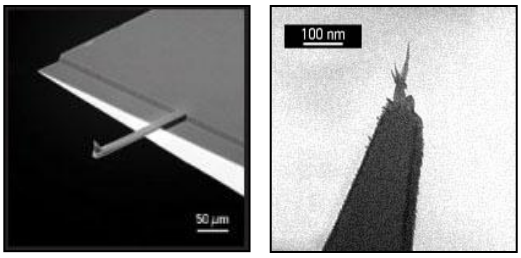

DP14 / HI'RES-C (Mikromasch):

Hydrophobic diamond-like extratip at the apex of silicon etched probe.

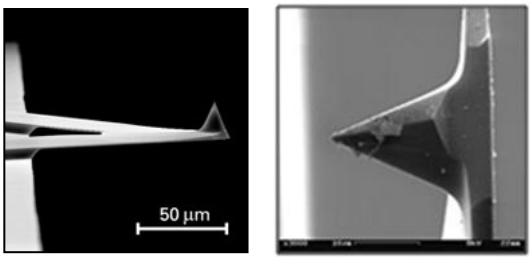

NSC11 (Mikromasch):

Two triangular cantilevers located on the opposite side. Each has a significantly different force constant and resonant frequency.

Figure 3.5: SEM images of some of the probes used in this research.

Nevertheless, once the AFM images started to show diminished results in resolution, the probes need to be changed with a new one. Blunt or broken tips falsify measurement results such as surface roughness or structures dimension considerably.

AFM images obtained were presented in an amber colour-contrast scheme and processed using the instrument's Nanoscope III v. 5.31r1 application software. Alterations or modifications to the original captured data were done in order to get better results with minimal distortions and imperfections using techniques such as flattening to remove background slope and erasing scan lines.

3.8 Conclusion

AFM has proved to make a great impact on the technical community by providing a new and unique tool to advance fundamental science and technology. This enabled the detection of nanoscale features on a wide range of surfaces that include biological samples and biopolymers. In this work, high resolution images of surface features of biological samples such as muscle cells and endometrial cancer cells were able to be captured on the replicas made from the newly developed Biopolymer (this will be explained in details in chapter 5). The use of sharp probes such as HI'RES/DP14 tips has helped to achieve molecular-scale resolution, which if they were not damaged in the engagement procedure and preserved from breaking in the low-force imaging. Excessive tip-sample forces could be avoided by using softer cantilevers though there were limitations caused by a need of the probe retraction from a surface in every oscillation cycle and light tapping conditions were used when scanning with sharp probes.

Despite the fact that so-called true atomic resolution was achieved in the frequency modulation and amplitude modulation imaging modes the value of these results is still questionable. The computer simulation of amplitude modulation imaging of polydiacetylene crystal showed that real atomic-scale resolution could be achieved only when the AFM probe has an

apex of the atomic size and imaging is performed in the low-force regime [81]. Otherwise, even the observation of the isolated atomic- or molecular-size defect does not mean that the molecular arrangement surrounding such defect is reproduced correctly. Consequently, there is still a lot of room for further improvement of high-resolution imaging that requires the use of sharp probes and better quality instrumentation allowing low-force imaging using such probes [82].

Further advancement in AFM and its probes hopes to bring a better future in high resolution imaging, especially in biological cells imaging. It is the wish of the author to see that biological sample imaging can be done *in vivo* in the near future, so that the true behaviours and characteristics of the cells can be investigated and examined systematically. Faster AFM scanning rates with instantaneous results would help to understand life-sciences processes such as biological mechanisms in high resolution images at atomic-scale resolution. The use of functionalized tips that not only can release various chemicals for chemical/biological sensing and detection, but also able to extract viruses or hazardous substrates from cells that can cause diseases or cancers will improve significantly in the area of medical diagnosis and clinical laboratory fields.

Chapter 4

Biochip

A Biochip is a platform of miniaturized microarrays arranged on a solid substrate that permits many tests to be performed at the same time in order to achieve higher throughput and speed. Typically, a Biochip's surface area is no larger than a fingernail. Biochip can perform thousands of biological reactions, such as sorting, trapping, and screening large numbers of biological samples for a variety of purposes, from disease diagnosis to detection of bioterrorism agents in just a few seconds. Another approach that has emerged from the Biochip technology is the Lab-on-a-chip (LOC) device. LOC is defined as a device that integrates one or several laboratory functions on a single chip and incorporating micro-fluidic channels for the handling of extremely small fluid volumes down to less than pico litres [83].

Biochip development is one of the major driving forces in the rapidly emergent biotechnology industry, which encompasses a very diverse range of research efforts such as in pharmaceuticals, genetics decoding, toxicological and biochemical research, among other activities. Further investigation would unravel the complex biological processes occurring

inside living cells, with the ultimate objective of understanding and be able to treat and cure human diseases.

As mentioned before in chapter 1, single-cell identification, imaging and analysis *in situ* using AFM faced a lot of difficulties as immobilizing the cells for direct cellular analysis is still a major challenge. One approach to overcome this problem was the use of organised arrangements like microarrays to trap the cells and placed them in a controlled manner. Studies indicate [84-86] microarrays architecture confers several operational advantages in cell sorting and microcell culture applications. This can be achieved by fabricating these microarrays on a special platform such as Biochip. To manipulate the cells' movements, an electrokinetic phenomenon known as dielectrophoresis (DEP) was used for that purpose. Non-uniform AC electric fields generated by the interdigitated microelectrode arrays provide an ideal method for manipulating and controlling particles [87]. Earlier work by previous researcher [88] has shown some interesting and promising results, where an electrode array chip known as the '*Biochip*' has been developed to trap single-cells within cavities for high resolution analysis. The cells were captured using positive and negative DEP forces in cavities placed at different locations within the electrode arrays. As some cells have no tendency to spread over substrates during culturing, the contact area between the cell and substrate is very small, often leading to cell

detachment by the scanning tip. Thus by employing the cavity trapping method, not only the cells were perfectly anchored to the surface but also their heights were lowered to within a set-scan level of the AFM, enabling faster time-to-analysis.

Unfortunately the trapping efficiency of this approach was poor and worked well only for polystyrene beads and dead cells. To solve this problem, a new design of Biochip microarrays was necessary. The requirement was that the Biochip must be able to perform as a platform to control and manipulate certain type of cells, and also as a substitute for cell culturing plate, with the intention to prolong culture times in order to reduce cell heights. However, since direct cellular imaging using AFM has resulted in low image quality and inadequate resolution, the idea of integrating the Biochip platform with the Bioimprint technique has become a major challenge. This chapter will elaborate on the work that has been done in the development of a new layout for the Biochip electrodes and some of the difficulties faced in applying DEP for cell manipulation. Suggestion for further improvement in the integration of Biochip and Bioimprint can be found in chapter 7.

4.1 Overview

Dielectrophoresis (DEP) is a phenomenon in which a force is exerted on a dielectric particle when it is subjected to a non-uniform electric field [89]. All particles exhibit dielectrophoresis activity in the presence of electric fields and this force does not require the particle to be charged. However the strength of the force depends strongly on the medium and particles' electrical properties, on the particles' shape and size, as well as on the frequency of the electric field. Consequently, fields of a particular frequency can manipulate particles with great selectivity. This has allowed, for example, the separation of cells or the orientation and manipulation of nano-particles [90].

The dielectrophoresis effects can be seen only when particles are in non-uniform electric field. Since the dielectrophoresis force does not depend on the polarity of the electric field, the phenomenon can be observed either with AC or DC excitation. Particles are attracted to regions of stronger electric field when their permittivity exceeds that of the suspension medium. When the permittivity of the medium is greater than that of the particles, the motion of the particles is to lesser electric field. DEP is most readily observed for particles with diameters ranging from approximately 1 to 1000 μm. For particles above 1000 μm, gravity overwhelms DEP; while for particles below 1 μm, Brownian motion overwhelms the DEP forces [89].

Phenomena associated with dielectrophoresis are electro-rotation and travelling wave dielectrophoresis (TWDEP). Dielectrophoresis can be enhanced using multiple frequencies, in what is known as multiple-frequency dielectrophoresis (MFDEP). For a field-aligned prolate ellipsoid of radius *r* and length *l* (*r* > *l*) with complex dielectric constant ε_p^* in a medium with complex dielectric constant ε_m^*, the time-dependent dielectrophoresis force is given by [91]:

$$F_{DEP} = \frac{\pi r^2 l}{3} \varepsilon_m \mathrm{Re}\left\{\frac{\varepsilon_p^* - \varepsilon_m^*}{\varepsilon_m^*}\right\} \nabla\left|\vec{E}\right|^2 \qquad (1)$$

The complex dielectric constant is:

$$\varepsilon^* = \varepsilon + \frac{\sigma}{j\omega}$$

Where ε is the dielectric constant, σ is the electrical conductivity, ω is the field frequency, and j is the imaginary number [90-92].

This equation is accurate for highly elongated ellipsoids when the electric field gradients are not very large (e.g., close to electrode edges). The equation only takes into account the dipole formed and not higher order polarization [91]. When the electric field gradients are large, higher order terms become relevant [91], and result in higher forces. To be precise, the

time-dependent equation only applies to lossless particles, because loss creates a lag between the field and the induced dipole. When averaged, the effect cancels out and the equation holds true for lossy particles as well. An equivalent time-averaged equation can be easily obtained by replacing *E* with E_{rms}, or, for sinusoidal voltages by dividing equation (2) by 2.

For a homogeneous sphere of radius *r* and complex permittivity ε_p^* in a medium with complex permittivity ε_m^* the (time-averaged) DEP force is [91]:

$$\langle F_{DEP} \rangle = 2\pi r^3 \varepsilon_m \mathrm{Re}\left\{\frac{\varepsilon_p^* - \varepsilon_m^*}{\varepsilon_p^* + 2\varepsilon_m^*}\right\} \nabla \left|\vec{E}_{rms}\right|^2 \qquad (2)$$

$$U(\omega) = \frac{\varepsilon_p^* - \varepsilon_m^*}{\varepsilon_p^* + 2\varepsilon_m^*} \qquad (3)$$

The factor in curly brackets is known as the complex Clausius-Mossotti (CM) factor [90-92] and contains all the frequency dependence of the DEP force. From the frequency dependent response of the CM factor it is apparent that DEP manipulation is best suited to being controlled by AC fields. As predicted by the polarity of $Re\{U(\omega)\}$, cells or particles may experience either positive (F_{DEP}), or negative ($-F_{DEP}$) DEP by attracting, or repelling from regions of higher or lower electric field gradients, respectively. If $Re\{U(\omega)\}$ is less than 0 then the cells are repelled from the electrodes using

negative DEP, on the other hand, if $Re\{U(\omega)\}$ is greater than 0 then the cells will be attracted to the electrode edges by positive DEP. Other factors also play a major role, for instance, when a cell is more conductive than its suspending medium then positive DEP occurs, but if the medium is more conductive then negative DEP occurs [88].

Dielectrophoresis can be used to manipulate, transport, separate and sort different types of particles. Since biological cells have dielectric properties [93], dielectrophoresis has many medical applications. Prototypes that separate cancer cells from healthy cells have been made [94]. The utilization of the difference between dielectrophoretic forces exerted on different particles in non-uniform electric fields is known as DEP separation. The exploitation of DEP forces has been classified into two groups: DEP migration and DEP retention. DEP migration uses DEP forces that exert opposite signs of force on different particle types to attract some of the particles and repel others [95]. DEP retention uses the balance between DEP and fluid-flow forces. Particles experiencing repulsive and weak attractive DEP forces are eluted by fluid flow, whereas particles experiencing strong attractive DEP forces are trapped at electrode edges against flow drag [96].

In this chapter a combined approach of capturing, trapping, and positioning cells at known locations using positive and negative DEP on the

Biochip platform was developed and tested. Both positive and negative DEP approaches were chosen in order to yield higher success rate in cells capturing and trapping. Later on the development of the electrodes platform will be presented along with the fabrication processes and outcomes.

4.2 Biochip design

The main components and concept of the Biochip system are illustrated in Figure 4.1. The design incorporated an array of micro-cavities aligned between a series of interdigitated electrodes. Cavities etched within the surface of the Biochip at regions of intense field act as incubators, trapping cells at known positions on the substrate's surface. Cavities created on top of the electrodes are targeted for positive DEP, while cavities in between the electrodes are for negative DEP. Each cavity has a unique locator enabling single-cell handling, addressing and identification throughout experimentation.

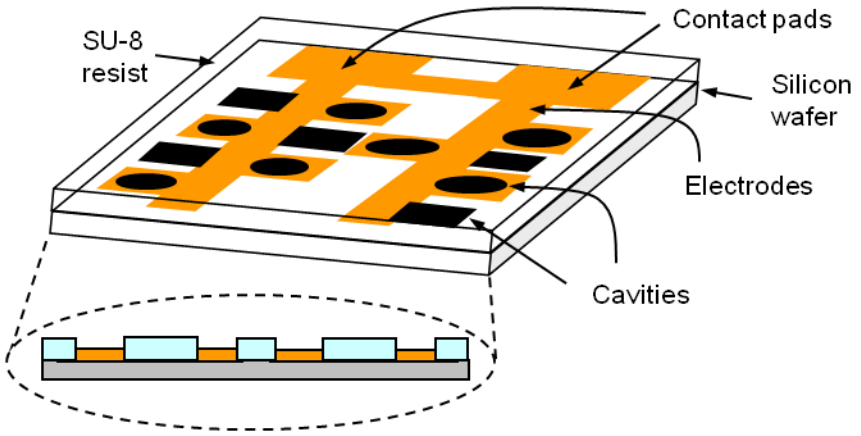

Figure 4.1: 3-D illustration of the Biochip design: Cavities were created on top of the electrodes by forming holes in the SU-8 resist (for positive DEP) and in between the electrodes (for negative DEP).

Cellular structures especially cells tend to have spherical morphological attribute when suspended in culture medium. Trapping them within the Biochip cavities allows the upper part of the cells to be analysed using AFM. The protruding part of the cell was low enough to enable imaging the exposed cellular body without breaching the AFM Z-limitation. This also helps to speed-up the analysis process without the need to wait at least 2 ~ 4 days for cells to settle down and spreading their membranes if standard culturing plates were used. Figure 4.2 ((a), (b)) exhibits microscope image and AFM micrograph of an etched cavity in the interdigitated position within the Biochip.

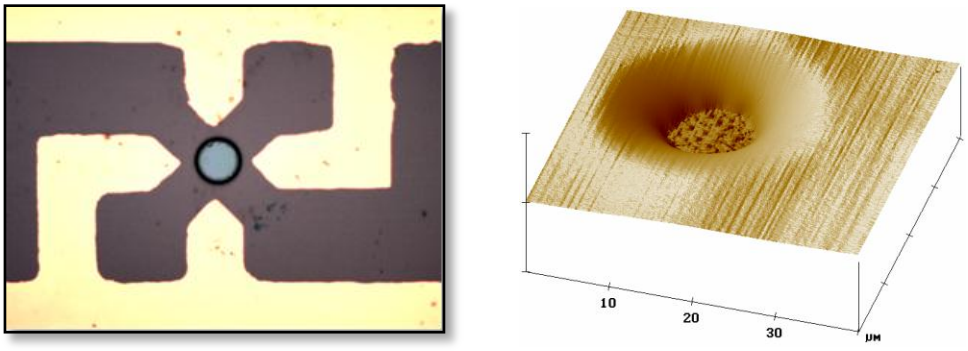

(a) (b)

Figure 4.2: (a) Microscope image showing a cavity etched within the Biochip right at the middle of a 4-pointed gold electrode plates. (b) AFM image of the cavity with rough and heavy texture visible at the bottom of the hole.

Growth and differentiation of anchorage dependent cells are strongly influenced by the material or structure offered as substrate. Cell growth rates can often be improved by surface coating with attachment factors such as fibronectin, collagen, gelatine or polylysine. Surface roughness and homogeneous structure of the surface of the Biochip also played an important role in cell adhesion. Besides being used as trapping mechanism, the cavities also serve the purpose of anchoring cells in position and preventing the AFM tip from dragging the particle during scanning.

In developing the Biochip, new materials were tested in order to find substrates that are biocompatible and suitable for cell culture. Based on

previous work [97], in order to prolong the culture times or for applying solvents to the cells for dehydration and drying, the cavities must be fabricated in a biocompatible and solvent-resistive material. One possible material is SU-8 (MicroChem Inc., MA, USA) which is available as a negative resist in photolithography fabrication process. It is a near-UV photoresist, epoxy-type based on EPON SU-8 epoxy resin (Shell Chemical) with relatively high thermal stability (T_g > 200 °C for the cross-linked exposed resist) and suitable for low-cost mould or microstructures fabrications.

4.3 Electrode-cavity design and fabrication

The design of the Biochip platform involved several key processes, starting with finding the ideas of how the Biochip should look like, how the geometry and shape of the electrodes and cavities should be, in order to sort and trap the cells. To achieve these aims, the configuration of the Biochip were designed to have at least 5 different sets of integrative microelectrode systems, such as the 2-pointed electrodes, 4-pointed electrodes, and interdigitated microarrays of electrodes and cavities placed side by side along a planar and rectangular electrode beam. For each of the electrode configurations, different settings were chosen in which some of them would

have diamond-like pointed tips, while others may just have square-flat tips. These tip designs were used to form a non-uniform electric field pattern on the Biochip to generate dielectrophoresis force on the cells/particles within the sample fluid/media.

The next step was to transform the design concept into reality. All ideas were transferred from drawing board to computer using L-Edit software (Tanner Research, USA), a draw type layout editor that is used primarily to design VLSI electronic circuits, printed circuit board layout and other computer aided design (CAD) work. Once the design was finished, it was transferred to a machine called Heidelberg µPG 101, a micro laser pattern generator for direct writing of photomask. The design files can be transferred in multiple data input formats (DXF, CIF, BMP). The photomask developed at this stage would be used later in the fabrication process.

Then to transfer the Biochip design from the masks to a silicon wafer, the mask aligner Karl Süss MA6 (Karl Süss GmbH, Germany) was used. It is a top and bottom side contact printer used to contact, align, and transfer features from a patterned mask to a photosensitive material by UV radiation exposure. A 350 W Mercury UV lamp with an intensity of 2.7 mW/cm^2 was used to expose the design from the photomask onto the photoresist material.

Two techniques in the design and fabrication of the Biochip were investigated. The same layout of cavities and electrodes positions was used for both schemes. The first scheme involved the fabrication of the electrodes and cavities using a three-stage process with photolithography, wet/dry etching, metallic deposition techniques and nanoimprint lithography. The full process flow of the pattern transfer scheme is shown in Figure 4.3. Firstly, a thin 20 nm adhesive film of nickel-chrome (NiCr) along with a 200nm layer of gold (Au) were thermally evaporated onto a 4 inch (100 mm) silicon wafer, insulated with 200 nm silicon nitride (SiN) layer. The electrodes are formed after Au and then NiCr wet-etching through a photolithography fabricated 1.5 μm positive resist mask – AZ1518 (Clariant Corp., NJ, USA), which was developed for 15 s in AZ300MIF (Clariant Corp., NJ, USA) and UV exposed for 12 s using the mask aligner. Later the wafer was hard-baked at 185 °C for 2 hours and O_2 plasma-cleaned for 10 minutes.

In the second stage, a microscope glass slide (75 mm x 25 mm) or a 5 inch transparent glass mask (127 mm x 127 mm) was spin-coated with 5 μm thick SU-8 layer and soft-baked at 65 °C and 95 °C for 1 and 4 minutes respectively. The SU-8 mould was created on the glass slide/mask after being developed using SU-8 developer (1-Methoxy-2-Propyl) Acetat after a photolithography exposure based on cavity mask pattern transfer.

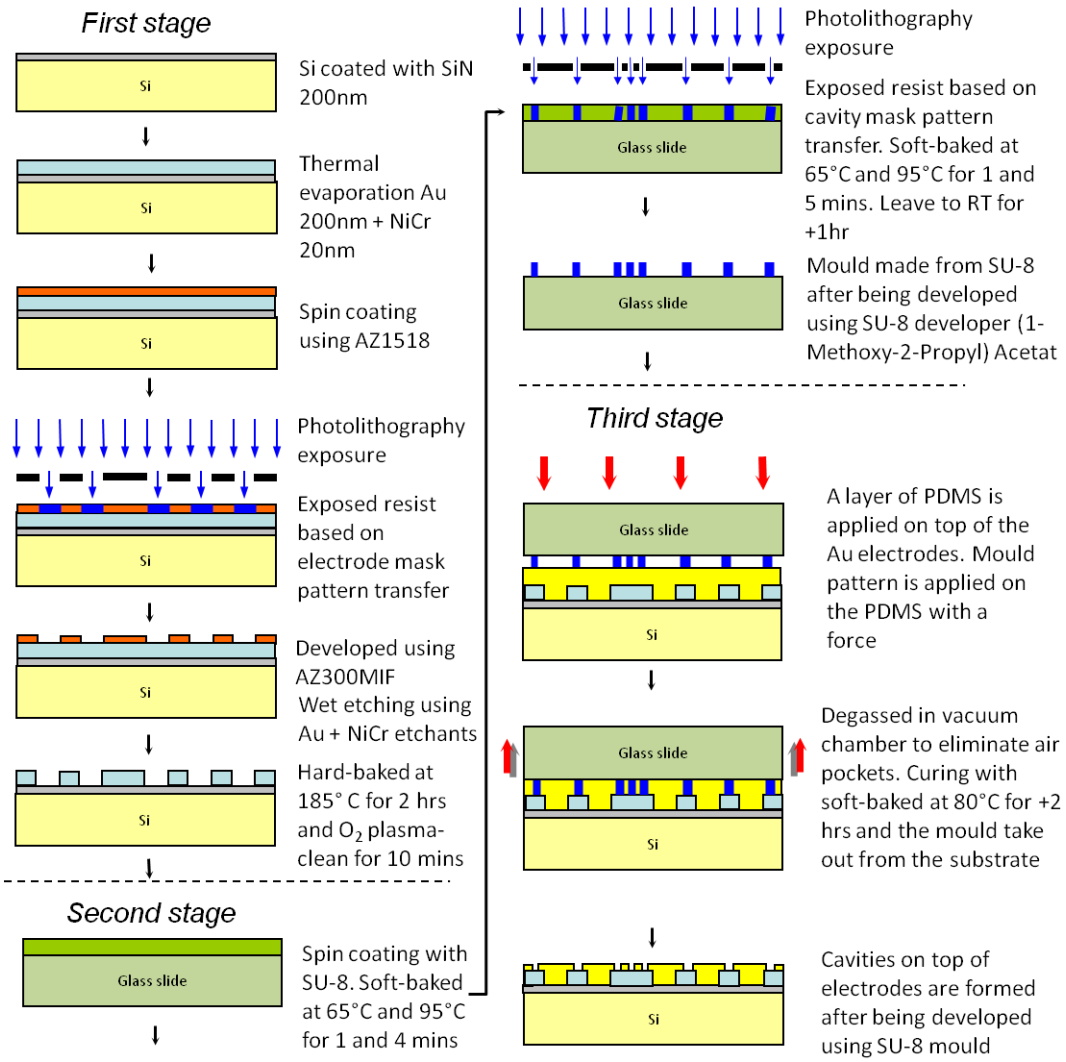

Figure 4.3: Three-stage Biochip fabrication processes: First stage – Formation of the electrode microarrays by metallic thermal evaporation, photolithography and wet etching process. Second stage – Formation of the mould with predefined topological patterns made from SU-8 using photolithography exposure. Third stage – Cavities were fabricated on top of the electrodes using nanoimprint lithography process by pressing an SU-8 mould on the substrate's PDMS layer.

Then the mould was soft-baked at 65 °C and 95 °C for 1 and 4 minutes respectively, and left to cool down to room temperature for 1 hour. Protruding pillar structures are formed on the SU-8 mould from the original cavity pattern mask.

In the third stage, a thin layer of PDMS was applied onto the sample substrate, and then the mould was brought into contact with the sample and they were pressed together under certain pressure, up to 0.3 bar (3 N/cm^2). The substrate together with the mould was then degassed in a vacuum chamber to eliminate air pockets. They were cured with soft-baked at 80 °C for +2 hours and after being cooled down, the mould was separated from the sample and the pattern was left on the Au electrodes.

To ensure alignment and uniform flatness between the mould and the substrate, a very precise and constant pressure need to be applied. The first attempt was to use a custom made metal enclosure that can hold both the glass slide mould and the Si wafer together, then a metal stamping block (with different weight; e.g. 250 g, 500 g, etc) was placed on top of the enclosure. This would pin-down the mould onto the PDMS layer on top of the Au electrodes. The metal stamping block was first removed before the substrate and the mould were cured. With this approach, pattern transfer i.e. the creation of cavities on the Au electrodes was possible but it had one

major problem, which was misalignment. It was very hard to get the cavities aligned correctly at certain positions like at the centre of the interdigitated electrodes (as shown in Fig. 4.2 (a)).

In order to solve this issue, a second approach was devised using the mask aligner. In this attempt, the same process used for photolithography exposure was followed. But instead of aligning a photomask to the sample substrate, the mould was brought into contact with the sample using hard contact program. Cavities were able to be aligned precisely and accurately at their positions and contact WEC (Wedge Error Compensation) was done automatically by the mask aligner to obtain a uniform flatness between the mould and the substrate. Unfortunately, the result was not as expected. Once the mould was removed from the sample substrate, the cavity pattern on the PDMS layer started to disappear and shrink before it was able to be cured thermally. On the other hand, to perform the curing with the mould and substrate still in contact would be inappropriate as PDMS takes more than 8 hours to cure at room temperature, and the mask aligner is not equipped with thermal cure capability.

PDMS was chosen during the initial design because it is a soft polymeric stamp, which provides a low surface energy and good conformal qualities. This attributes its ability to conform to the total thickness variation

(TTV) of the imprinted substrate, while maintaining the fidelity of the desired features defined by the mould. But, PDMS requires a long, thermal cure under pressure which is very time consuming and can take several hours [98]. The material also has other issues like swelling when in contact with organic solvents and it also experiences shrinking during the curing process which requires biasing of the features on the mould.

So, to overcome these issues, a new technique was formalized and it was simpler and easier with shorter fabrication period compared to previous approaches. In this second technique, it involved the fabrication of the electrodes and cavities using a two-stage process with photolithography, metallic deposition techniques and wet/dry etching. The full process flow of the pattern transfer scheme is shown in Figure 4.4. Firstly, a thin 20 nm adhesive film of NiCr along with a 200nm layer of Au were thermally evaporated onto a 4 inch (100 mm) silicon wafer, insulated with 200 nm SiN layer. The electrodes are formed after Au and then NiCr wet-etching through a photolithography fabricated 1.5 μm positive resist mask (electrodes pattern) – AZ1518 (Clariant Corp., NJ, USA), which was developed for 15 s in AZ300MIF (Clariant Corp., NJ, USA) and UV exposed for 12 s using the mask aligner.

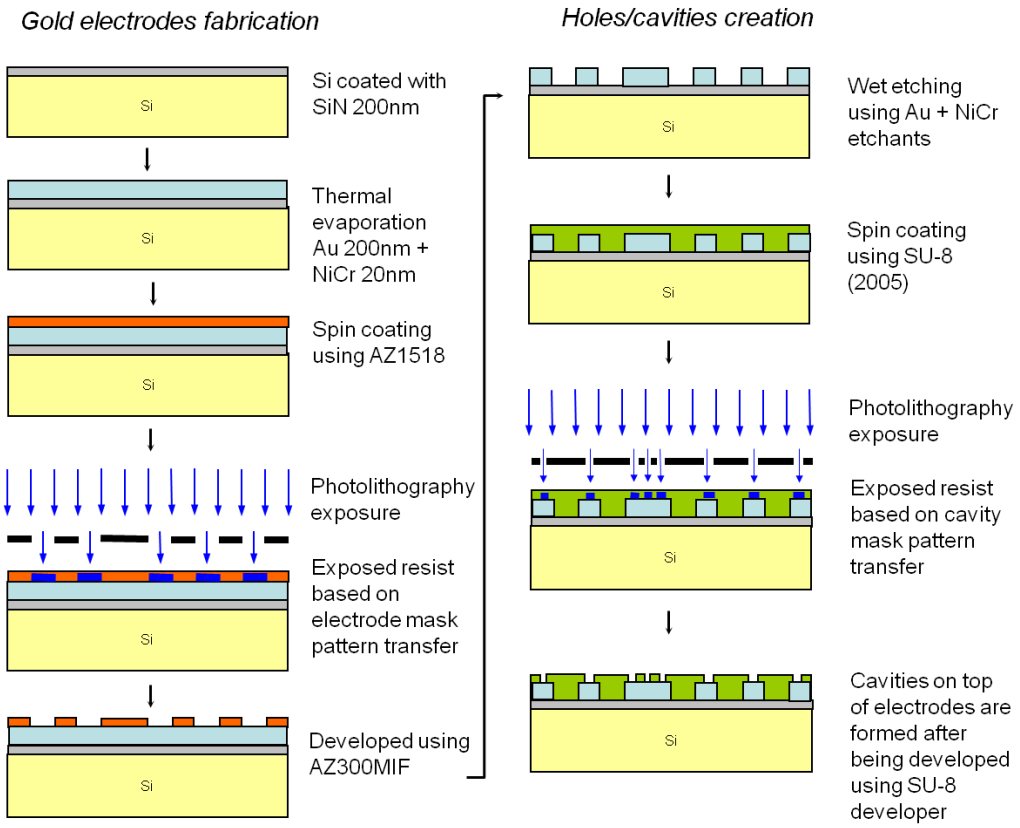

Figure 4.4: Two-stage fabrication process: First stage - Formation of the electrode microarrays by metallic thermal evaporation, photolithography and wet etching process. Second stage - Formation of the cavities on top of the Au electrodes after chemical development using SU-8 developer.

In the second stage, a layer of SU-8 was spin-coated on top of the Au electrodes and the thickness of the SU-8 layer can be controlled by changing the type of SU-8 resists used or the spinning speed. To get a layer with the thickness of ± 5 µm, SU-8 2005 series (MicroChem) was used. It was

followed by soft-baked at 65 °C and 95 °C for 1 and 2 mins respectively. Then the sample substrate was exposed to UV-light exposure based on cavity mask pattern transfer and followed by post exposed-baked at 65 °C and 95 °C for 1 min respectively. It was then followed by hard-baked at 185 °C for 5 mins. The entire baking process is to harden and fully cure the SU-8 polymer. Cavities on top of the electrodes are formed after the sample being developed using SU-8 developer (1-Methoxy-2-Propyl) Acetat. Careful handling and selection of process parameters such as sample pre-treatment and preparation are very crucial in determining the quality of the SU-8 layer and the Biochip electrodes structures.

Table 4.1: Process parameters for cavities fabrication on SU-8 (2005) resist.

Substrate Pre-Treatment	Plasma O_2 asher and hard-baked at 185 ºC for overnight
Coat	SU-8 2005 with speed 500 rpm, 30 sec and 3000 rpm, 30 sec
Soft-baked	1 min at 65 ºC, followed by 2 min at 95 ºC on hot plate, leave to cool to RT at least 1 hr*
Exposure	Vacuum contact (Vac), multiple exposure – 10 sec, 5 cycle with 60 sec waiting period
Post Exposed-baked	1 min at 65 ºC, followed by 1 min at 95 ºC on hot plate, leave to cool to RT more than 1 hr*
Develop	Use Su-8 developer (1-Methoxy-2-Propyl) Acetat without using ultrasonic bath for 5 mins. Rinse with IPA and dry
Extra Steps	Hard-baked at 185 ºC for 5 mins.

*Temperature step down must be done slowly

The complete process parameters for obtaining the finest fabrication of cavities from SU-8 resist are shown in Table 4.1.

4.3.1 Biochip with SU-8 layer

Based on the limitations of the first Biochip configuration an improved design was developed for fabricating cavities on a SU-8 resist layer. Selective sites were etched to form cavities designed to incubate single cells above the interdigitated electrode plane, which has high electrical field intensity regions. Regions surrounding the cavities on the electrode are suppressed by the insulating SU-8 layer, providing isolated locations and insulations for more effective cell trapping by positive DEP [88]. Some of the cavities were also placed on selected positions of low electrical field intensity areas. SU-8 was chosen as the functional material in Biochip design as it is one of the biocompatible materials known and is often used in bio-MEMS fabrications. After exposure and developing, its highly cross-linked structure gives it high stability to chemicals and radiation damage.

During the first trial of fabrication, the SU-8 layer formed on top of the Au electrodes showed some deformation in the form of cracks originating from the cavities and extended towards the upper side of the surface. These

cracks can be seen clearly in Figure 4.5 ((a) and (b)) and in agreement with a number of literatures. It was noticed that the thermal mismatch between SU-8 and the silicon substrate material generates high film stress in the spin-coated SU-8 causing crack formation in the microstructures [99].

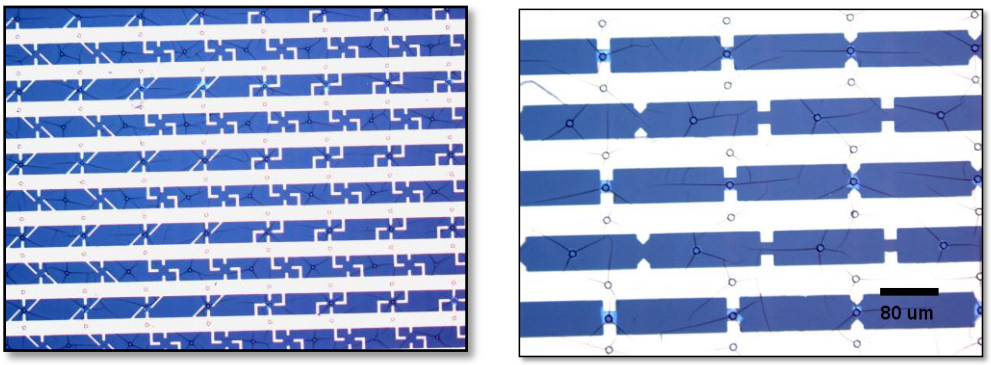

(a) (b)

Figure 4.5: SU-8 layer after exposure, development, and post expose bake (PEB) clearly showing crack formations on the SU-8 surface.

After extensive testing and investigations, additional baking parameters were found to be working in minimizing the crack formations. The extra step was to hard-baked the sample substrate at 185 °C for another 5 minutes after the development process has completed. But the most important thing is to make sure that the temperature ramping down must be done as slow as possible.

Using this additional step, the crack formations can be avoided, as long as the temperature step down is done very slowly and under controlled condition. In Figure 4.6, we can see that the cracks were gone completely from the surface of the SU-8 layer after the hard-baked and temperature step down process has finished. While in Figure 4.7, a cross-section analysis shows that the cavities have average sizes between 10 ~ 15 µm, and deepness of 2.2 ~ 2.6 µm.

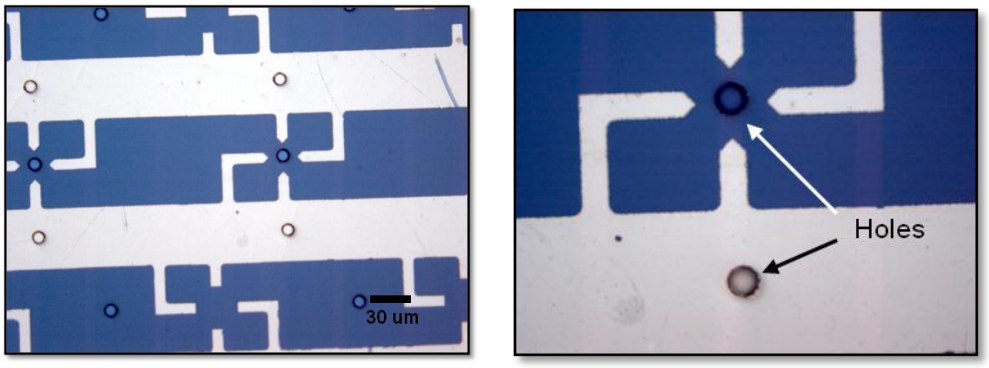

(a) (b)

Figure 4.6: Both microscope images showing the cracks that were visible as in Figure 4.5 has disappeared from the surface, leaving an even and smooth film of SU-8 deposition.

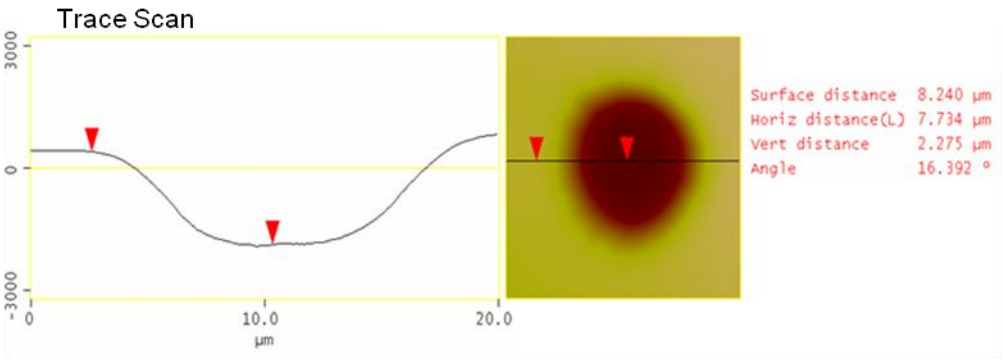

Figure 4.7: Cross-section AFM image of a single cavity with diameter of 10 ~ 15 µm and deepness of 2.2 ~ 2.6 µm.

4.3.2 Biochip electrode configurations

Various electrode geometries were used intermittently in the design of the Biochip. Different patterns would create electric fields of intense and weak strength at different locations. Figure 4.8 demonstrate some of the electrode pattern designs currently used for the Biochip fabrication. At certain positions, the cavities are located at the centre of the 4-pointed electrode plates or in between two parallel electrodes, which is suitable for trapping cells using negative DEP. At the same time, some of the cavities are placed near the sharp end of a NiCr, diamond tip electrodes and on top of the electrodes, which are more suited for positive DEP.

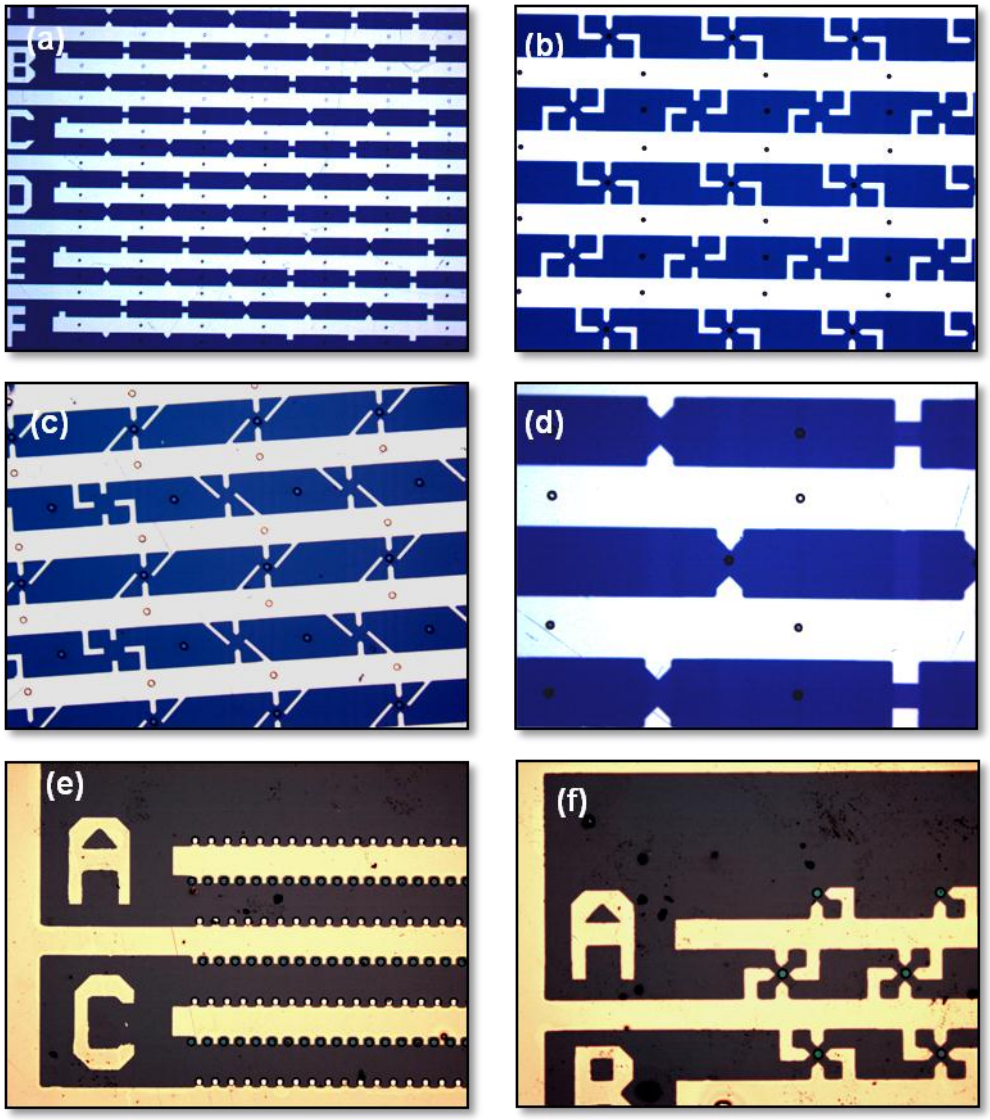

Figure 4.8: Some of the electrode pattern configurations fabricated on the Biochip. 4-pointed electrodes pattern with cavities in the centre to trap cells that respond to positive DEP (pictures b, c and f). Microarrays pattern with planar interdigitated electrodes/cavities were designed to accommodate higher and lower electric field gradients, suitable for F_{DEP} and $-F_{DEP}$ respectively (pictures a, d and e). Each electrode and cavity has a unique locator for individual addressing and identification.

4.4 Polystyrene-beads trapping

The Biochip was first tested using polystyrene microsphere beads with different sizes (e.g. 10 µm, 15 µm and 25 µm). To position the bead within cavities by either positive or negative DEP, they were resuspended in de-ionized water (DIW) with an estimated conductivity of < 10 µS/cm and total dissolved solids of < 10 mg/L. Its dielectric constant is relatively high (~ 80) dominated largely by ionic conductivity and dipoles. The used of a low conductive medium generated more polarisable polystyrene beads due to the inability of ionic charges to move freely through the liquid, thus increasing the net DEP force while avoiding electrolysis. A limited volume of beads in suspension was placed on top of the Biochip while pin-connect clips deliver the desired signal to the contact pads.

The experiment was conducted in our BioLab (PC2) which has all the necessary equipment for carrying out experiments related to biological cells. Trapping activity was observed and recorded using an Olympus BX-60 microscope and Nikon digital camera at room temperature of 22 °C. The power delivered onto the Biochip for DEP forces was taken from a function generator – HP3312A, Hewlett-Packard (CA, USA) in a sinusoidal waveform between 10 Hz to 10 kHz and a voltage range of 1 ~ 25 $V_{p\text{-}p}$. A

HP4523, Hewlett-Packard (CA, USA) oscilloscope was used to monitor all signals delivered by the function generator to the Biochip.

A sinusoidal 50 Hz waveform with amplitudes ranging from 1 ~ 25 V_{p-p} was applied to the electrodes and within 1 hour after that, the result was that the microbeads had arranged themselves along the electrodes, either at the edges or over on top of the Au electrodes. This can be seen clearly in Figure 4.9 (a) where it shows the microbeads are scattered all over the Au electrodes, but not on the silicon layer, while Figure 4.9 (b) shows a close-up view of a section on the Biochip. Positive DEP has forced the beads to move towards the higher electric fields with some of them being evenly distributed in parallel along with the electrodes.

Experiments were conducted not to exceed more than 1 hour at voltage higher than 12.5 V_{p-p} as prolong DEP exposure at higher voltages will introduce Joule heating that can cause hydrodynamic effects which result in formation of an inhomogeneous liquid medium, allowing the creation of space charges in the bulk that interact with the externally generated electric field. The effect of this interaction is fluid motion in and around the cavity structures and levitation of particles above the substrate [100] and can also cause dehydration to the suspending medium. This heating effect also caused the temperature of the media to rise and started to

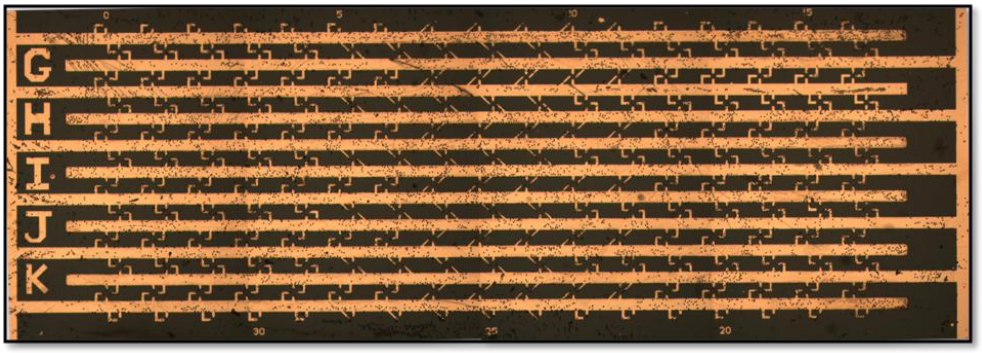

(a)

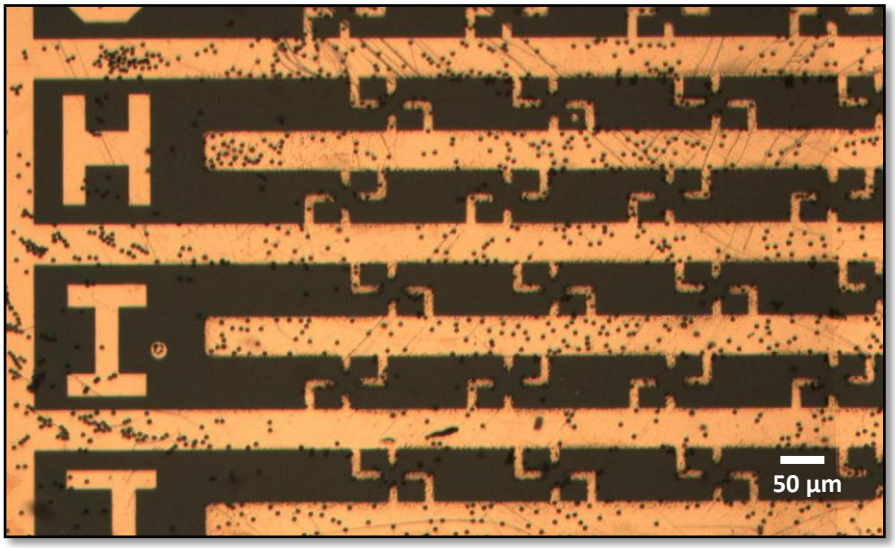

(b)

Figure 4.9: Image (a) showing Biochip electrodes overview under optical microscope with 10 µm polystyrene beads. While image (b) showing a close-up view of a section on the Au electrodes with positive DEP forcing the beads towards higher intensity field near and on the electrodes themselves.

evaporate if being left for so long. This not only affects the liquidity of the media, but also can cause some degree of structural damages to the Biochip platform due to overheating and the presence of crystallized salt from the media.

Another sinusoidal waveform with amplitudes ranging from 1 ~ 25 V_{p-p} was applied again to the same Biochip setup. This time the frequency was changed to 5 kHz and applied for at least an hour. The result showed the beads have moved in opposite directions, in which they were repelled away from the electrodes or in this case, the regions of intense electric field gradients. Negative DEP has forced the beads to move towards the lower electric field intensity and away from the electrodes. Most of the beads had formed structures that resemble a line bridge connecting between two parallel electrodes. This phenomenon can be seen clearly in Figure 4.10 ((a) and (b)). In (a) it depicts the overall view of the whole platform, while in (b), a close-up view of an area where the beads can be seen clumping together at positions near the weak intense electric fields.

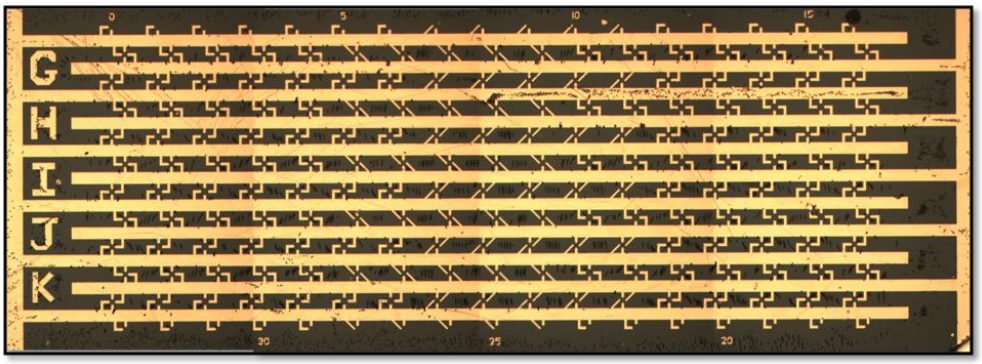

(a)

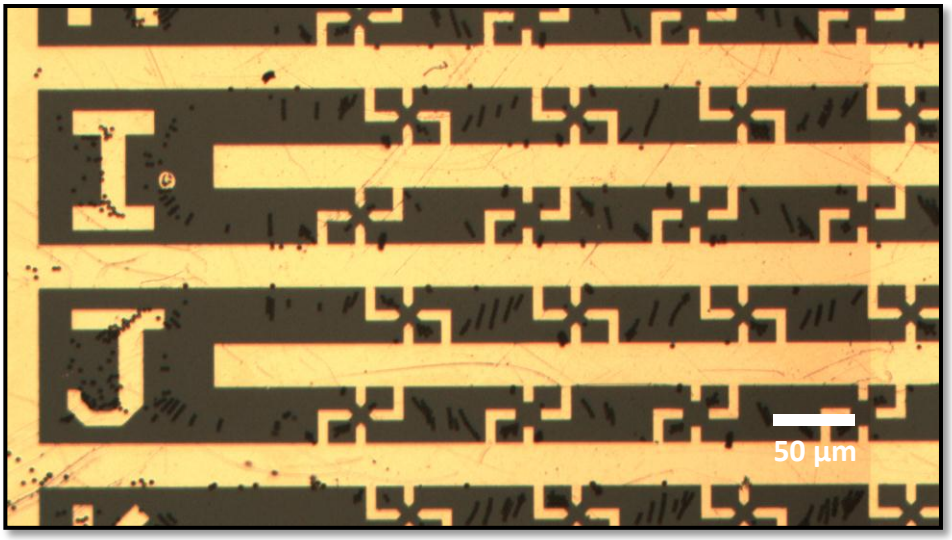

(b)

Figure 4.10: The optical microscope images in (a) and (b) show how the polystyrene beads were moved towards the lower electric field regions by negative DEP. The beads were forming ‘bridges’ as if they were trying to connect between two-adjacent parallel electrodes together. No beads were found on the high electric field regions (e.g. centre of the 4-pointed electrodes).

4.5 Discussion

As mentioned earlier in this chapter, there were quite a few problems faced during the experiments. For instance, in the polystyrene beads experiment, there were no cavities etched on top of the Biochip Au electrodes, as it was not coated with a layer of SU-8 in the first place. The objective of the setup was to test the electrodes configuration first, in order to test the new design layout was working as expected. The outcomes were clearly shown in Figure 4.9 and 4.10 respectively, which indicates that the first stage of the Biochip design process has achieved its goal.

Taking the process next step further, a second experiment was conducted and this time the Biochip has a SU-8 cavities layer on top, which was intended to be used as traps for the polystyrene beads. Unfortunately, the experiment did not go very well and according as planned. The problem was that the beads were sticking to the SU-8 surface and unable to move either by positive or negative DEP forces. The beads were jammed together forming small clusters and not spreading evenly over the surface area. The main reason might be related to the sticking problem between the beads and SU-8 layer, which is due to the surface properties of SU-8 resist. Nevertheless, SU-8 deformation will still remain a critical aspect of design in microstructures fabrication on silicon wafers.

Further testing and experiments on the Biochip were not performed as there was a change of emphasis to Bioimprint and focusing on investigating and developing the Bioimprint technique using the new Biopolymer developed in collaboration with the New Zealand Institute for Plant and Food Research Limited. Another measurement factor, namely the quantitative analysis should have been performed to verify the results, but it is beyond the scope of this work and that a new postgraduate student is performing this analysis currently.

4.6 Conclusion

A new technique was formalized in fabricating the Biochip which was simpler and easier with shorter fabrication period compared to previous approaches. The fabrication process of the electrodes and cavities involved a two-stage process comprising of photolithography, metallic deposition techniques and wet/dry etching steps. SU-8 resist was used as the material to cover the upper side of the electrodes, and was etched at numerous known locations to form the holes or cavities. To overcome crack formations problem which is a common on SU-8 material, additional baking parameters were necessary to minimise the cracks. However the most important step was

to cool down the SU-8 layer very slowly with the ramping down temperature being dropped as slow as possible.

The Biochip electrode design has worked as expected in manipulating the beads movement, extracting them towards the electrodes, or repelling them away from the electrodes, using either positive or negative DEP forces. With this design, low frequency ranges and V_{p-p} were sufficient to manipulate the beads mobilization. On the contrary, the beads were immobilised and stuck to the SU-8 layer, grouping in small clusters scattered all over the Biochip platform. This was the case for the Biochip with a layer of SU-8 on top forming the electrode-cavity design pattern.

In order to prove that the electrode-cavity design will work, further investigation should be done to determine whether the sticking problem would occur if real cells were going to be used. It is interesting to know what will happen, as there are still no available literatures that can confirm on this matter. Few reports only mentioned that some work has been done to culture biological cells on SU-8 layer and it seems that there is a ‘good’ biocompatibility of this material with biological samples.

Chapter 5

Bioimprint

"Bioimprint™" is a term describing a technique for permanently capturing a replica impression of biological cells, which has been developed to facilitate analysis using nanometer resolution imaging tools, namely the atomic force microscopy (AFM). In this chapter, a new Bioimprint approach and materials developed and investigated for this work will be described in details, together with the improvements and advantages it offers when compared to the previous technique and materials employed by Dr. James Muys.

To view the topography of an object, such as soft cells surface under a microscope, can be very challenging; which is why replication techniques were developed to overcome this problems. Some replication technologies have already been used for light and transmission electron microscopy (TEM) [101, 102] well before the introduction of the scanning electron microscope (SEM). In principle the replica of a surface can be a negative (or direct) impression, or alternatively a positive impression, obtained consequently through two-steps replica.

In this case, the replica must be able to capture a faithful replication of the original sample in a high resolution scale. The material used should be biocompatible as to minimize any harm or stress to the cells during polymerization. It should only introduce very minimal defects or artifacts during the replication process as complete elimination is impossible. Ideally it will be able to keep the cells alive during and after the replication process ended.

The replication materials that will be used for the biological cell replications must be able to meet these few requirements; have fast curing time, easy to peel and handle, able to produce a permanent hard copy of the sample, scaling up capability, and have excellent compatibility with cells and cell culture substrates. The best condition for replication is to have the replication material with an initial fluid character, so as to fill out the finest details of the surface to be depicted in the first step of a two-steps replication process. In the second step the replication material should cure to form a coherent layer that can be loosened from the surface to be replicated without leaving any material deposited on the replicated surface or extracting any material from the surface. A third feature of importance in biological applications is that the replicating material should be as applicable on wet as on dry surfaces [103].

To explore these possible ideas a Bioimprint replication technique was developed by our laboratory [26]. The motivation was to keep a high resolution record of cells, which is easy to be imaged by AFM. It was also because of the deficiencies in most vacuum-based nanoscale imaging technologies that require harsh drying and modification techniques for biological sample. This can lead to cell deformation and thus misrepresenting the true cellular structure. Bioimprint also overcomes many of the difficulties associated with *in vitro* cellular analysis, which results from the impact of the sharp scanning probe on the soft cell membrane, thereby facilitating the utilisation of the AFM as a non-destructive tool in biology imaging [88].

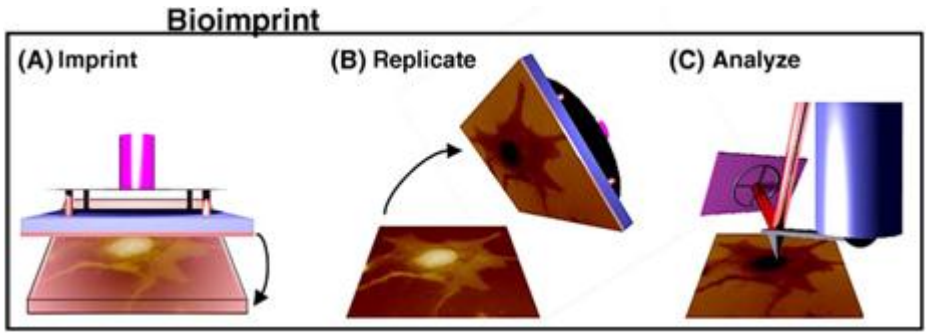

Figure 5.1: Illustration demonstrating the Bioimprint replication process [88].

Figure 5.1 shows a cartoon illustration that described the Bioimprint replication process and the imaging of cell replicas. By using a heat-curable elastomer composite (i.e. PDMS), cell impression can be obtained by submersing the cells in a liquefied polymer material and curing conditions are applied to permanently transfer the complete topography of the cells. Once the polymer has set after several hours, the cells and the replica are separated and the replica is then imaged under the AFM and digitally inverted to yield a positive replica [88]. One main disadvantage of this method is the dehydration effects, which results in the appearance of indentation profiles across the cell surface from collapse of the nucleus or of its dematerialisation. At first these effects were thought to be formed as a result of the pressure of the polymer on the nuclei. However, the indentation effects proved to be more intense with longer polymer curing times and temperatures, and thus were linked to dehydration effects [88].

5.1 Overview

A common approach used to reproduce structures of a surface is templating, which has been a general practise in dentistry. Templating is a simple technique for copying of surface structures where the master surface

represents the template, and replication material is pressed or filled in. Moulding is an example of a templating technique. A moulding material is used to fill a master surface, and once it hardened and separated, a negative replica is produced. Moulding is a relatively reliable way of surface structure replication and can reach a precision of a few tens of nanometers [104, 105].

Various types of materials have been reported being used as the moulding material for biological tissue replication. Silicone-elastomer replication has its basis in products developed for use in clinical dentistry [106, 107]. Forslind work demonstrated the use of silicone plastic (Provil-L, Bayer Dental, Germany) that was mixed with a catalyst and cured within 3 minutes. The negative replica was subsequently covered with an Araldite plastic (CIBA-Geigy, Basel, Switzerland) which cured within 3-5 hours depending on the volume applied. But the work only involved replicating large area of biological tissue such as skin surface. They have also reported to use methacrylate (Sigma, St. Louis, MO) designed for whole-mount embedding of e.g., insects and has longer curing time [108]. Nevertheless, not much has been reported or discussed concerning the ability of this approach in replicating nano-scale and high-aspect-ratio biological structures.

Another group lead by Kerstin [109] demonstrated the use of dental wax, polyvinylsiloxane (PLB, Hamburg, Germany) as the material for moulding and used three types of different fillings for the moulds. The fillings consist of a water-based acrylic lacquer (Acryllack, Knauber/Knauber Freizeit GmbH, Bonn, Germany), Epoxy resin (Epoxydharz, Conrad electronics, Hirschau, Germany) and Spurr resin (Plano, Wetzlar, Germany).

The work mostly involved the use of plant surfaces as their models for the replication which was targeted for the development of biomimetic, e.g., super hydrophobic, self-cleaning materials [109]. The replica method they presented was precise for nanostructure replication, fast for water-containing biomaterial replication and could be used without any expensive equipment for moulding of surfaces.

However, the main inspiration behind the development of the Bioimprint technique came from the nanoimprint lithography processes developed for the fabrication of electronics and optical devices. Nanoimprint lithography is a method of fabricating nanometer scale patterns involving simple nanolithography process with low cost, high throughput and high resolution. With this technology, patterns are created by mechanical deformation of imprint resist and subsequent processes. The imprint resist is

typically a monomer or polymer formulation that is cured by heat or UV light during the imprinting. Adhesion between the resist and the template is controlled to allow proper release.

Nanoimprint technique is one of the leading technologies in the nanofabrication field, but it has not been utilised fully for biological samples replication. Not only until recently was that this technique adopted for the fabrication of mould from soft cell samples, and replicas of soft cells were able to be produced [110]. 3-D specimen reproducibility in high resolution, low degree of cell structure damage during replication, and less formation of artifacts such as air bubbles and biological wastes were highly achievable and proved this technique has enormous potential in biological studies and research.

5.2 Materials and methods

As mentioned earlier, there were several problems associated with the Bioimprint technique during its initial development. Some of the problems were related to the dehydration effects caused by the heat-curable polymer used for the replication process. Others were linked to the introduction of artifacts or organic wastes during or after the replication process, caused by

the interaction between the heat-curable polymer and the photo-initiated elastomer with the biological cells. The lack of replica resolution was also another issue with the first Bioimprint method. It was caused by interfacial fluid layer remaining after aspiration and this had inhibitory effect in the resolution transfer of cell topography into the polymer.

To overcome these problems, a new material for soft cell replication was developed recently to replace the previous polymers used in the Bioimprint technique. A new Bioimprint method was also investigated. In this chapter, the new material will be described in details and is introduced as the "Biopolymer". For this research, three requirements should be fulfilled by the new Biopolymer replication method. First, the replication materials should cause no artifacts by shrinking or expansion and should be precise for nanostructure replication. The second requirement is the replication of biological surfaces of living cells with extracellular structures. Replicas should be without artifacts, caused by shrinking of the cells or squashing of the fragile three-dimensional cellular membranes. Thus, for water-containing biocompatible materials, a fast technique is required and replication of fragile structures must be performed with low pressure and at room temperature. Third, a comparison of the structure and morphology of the living cells and their replicas should show how faithful structural properties of cells can be transferred into artificial surfaces by the replication.

5.2.1 Materials

A new Biopolymer was developed for this purpose by the New Zealand Institute for Plant and Food Research Limited, Hamilton, under the direction of its chemical scientist, Dr. John S. Mitchell. The new Biopolymer cures in 10 s under UV-light exposure. The Biopolymer is biocompatible and can replicate soft materials such as living cells with high resolution. The composition of this material will be described in the following paragraph.

The polymerization mixture was composed of triglyme (Sigma Aldrich, St Louis, USA), ethylene glycol dimethacrylate, methacrylic acid and IRGAcure 2022 (CIBA Specialty Chemicals, Basel, Switzerland). The recipe consists of 1.2 ml of triglyme, 0.425 ml of EGDMA, 0.0425 ml of MAA and 20 µl of IRGAcure (photo-initiator). To get the best result, application volume for replication was optimized at 125.5 µl to give suitable coverage and thickness.

Triglyme or better known as triethylene glycol dimethyl ether is a clear colourless liquid with a mild ethereal odour. It is water soluble and has a hygroscopic type of chemical sensitivity. There is a risk of impaired fertility due to its toxicity and may cause harm to internal organs if it is not handled properly. Figure 5.2 depicts the molecular structure of this compound. Triglyme is added to this mixture in order to increase the

viscosities which assist the dispersion of the polymer over a large area of sample.

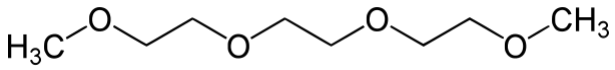

Figure 5.2: Molecular structure of triglyme with molecular formula of $C_8H_{18}O_4$.

Ethylene glycol dimethacrylate (EGDMA) is a diester formed by condensation of two equivalents of methacrylic acid and one equivalent of ethylene glycol. The liquid is clear with a bit of yellowish in colour and has a very low solubility in water. Ethylene glycol dimethacrylate is mainly used in plastic and rubber industries, e.g. acrylic acid sheet material, plastic tubing, fibreglass enhanced polyester, polyvinyl chloride (PVC), and known as ethylene-acrylic copolymer. Any polymer mixture that contains EGDMA will develop several augment characteristics like higher rigidity, heat-resistant, weathering resistance, solvent resistance and improved frictional ability.

Besides that, ethylene glycol dimethacrylate can be used as a high purity monomer for contact lens application, dentistry material, latex copolymer, rubber modification, adhesive material, and in printing ink and

paper making industries. Other than that, EGDMA is also used as a cross-linking agent in free radical copolymer cross-linking reactions, with bridging or specialty capability between polymer chains. Figure 5.3 illustrated the molecular structure of EGDMA with molecular formula of $C_{10}H_{14}O_4$.

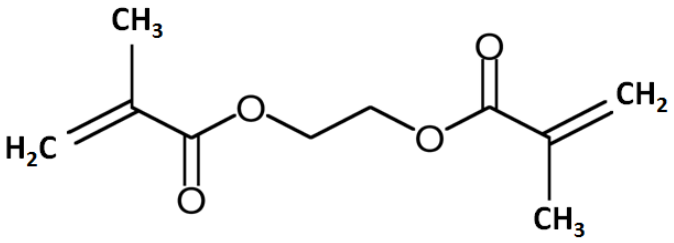

Figure 5.3: Molecular structure of ethylene glycol dimethacrylate.

Methacrylic acid (MAA) is a carboxylic acid with an acrid, repulsive odour. This colourless, viscous liquid is soluble in warm water, alcohol, ether and most organic solvents. The smallest part of this methacrylate group is the acrylic acid, which is the simplest unsaturated carboxylic acid that has double bond on its molecular structure. Acrylic acid undergoes the typical reactions of a carboxylic acid and forms acrylic esters. The basic alkyl esters are methyl, butyl, ethyl acrylate, and 2-ethylhexyl acrylate. Acrylic acid and its esters undergo the reactions of the double bond which readily combine

with themselves or other monomers, e.g. amides, methacrylates, acrylonitrile, vinyl, styrene and butadiene to form homopolymers or copolymers which are used in the production of coatings, adhesives, elastomers, super absorbent polymers, flocculants, as well as fibres and plastics. Acrylate polymers show a wide range of properties dependent on the type of the monomers and reaction conditions. The formula for methacrylic acid is $C_4H_6O_2$ and the molecular structure can be seen as shown in Figure 5.4.

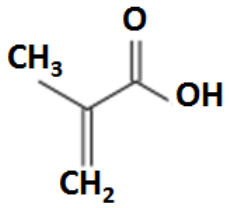

Figure 5.4: Molecular structure of methacrylic acid.

IRGAcure 2022 is a clear and viscous liquid, yellow in colour and miscible with most organic solvents but poorly soluble in water. It is a highly efficient liquid curing agent that is used to initiate radical polymerization of unsaturated resins after UV light exposure. Unsaturated resins that are mostly suited are those based on a pre-polymer, e.g., acrylates or unsaturated polyesters which goes in combination with mono- or multifunctional

monomers as reactive diluents. IRGAcure has a very good reactivity and a well-balanced ration between through-cure and surface cure. IRGAcure 819 is the main chemical composition of IRGAcure 2022 and it determines other components required to perform most of the needs to cure the clear or pigmented coatings.

5.2.2 Methods

In chapter 2, detailed elaboration and explanation have been presented on the subject of experimental techniques involving cell culture protocols and preparation. In this part, the explanation is continued by introducing the new Bioimprint methodology, proposed and developed in collaboration with Dr. John S. Mitchell from The New Zealand Institute for Plant and Food Research Limited, Hamilton.

As previously mentioned in details in chapter 2 (Section 2.7: Cell culture plates and chambers), cells were grown either on cover slips in well plates or on glass slide with chambers. For experiments using 6-well plates, the cell-coated cover slips were removed from the medium using tweezers on the edges of the glass so that the adhered cells are not removed. They were washed by immersion in 1 M phosphate buffered saline pH 7.4 and followed by drying using absorbent paper from the corners of the cover slip and then aspiration of excess fluid from the extreme edges.

The cover slip was then immediately mounted on to a spin coating apparatus (Laurell Technologies Corp.) and coated with the pre-prepared Biopolymer mixture. Optimum volume recommended is 125.5 µl but the range can be between 120 – 130 µl. The polymer was coated by dropping the polymer on top of the sample using a micropipette within 1 - 3 mm in distance. The cover slip was then irradiated with a Omni Cure Series 1000 UV lamp (100 W Hg arc lamp, 20% iris setting, 250-450 nm filter, EXFO Photonic Solutions Inc, Singapore) and immediately spun at 50 rpm for 10 s and then continued irradiation while spinning for another 15 minutes to harden the cured Biopolymer. Lamp distance to sample should be between 5 – 10 mm, depending on the size of sample. If the sample was bigger (e.g. more than 22 mm x 22 mm), then the distance should be further.

After polymerization, the Biopolymer can easily peel off the glass cover slip. Optical microscope images were collected with a CCD camera at each stage in the imprinting process and compared to images of the cells before removal from the culture media. The polymer was then cleaned with deionised water followed by ultrasonication for 15-20 s to remove cellular material from the polymer. The resulting polymer imprint could then be imaged under AFM. The soft lithography process is best being described as in the illustration in Figure 5.5.

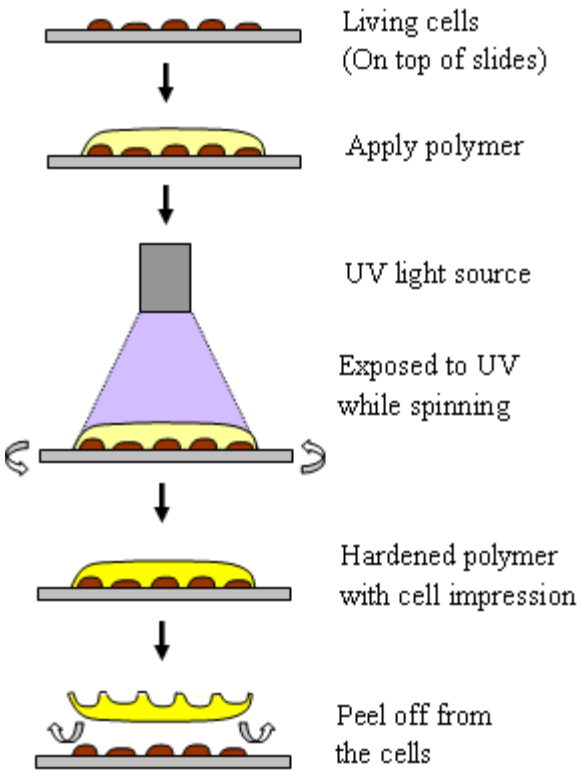

Figure 5.5: Schematic of the Bioimprint process showing immobilized live cells being coated with monomer mixture, polymerized under UV light, and peeled away from the glass support.

5.3 Imprints and AFM imaging

Rat muscle cells and Ishikawa endometrial cancer cells were used extensively in this work for the purpose of assessing the potential of the proposed polymer mixture. Cells were replicated and the replicas were

analysed under AFM to obtain high resolution imagery of extra-cellular features and nano-structures that could be found on the surface of the cell's membrane [30, 31].

5.3.1 Polymerization to produce imprints

To accurately replicate the surface features of a living cell using polymer imprint fabrication technique, it is essential to achieve polymerization rapidly so as to minimize the time over which process-induced alterations may take place. Additionally, the monomer solution mixture should be biologically inactive so that cell responses to it are minimal. These conditions must also be combined with a final polymer composition that is sufficiently flexible to mould the nanoscale features of the cell surface and not subsequently swell or shrink in such a way that these features become distorted. Our results suggest that a copolymer of MAA and EGDMA has these properties. Moreover, it is possible to lock in cell surface features through polymerization as the polymer is set using rapid UV initiation without the need for long heat curing that might introduce artifacts and distortions to the imprint. The UV-initiated polymerization is summarized in Figure 5.5.

5.3.1.1 Polymerization of muscle cells

Muscle cells growth was observed continuously with the cell culture media was changed every second of third day. Culturing period was maintained not to exceed 6 ~ 7 days to ensure the maximum number of adhered cells. Furthermore, the confluent state of the cells must be kept below 80% so that the cells were not crowded to the extent that their growth and development were being hindered by other neighbouring cells. This is also to ensure minimal overlapping of the cells which would prevent imaging of discrete cells and their surface features. Prompt handling of the cells combined with rapid setting of the polymer (very thin polymer layers can set within 15-30 s; thicker layers can take 120-180 s) allowed morphology to be preserved. This could be seen in the first instance by comparing the muscle cells growing in cell culture media to cells encased in the polymer coating in Figure 5.6. From this one can see that the characteristic cellular shapes have been preserved in the polymer. Circular features in the growth medium and polymer matrix are small accretions of salt or dust and can be removed in the washing process.

The polymer matrix is largely composed of ethylene glycol units and indeed polyethylene glycol polymers are well known for being non-toxic and non-immunogenic [22] and are used in a number of clinical products,

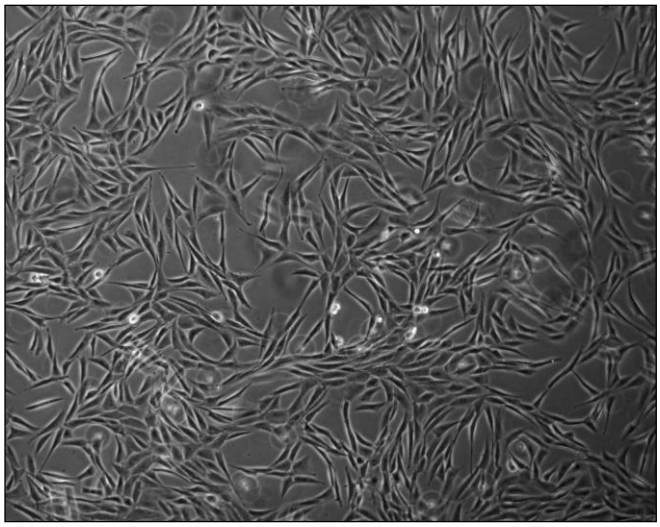

(a)

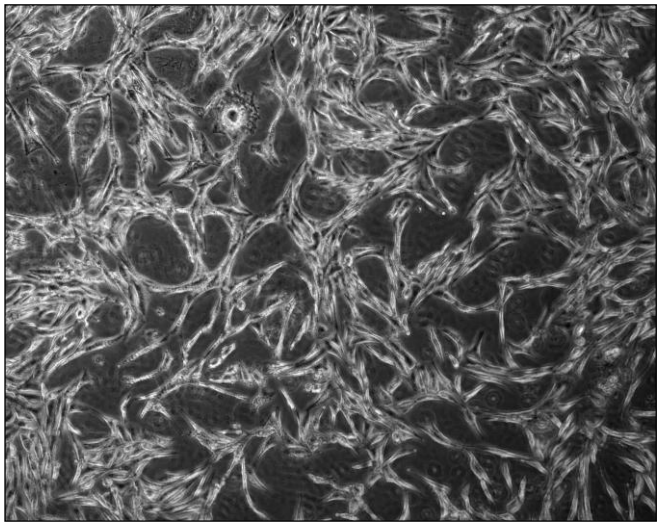

(b)

Figure 5.6: Light microscopy image at 20x magnification showing L6 rat muscle cells (a) in culture medium before imprinting and (b) after imprinting with methacrylic acid/ethylene glycol copolymer coating (which is transparent) in place.

including skin cream. This is likely to confer low toxicity on the polymer as a whole and further aid the preservation of cellular features. Low spin speeds were applied to ensure an even coating across the surfaces of the cells but not high enough to cause significant spin-off of the polymerizing matrix.

The triglyme is added to boost the viscosity of the polymer and to act as a porogen. Thick coatings of this polymer are inflexible and quite firm, which makes it easy to break if not handled carefully and it is not as malleable as PDMS. The amount of fluid in the layer between the cell and the polymer after aspiration affects the quality of the imprint, if it is too high it will cause degradation in resolution transfer of cell topography by diluting the monomer mixture and interfering with the intimate contact of the polymer solution with the cell surface.

High UV irradiation strength is required to ensure rapid setting of the polymer. A slow, long time curing process would likely affect the impression when rapid cellular processes are occurring and so it is possible that fast UV-curing may have a better chance of realizing snapshots of these processes as they occur. Muscle cells were chosen as a model in this case as they have excellent adherence to solid surfaces, which is especially important for coating on glass which has been found to be a difficult matrix for immobilization of cells. Furthermore, the L6 cell line is commonly used in

the study of tissue development and the study of the effects of nutrition and exercise on muscular development.

5.3.1.2 Polymerization of Ishikawa cells

Besides muscle cells, Ishikawa endometrial cancer cells were also tested with the same replication process as the muscle cells had gone through. Based on the observation on these cancer cells, during UV light exposure the cells will ultimately die, but cell survival is not crucial at this point as the imprint has already been taken. The polymer sets around the cells within the first 10 – 15 s, and further 15 min irradiation facilitates copolymer cross-linking reactions, especially when the application volume and thickness required are greater than the optimum volume (125.5 μL). 15 s exposure of the cell to UV at this intensity would be unlikely to generate sufficient free radicals to alter the cell's membrane. In this time, the polymer would have attained its final shape; the longer duration of UV is to increase the rigidity of the polymer to enable subsequent AFM scanning.

The polymerization process will freeze all cell activities, either changes in the cell structure or the internal molecular processes at the point of imprinting. This could be seen in the first instance by comparing the endometrial cells growing in cell culture media before being exposed to the

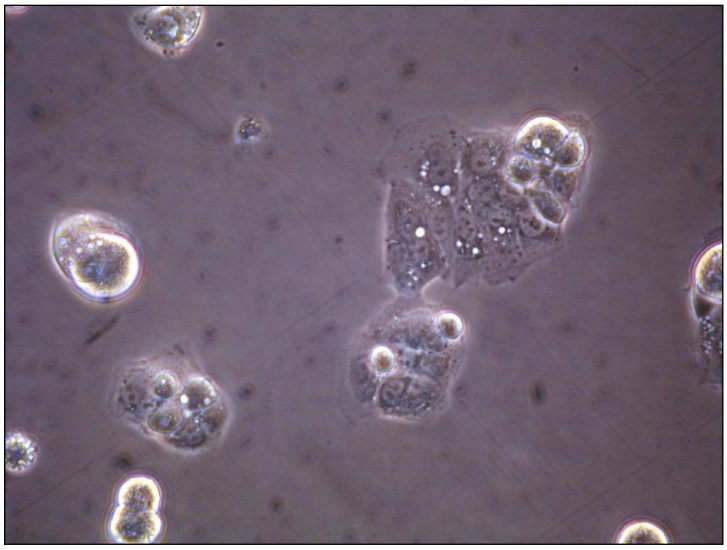

(a)

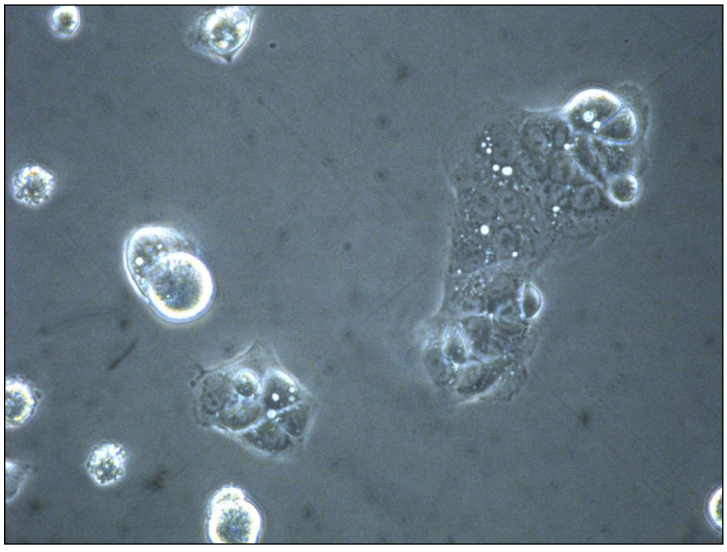

(b)

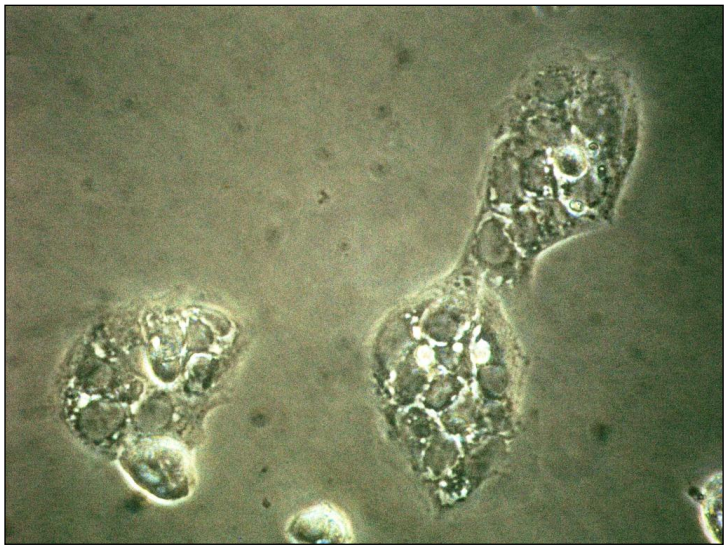

(c)

Figure 5.7: Light microscope image at 40 x (0.55) magnification showing Ishikawa endometrial cancer cells (a) in culture medium before UV-light exposure, (b) after the UV exposure for 15 seconds and (c) after chemical fixation using 4 % paramormaldehyde. Cell image in (c) is not the same as in (a) and (b), but they are from the same sample on the same slide.

UV-light to the same cells after the UV-light exposure for 15 seconds and also compared to the similar cells that have been preserved using chemical fixation method in Figure 5.7. From this, one can see that the characteristic cellular shapes of the cells (e.g. overall size and structure of the cells) remain the same without any significant changes in sizes and compositions, such as shrinking or deformed into spherical structure (this would suggest the cell was dead) [31].

5.3.1.3 Replica versus direct cellular imaging

To confirm the polymerization was able to replicate significant surface features and topographies of the cells, comparison between the AFM image of the imprint and the image of a direct cellular AFM scanning in semifluid-tapping mode were done. Figure 5.8 (a) shows a lumps of Ishikawa endometrial cells taken using DP14 SPM probe silicon cantiliver in direct cellular contact, with scan rate of 0.1296 Hz and drive frequency of 505 kHz, at 21 ºC (26% humidity). While Figure 5.8 (b) exhibits an AFM image taken from the replica of similar lumps of cells. Through these images, we can validate that the replication process managed to replicate these cells without destroying the cells morphologies, and showing no effects of dehydration, artifacts or inclusions whilst the cell still retained its structure. Infact, from this comparison, the AFM image of the replica managed to show the faithful replication of the cancer cells, before any deformation effects or structural changes had the chance to alter them. On the contrary, direct cellular AFM imaging was not able to produce the same results. Since the cells were suspended in semifluid condition, the cells were probably in stress and 'unhappy' situation that have led to cells deformations, shrunk in sizes, and structural changes to the walls and cell boundaries. Prolong AFM scanning time (20 ~ 30 minutes for 100 µm x 100 µm scan size) also caused the cells to change in their structure and morphology.

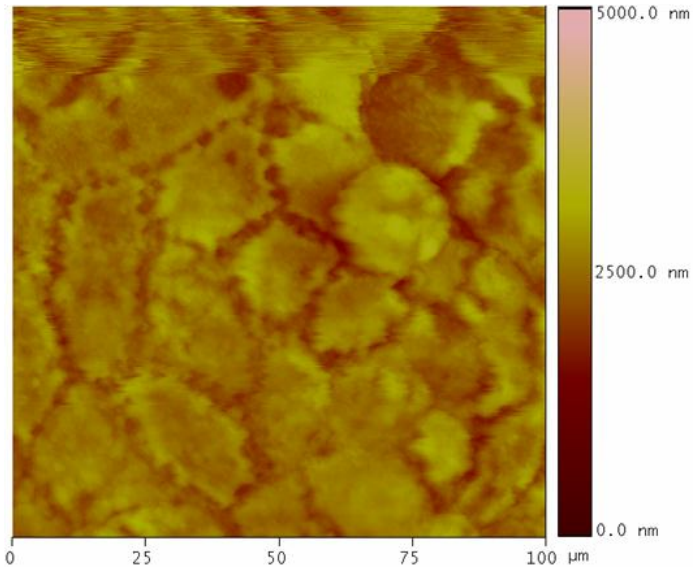

(a)

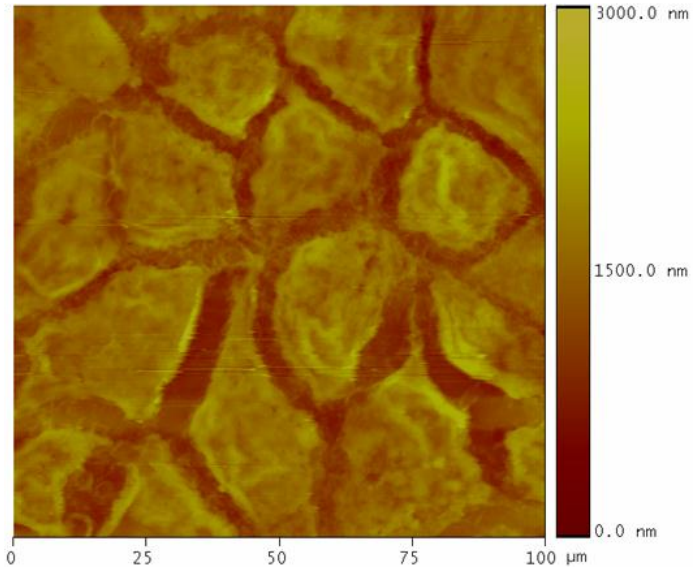

(b)

Figure 5.8: AFM images showing lumps of cancer cells (a) obtained through direct cellular imaging in semifluid-tapping mode and (b) cell imprint of similar lump of cells.

5.3.2 AFM imaging of cellular features

5.3.2.1 Rat muscle cell imprints

Figure 5.9, Figure 5.10, and Figure 5.11 show the top view and angle view images of the muscle cells captured using the AFM. Figure 5.9 (a) clearly shows the topography and the surface structure of the cells, while Figure 5.9 (b) shows that the polymer replica has captured at the nanometer scale detailed features consistent with a functioning cell.

At higher magnifications the range of membrane topography is observable. Structures that resemble fusion pores are shown in Figure 5.10. In Figure 5.10 (a), the replica of several cultured cells with abutting plasma membranes are highly visible. The angle-view imagery in Figure 5.10 (b) highlighted craters which are thought to be a result of fusion pores forming on the membrane by underlying granules. Our hypothesis is that these craters are steps on a transitional series of sequential structures that represent either an endocytotic or exocytotic process. On the other hand, the possibility that these structures have other functions or they are cell permeation artifacts resulting from the polymerization process cannot be ruled out.

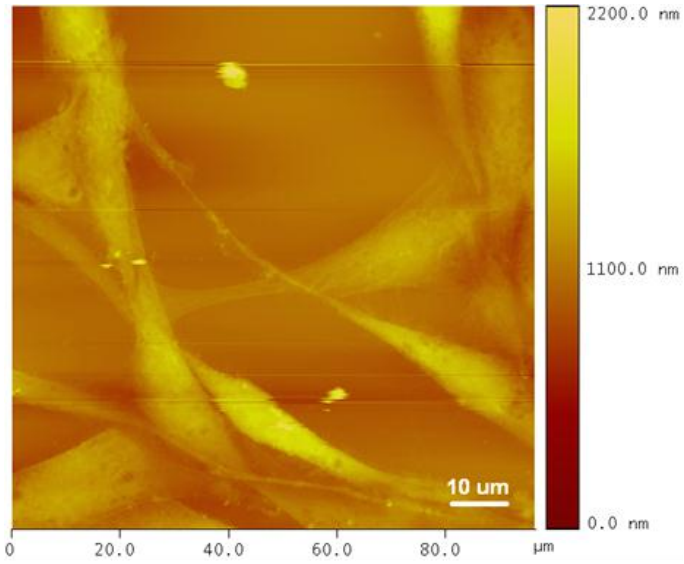

(a)

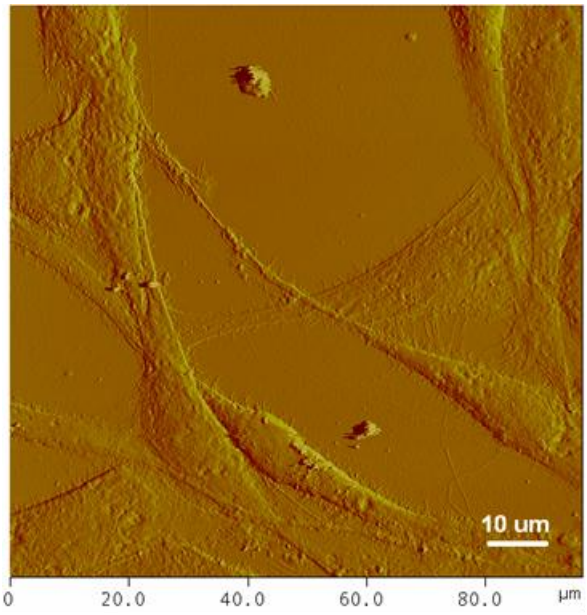

(b)

Figure 5.9: AFM images of the MAA/EGDMA polymer imprints of rat muscle cells with (a) imprint showing a group of cells obtained in phase mode, and (b) image of cells obtained in amplitude mode.

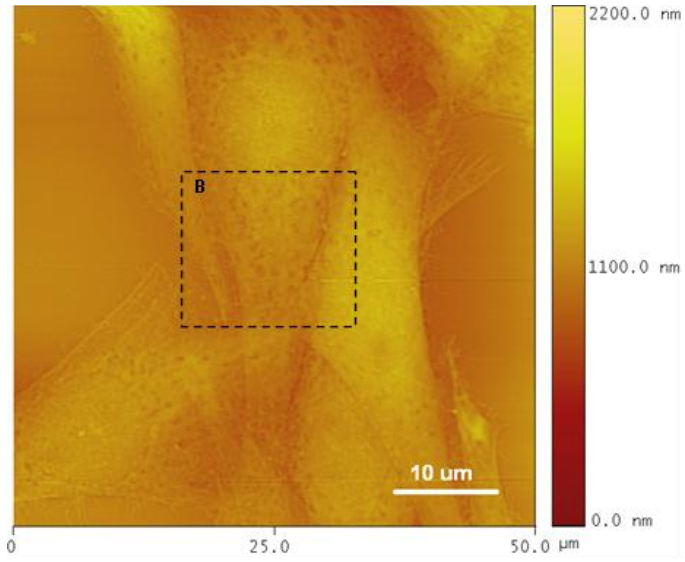

(a)

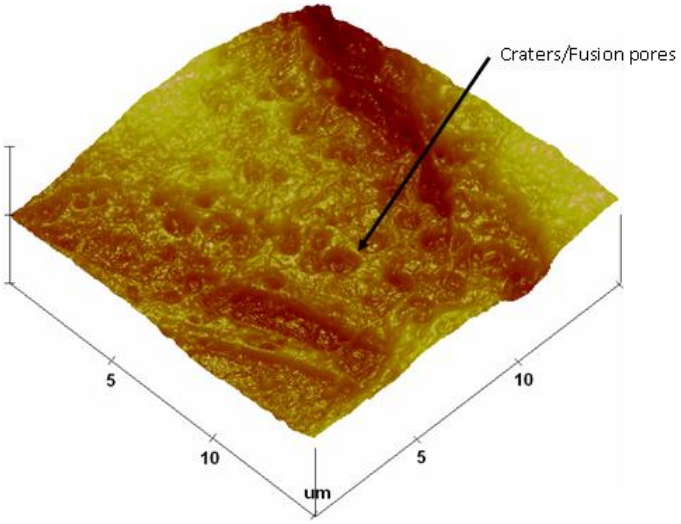

(b)

Figure 5.10: AFM images showing the topography and morphology of the polymer imprint of L6 rat muscle cells. (a) Several cultured cells with abutting plasma membranes and (b) angle-view imagery with visible fusion pores.

In addition the polymer has also succeed in replicating the cell submembraneous structures. Figure 5.11 depicts elements on the sarcolemma of the cell, which is the cell membrane of a muscle cell. The Bioimprint resolves numerous thin collagen fibrils in the form of fine fibers that extend from the outer coat of the membrane, which is made of a thin layer of polysaccharide material as shown in Figure 5.11 (a). At each end of the muscle fibre, this surface layer of the sarcolemma fuses with a tendon fibre, and the tendon fibres in turn collect into bundles to form the muscle tendons that then insert into bones. The membrane is designed to receive and conduct stimuli. Both Figure 5.11 (a) and (b) also display the presence of a structured cytoskeleton consisting of the intermediate cytoplasm filament proteins along with actin filaments. Actin filaments attach to the sarcolemma by focal adhesion in a spiral corkscrew fashion, and contractile proteins can organize into zones of actin and myosin along the axis of the cell.

Figure 5.12 shows a 3-D AFM image of the muscle cell illustrating the preserved morphology of the cell after imprinting process. There was no evidence of any damage to the imprint from the tip of the AFM probe such as tears or scratches in the imprint. This indicates that the polymer is firm enough to resist abrasion during the microscopic imaging process and thus is suitable for use in imaging cells on the nanoscale.

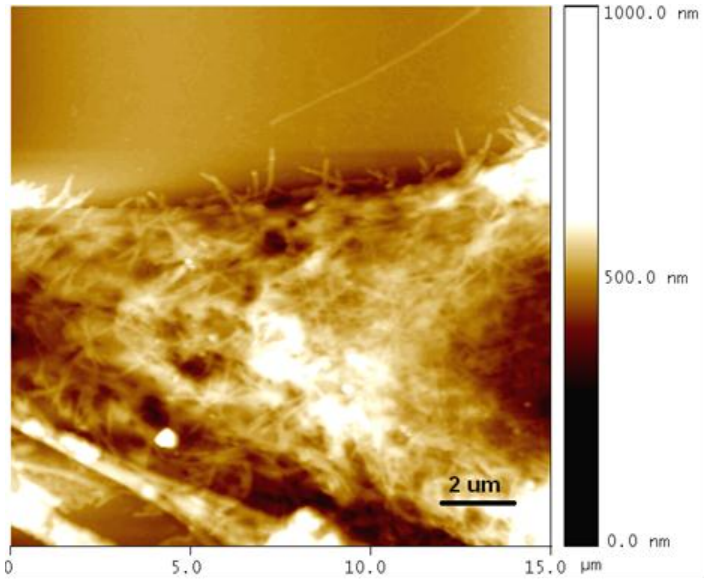

(a)

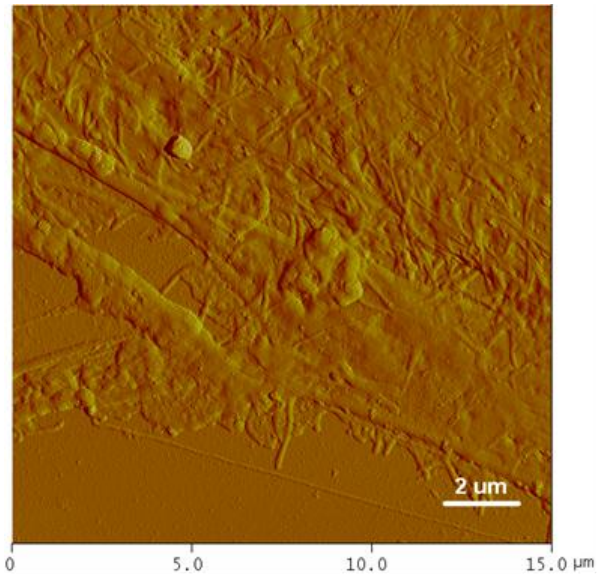

(b)

Figure 5.11: Images of cell intrusions and fibres illustrating the presence of ribosome on the membrane in muscle cell imprints with (a) visible fine micro-fibres on the cell membrane, and (b) polysaccharide material that form thin collagen fibrils [111].

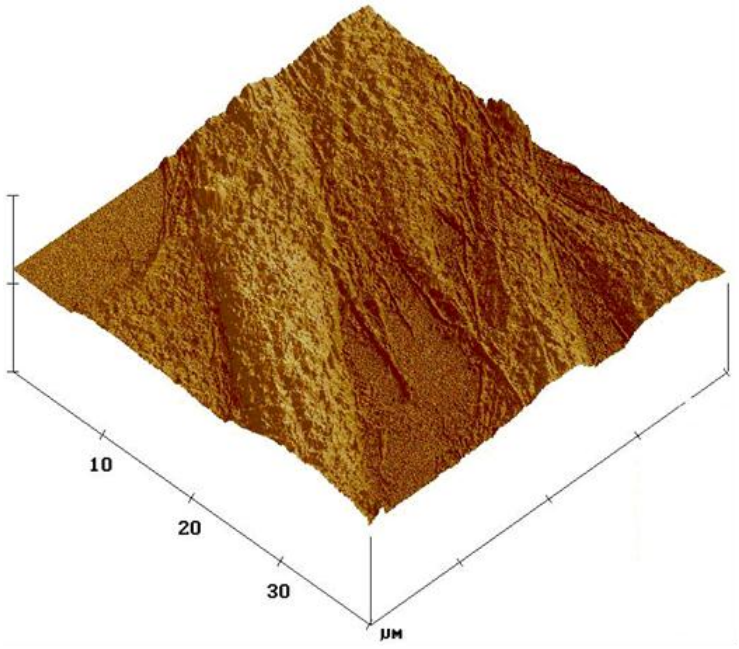

Figure 5.12: AFM contour image of L6 rat muscle cell imprint showing micro-fibrils at the ends of the muscle cells.

5.3.2.2 Endometrial cancer cell imprints

Figure 5.13 and Figure 5.14 show the AFM scanning images of the Ishikawa endometrial cancer cells. Figure 5.13 (a) clearly shows the topography and the surface structure of the cells, while Figure 5.13 (b) shows that the polymer replica has captured at the nanometer scale detailed features consistent with a functioning single cell.

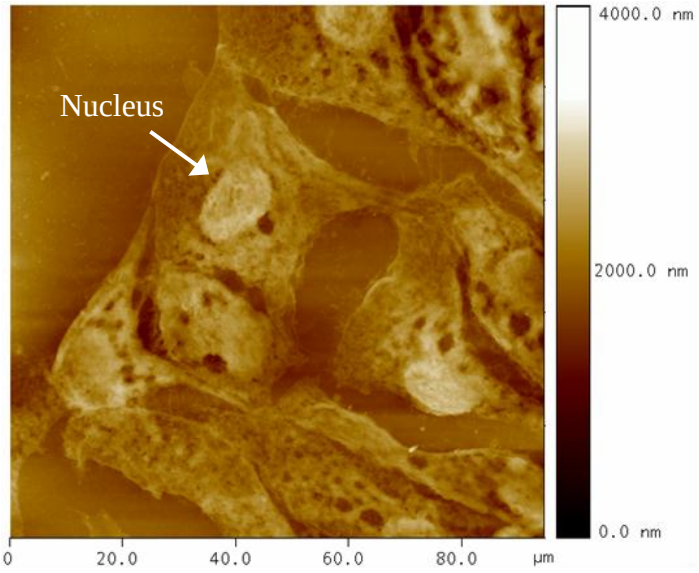

(a)

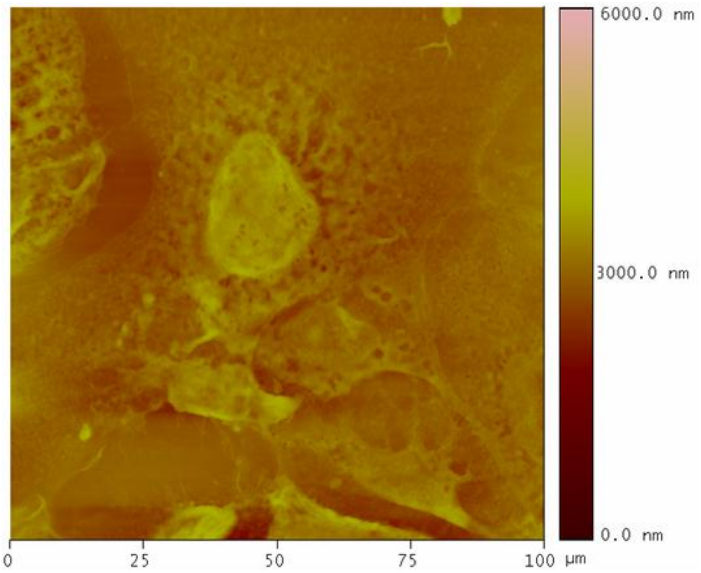

(b)

Figure 5.13: AFM images of the polymer imprints of Ishikawa endometrial cancer cells. (a) A group of cells connects to each other through the elongated membranes within the extracellular matrix. (b) Imprint of a functional single cell with membranous structures surrounding its nucleus.

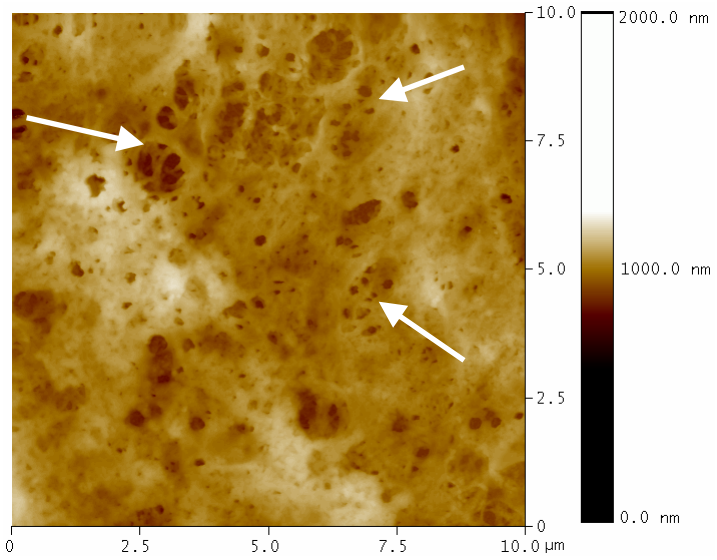

(a)

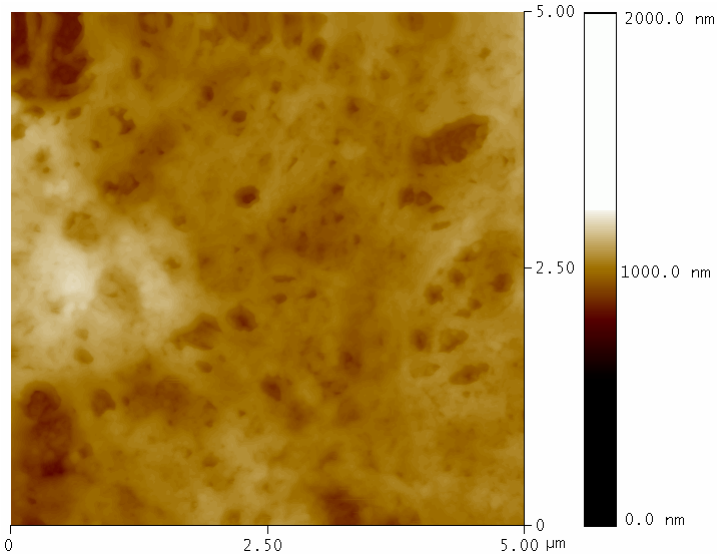

(b)

Figure 5.14: AFM images of cell's membrane showing intrusions or craters that may suggest the result of fusion pores forming on the membrane of the cell by under laying granules.

At higher magnifications, the membrane topography of the cell's nucleus is observable. Structures of craters that resemble granules are shown in Figure 5.14. There is a possibility that nano pores can be found in these granules. In Figure 5.14 (a), the replica of a cell's membrane with highlighted craters which are thought to be a result of fusion pores forming on the membrane by underlying granules are highly visible. The top-view imagery in Figure 5.14 (b) shows a single crater (in the middle of the figure) with the size of 230 nm and deepness of 130 nm.

5.3.3 Imprints as 3-D scaffolds for tissue culture

Preliminary work has begun in finding and designing new materials and techniques that can work really well in tissue culture system. The aim is to help researchers and scientists get a more accurate picture of how cells grow and behave in the body. New synthetic structure can provide a more conducive microenvironment for tissue cell cultures and tissues used in regenerative medicine, such as skin grafts or epithelial cells to replace organ cells such as liver which are lost to injury (*Cirrhosis*) or disease (cancer). The scaffold itself can be transplanted directly into the body with no ill effects. This has huge potential in medical implant field and cell regenerative study.

In the biological science field, people especially the biomedical researchers have become increasingly aware of the limitations of growing living cells in coated, two-dimensional Petri dishes and glass slides. Cells on flat surfaces tend to exhibit skewed metabolisms, gene expression and growing patterns, compared to normal cells living in the body. A normal cell environment is a complex network of tiny fibres, gaps and pores through which oxygen, hormones and nutrients are delivered and waste products filtered away. To support the cells in the body, other cellular structures and proteins are attached to them and this helps the cells to move within their natural environments in response to chemical signals or other stimuli. Only a few choices of schemes are available to imitate these conditions such as using glass lab ware and a product called Matrigel, a gelatinous protein mixture secreted by mouse tumour cells. Even though Matrigel does resemble a complex extracellular environment, it also contains growth factors and unknown proteins that limit its desirability for experiments requiring precise conditions. As the technology used in biological research getting advanced and better, the time has come to move on from two-dimensional incubation dishes to cell culture systems that better represent the natural context of cells in tissues and organs [112].

In this study, the work involved in cell replications using Bioimprint has triggered the idea of 3-D tissue scaffolding, which presents the potential

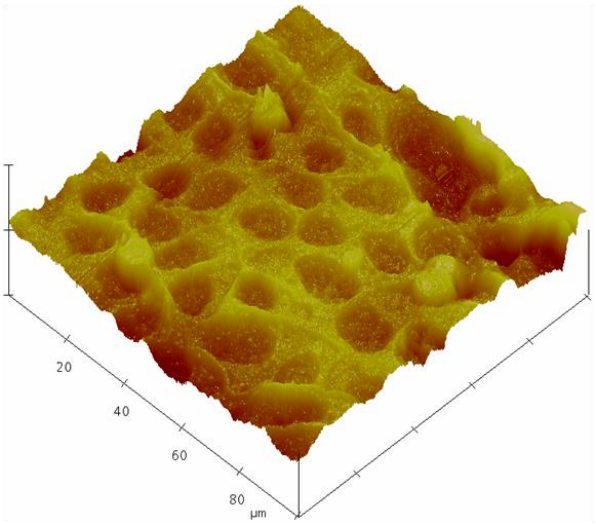

(a)

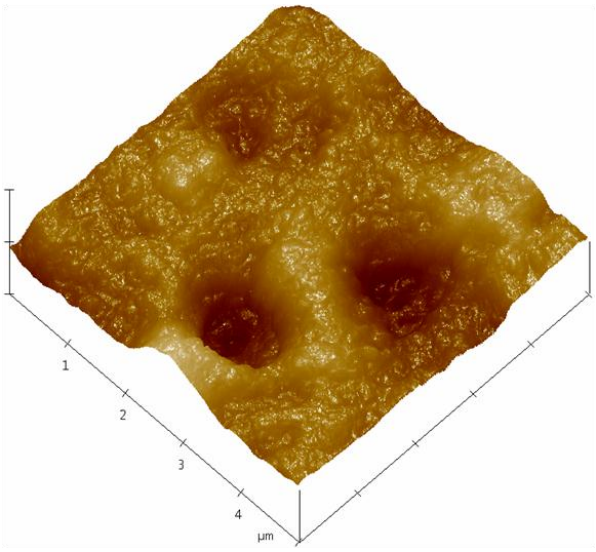

(b)

Figure 5.15: (a) AFM images in 3-D of negative impression of the endometrial cancer cells. A high resolution image in (b) that shows the surface topography clearly indicates that the cell structural arrangement is rough with heavy texture.

of this newly developed Biopolymer has to offer as a biomedical procedure for forming 3-D biocompatible and bioactive scaffolds for tissue culture. Tissue and cells interactions to their replicas would be a great area of interest to study and how the cells attached and detached to surfaces that have the same structural arrangement to them would open new possibility in biological and medical science, especially where these new findings can help to offer a second chance to patients with lower stages of cancer or other health problems that requires tissue or organ transplants. Figure 5.15 shows 3-D AFM images of these replicas that may be used for 3-D tissue/cell culture and bioactive scaffolding.

5.4 Conclusion

This research reports the development of a new material called Biopolymer that works as an imprint resist for the Bioimprint technique, developed by our team here in The Nanostructure Engineering Science and Technology (NEST) group laboratory, Canterbury University, in collaboration with The New Zealand Institute for Plant and Food Research Limited. The new Biopolymer offers remarkable improvements in terms of reliable and faithful replication of soft cells samples. Fast UV-irradiation of just below 10 s helps the Biopolymer to lock cellular processes; especially those related to the

exocytotic mechanisms which may last only a few seconds. This new Biopolymer is also biocompatible to biological samples, as the main compositions of the polymer matrix are all known to be non-toxic and non-immunogenic. Low level of toxicity confers the Biopolymer to further support the preservation of cellular features.

As described in details before, the new Biopolymer has able to replicate soft biological cells without introducing any defects or artifacts during the replication process, with all experimental work related to the handling of the biological samples were done in culture hood under sterile and contamination-free conditions. The Biopolymer mixture is also biologically inert, which make the cell responses to the polymer during direct contact is very minimal. The final polymer composition that is sufficiently flexible to mould nanoscale features of the cell surface and not subsequently swell or shrink plays an important role in determining the true level of a faithful replication of the cellular features.

This new Biopolymer may have numerous impacts on the development of the Bioimprint technology. It may put Bioimprint as one of the principal methodology in life sciences study, in par with other sample preparation techniques such as chemical fixation, dehydration, and cryofixation.

Even though there were a few issues such as the requirement to use ultrasonic cleaning to remove cellular debris might suggests the cells were harmed significantly and completely destroyed, the conditions of the cells at the end of the polymerization process were not important. The cells would eventually die after being exposed to high intensity UV-light for more than 15 minutes, but what most important was that the imprint of the cells were able to be captured within the first 10 s. The imprints were washed as to get rid any excess of the cell structures that might still adhered to the surface and could affect the result when the imprints were brought-in for the AFM scanning.

Another issue was about the time it would take to complete the polymerization. It was suggested that longer polymerization times will cause problems to the process. It is true to say that longer and slower polymerization would lead to cells start to deform (e.g. shrinking, dehydrate), which could cause the samples being tampered by artifacts, air bubbles etc. That is why it was essential to achieve the polymerization so rapidly so as to minimize the time over which process-induced alterations may take place. No comparison between long and short polymerization times were done as it was deemed not necessary.

Chapter 6

Bioimprint of cancer cells

This chapter will elaborate further the research work that has been done in the investigation of the Ishikawa endometrial cancer cells. Some of the results will be presented here and will be discussed in details. Endometrial cancer is cancer that forms in the tissue lining the uterus of a woman. Most endometrial cancers are adenocarcinomas (cancers that begin in cells that make and release mucus and other fluids). Based on a report by the National Cancer Institute, estimated new cases and deaths from endometrial (uterine corpus) cancer in the United States alone is about 43,470 of new cases and 7,950 of deaths. These estimations are for this year (2010).

For most cases of women who have symptoms that suggest endometrial cancer, their doctors usually perform general health check, together with blood and urine tests. The doctors may also perform one or more exams or tests such as pelvic exam, Pap test, transvaginal ultrasound, or even biopsy by removing a sample of tissue from the uterine lining to determine the presence of any cancer cells. In some cases, however, a

woman may need to have a *dilation and curettage* (D&C). D&C refers to procedure that involves the processes of dilation of the cervix and surgical removal of part of the lining of the uterus or its contents.

Abnormal cells that generally make up tumours differ from normal cells in terms of having distinct structural changes to their appearance and other characteristics. They are related to certain functional alterations such as *hypertrophy* (an increase in the size of individual cells), *hyperplasia* (an increase in the number of cells within a given zone) or *anaplasia* (a reversion of differentiation of the physical characteristics in cells). Anaplasic tumour cells are poorly differentiated cells with a primitive look rather than an appearance like normal healthy cells.

At present, tumour cells detection are done by performing histomorphological analysis using stains and antibodies to underline morphological differences against normal healthy cells. These histological analyses are typically done in vitro on fixed tissue samples taken from a patient by invasive procedure (i.e. biopsy, D&C). Although the analysis may be simple, it often suffers from low sensitivity or specificity in the quality of the images obtained, and lacks of high resolution imagery for better understanding of cell structures at nanoscale.

As described before in chapter 1 and 5, AFM superior resolution enables exploration of new topographic identities, which is suitable for cancer cell identification and accurate detection. This chapter presents further results from AFM analysis on the endometrial cancer cells and the investigation into cell structure during the regulation of VEGF receptors while monitoring the effect of using certain organic or inorganic compounds such as cobalt chloride in exaggerating the expression of the growth factor.

6.1 Cellular features on membrane surfaces

Figure 6.1 (a) and (b) show the AFM scanning images of an imprint of the Ishikawa endometrial cancer cells. See Appendix A.2 Protocol for cancer cell culture and cloning for procedure described in this part. In (a), it clearly depicts the surface structure and the topography of the cells, and the replica has captured at the nanometer scale detailed features such as intrusions in the form of nanopores on the membranes surface of the cells. A group of 4 to 5 cells forming a small cluster with dissymmetrical structures and partially lacking vascular walls. This type of cells multiplies and grows on top of each other, as they have lost the restraints on growth that characterize normal cells.

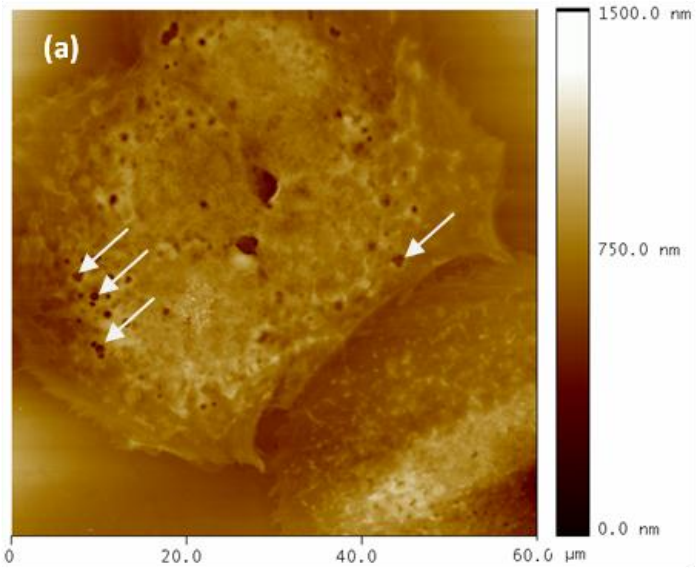

(a)

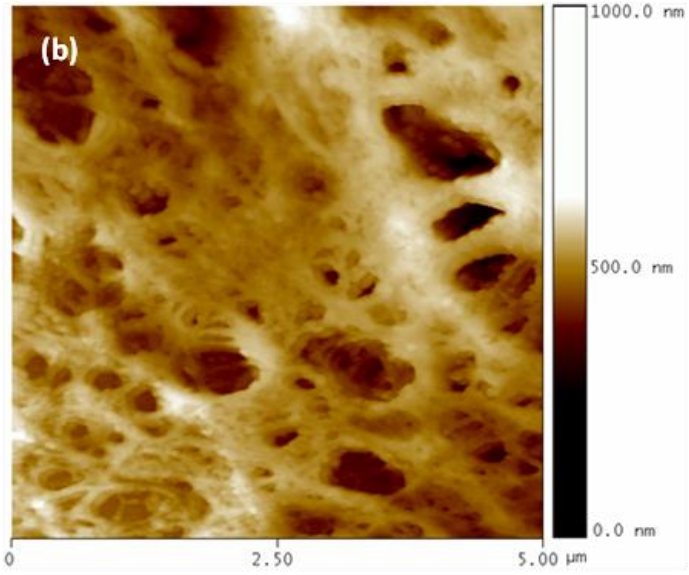

(b)

Figure 6.1: AFM image of (a) Bioimprint polymer showing a group of 4 to 5 Ishikawa endometrial cancer cells, (b) intrusions in the form of nanopores are highly visible on the membranes surface of the cells.

For example, cancer cells are genetically unstable and prone to rearrangements, duplications, and deletions of their chromosomes that cause their progeny to display unusual traits. A higher resolution image in (b) describes the membrane structures as multilayered filaments of phospholipids with pores in different sizes and depths. As described in [113], the nucleus of neoplastic cells plays through its changes a main role in the assessment of tumour malignancy. Changes concern its surface, volume, the nucleus/cytoplasm ratio, shape and density, as well as structure and homogeneity.

Ultra-structural characteristics are related to nucleus segmentation, invaginations, and changes in chromatin, increase in certain type of granules, and also the increase of nuclear membrane nanopores, together with the formation of higher number of inclusions. On the surface of malignant cells such as Ishikawa cell, atypical microvillus, pseudo-pods and vesicles with extremely active enzymatic equipment would appear [114] which correlates well with the appearance of the multilayered structure of pores and granules shown in Figure 6.1 (b). Recently, a new technique called Ion conductance microscopy (ICM) managed to capture the image of a live human breast cancer cell that shows the same topography features and appearances as demonstrated before in Figure 6.1 (b). The image, shown here in Figure 6.2 (scan size: 50 μm) clearly support the argument that cancer cells demonstrate

complex reactions and activity at the membrane surface. ICM is a non-invasive in-liquid scanning probe technique that does not apply any force over its sample surface, making it ideal for nanoscale imaging of soft cellular membranes in dynamic conditions [115].

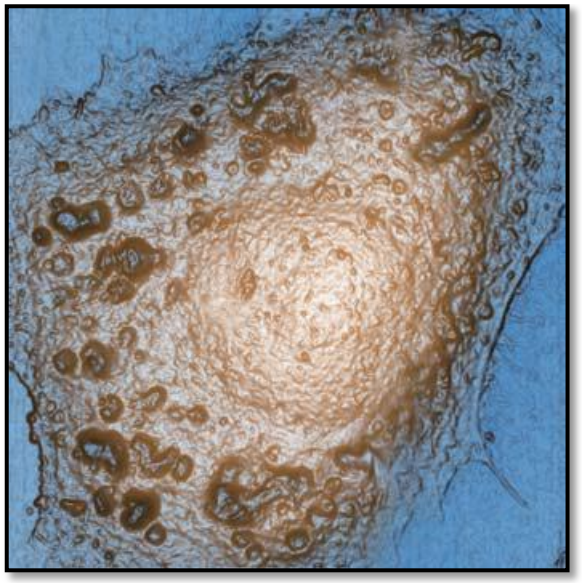

Figure 6.2: An image of a live human breast cancer cell taken using Ion conductance microscopy (ICM) with scan size of 50 μm [115].

6.2 Cell structure during VEGF regulation

The Vascular Endothelial Growth Factor (VEGF) has emerged as one of the promising therapeutic target in the treatment of cancer, and VEGF proteins are expressed on the endothelial cells lining blood vessels, which are normal, untransformed cells. VEGF proteins contribute to tumour growth by triggering vessel growth which is essential to supply nutrients to a growing tumour. However, if VEGF proteins are over-expressed, it can lead to cardiovascular disease which will affect the blood vessels. Consequently, the tumour growth will be halted and continuous lack of blood and nutrients supplies makes the cancer cells weaker and ultimately dies after a period of time.

For this research work, studies were concentrated on observing the cell structure in high resolution imagery during the regulation of VEGF and the effect of using certain organic or inorganic compounds such as cobalt chloride ($CoCl_2$) in exaggerating the expression of the growth factor. It was reported that for certain type of cells, the expression of VEGF protein after $CoCl_2$ treatment was likely three times as much as that at the start of treatment [116]. Bioimprint replicas of the treated cells are shown in Figure 6.3. They demonstrated the different characteristic behaviour between control cells which were cultured under normal conditions (without any

stimulation) and cells induced by $CoCl_2$. In (a), control cells showing less activity related to exocytosis process on the membrane surfaces while in (b), the cells showed higher activity level with increased number of visible pores on the membrane and (c), their numbers were significantly escalated in areas where the confluent states were higher than 80% with cells forming multiple layers by growing overlapping each other.

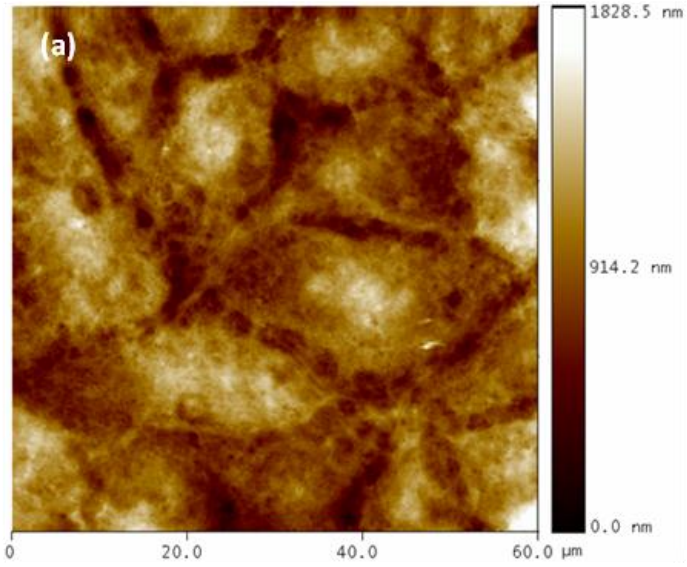

(a)

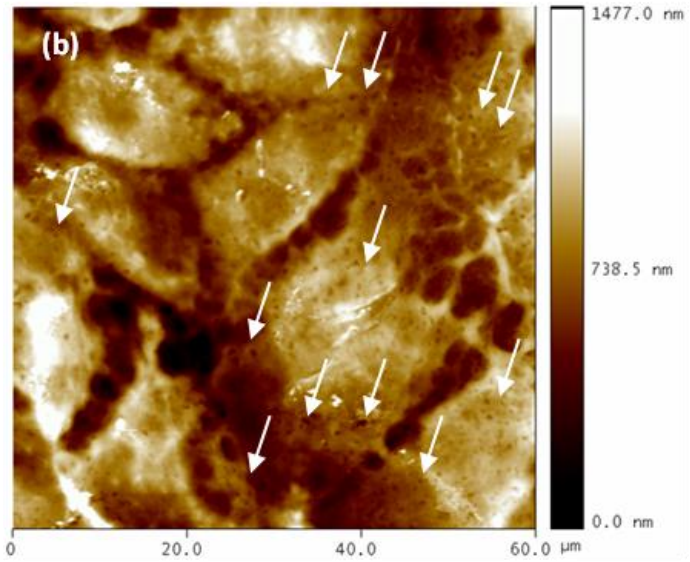

(b)

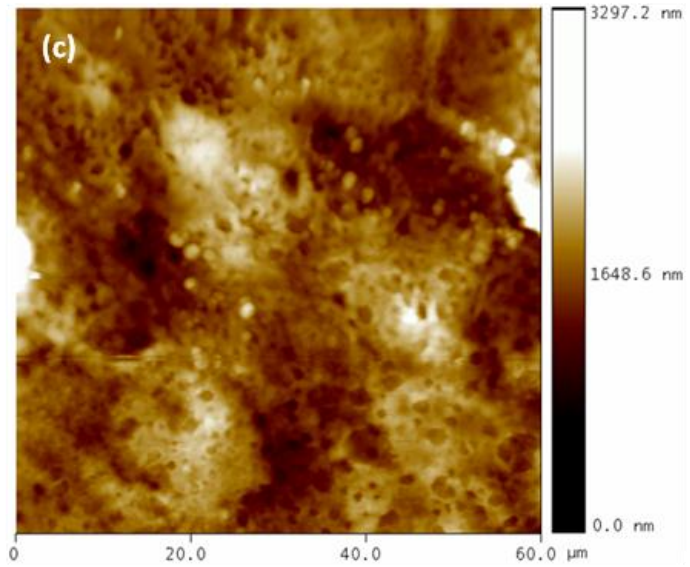

(c)

Figure 6.3: AFM images of cancer cells replicas. (a) Control cells, (b) increased number of visible pores after $CoCl_2$ treatment and, (c) higher expression of VEGF was observed with number of pores escalated considerably at numerous areas of the cells population.

6.3 VEGF time course expression

Cell membrane examination under the influence of this chemical agent was targeted in order to establish the time course for VEGF proteins expression during different periods of $CoCl_2$ treatment. Ishikawa endometrial cancer cells were up-regulated with $CoCl_2$ for a 24 hours period, and VEGF expression values at 1 hour, 10 hours and 24 hours time points were extracted from the same cell line. Each time point values were compared to a common reference set by the control cells (not stimulated by any types of stimuli).

Supernatants from each time points were collected and evaluated using enzyme-linked immunosorbent assay (ELISA). Data obtained from the ELISA standard curve were linearized by plotting the log of the VEGF concentrations (ng/ml) versus the log of the time course (hour/s). In this experiment, $CoCl_2$ was found to significantly elevate VEGF proteins expression at different time intervals. At 10 hour after the treatment, the expression of VEGF proteins was almost three times greater than at the start of the treatment. The result in Figure 6.4 showed that the VEGF expression profile was gradual and time-dependent. It also shows that $CoCl_2$ stimulation mediated the increase induction of VEGF proteins nearly two-fold than the untreated cells [117].

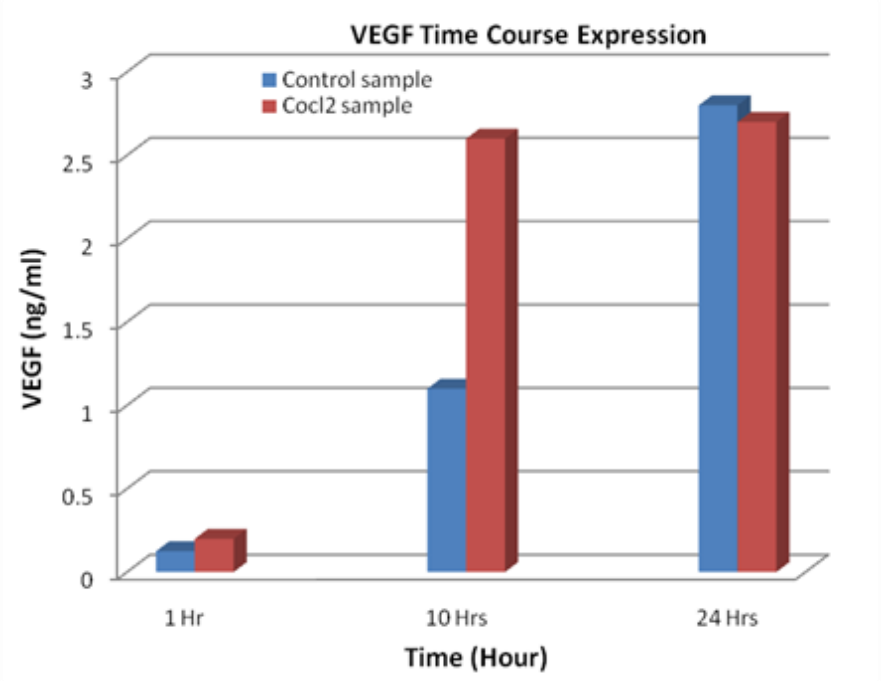

Figure 6.4: VEGF concentration (ng/ml) versus time (hour/s) with control and $CoCl_2$ induced samples.

These results indicated that cancer cells produced more VEGF proteins after $CoCl_2$ treatment which would stimulate the growth of new blood vessels to support tumour development and proliferation. Cancer cells cannot grow beyond a limited size without an adequate blood supply, which means cancer cells that can express VEGF are able to grow and metastasize. It is part of the system that restores the oxygen supply to tissues when blood circulation is inadequate. Consequently, over expression of VEGF can cause cardiovascular disease, primarily affecting the blood vessels.

Numerous studies have shown that there is a decrease in the overall survival and disease-free survival in those over expressing VEGF tumours. VEGF release can cause several responses, for instance it may cause a cell to survive, move, or further differentiate. Hence, VEGF has become a potential target for the treatment of cancer [83, 118]. Approved anti-VEGF drugs have been used since 2004 such as *bevacizumab* with approximately 10-15% of patients benefit from the therapy. Bergers and Hanahan concluded in 2008 that anti-VEGF drugs can show therapeutic efficacy in mouse models of cancer and in an increasing number of human cancers [119].

To understand the process described in this part of the chapter, please refer to Appendix A.3 Protocol for cell culture and regulation using cobalt chloride / cyclohexamide and Appendix A.4 Protocol for DuoSet® ELISA development system to measure human Vascular Endothelial Growth Factor (VEGF). Once the supernatants from each time point have been collected for ELISA analysis, the endometrial cells left in the culture chambers were replicated using Bioimprint technique. Replicas in Figure 6.5 exhibits the membrane behaviours of the cells under the influence of $CoCl_2$ measured during the 24 hours' time course duration. Based on the results, they clearly show that the number of intrusions that resembled the exocytotic pores correlated well with levels of VEGF that were secreted by the cells, resulted from the exocytosis mechanism.

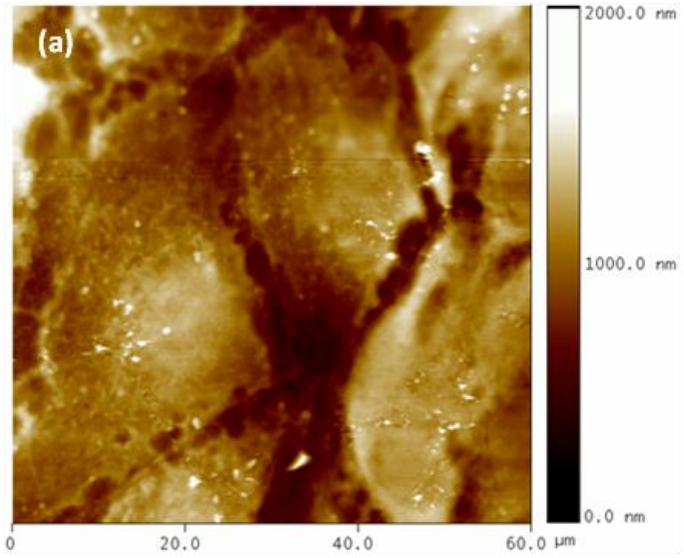
(a)
2000.0 nm
1000.0 nm
0.0 nm
0
20.0
40.0
60.0 µm

(a)

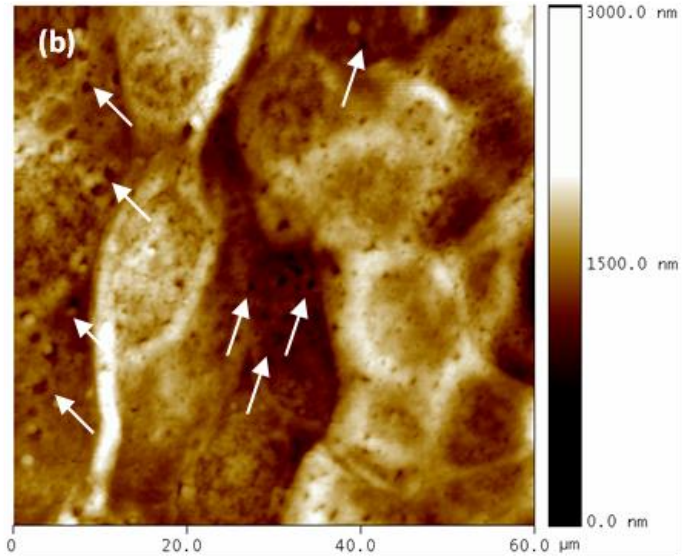
(b)
3000.0 nm
1500.0 nm
0.0 nm
0
20.0
40.0
60.0 µm

(b)

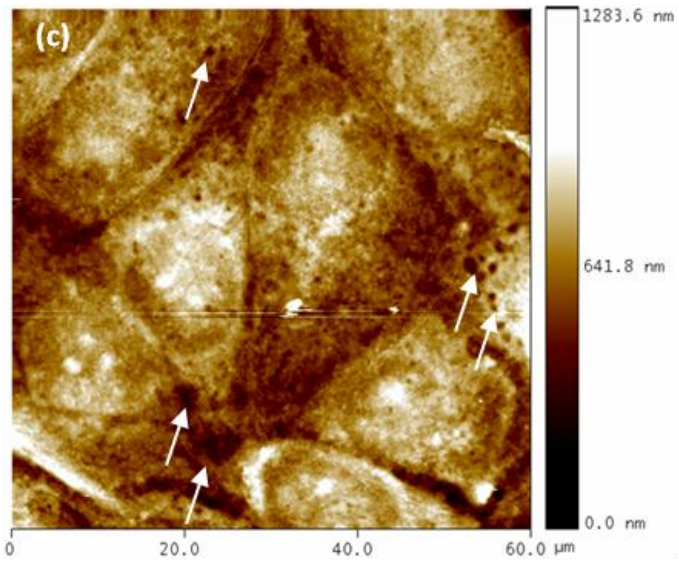

(c)

Figure 6.5: Cells induced by $CoCl_2$ and underwent VEGF time course experiment. (a) Cells after 1 hour; low visibility of pores on surface membranes. (b) Cells after 10 hours; increased number of visible pores on membranes, especially in areas surrounding the nuclei, and (c), cells after 24 hours; slightly lower number of visible pores, which can be due to the VEGF secretion has reached its saturated level.

Pores with bigger openings were highly visible on the membrane surface ((b) and (c)). Higher number of visible pores was achieved after 10 hours $CoCl_2$ treatment and the volume seemed to be slightly lower after 24 hours, which can be due to reasons such as the VEGF secretion has reached its saturated

level, or the exocytosis process of expressing the VEGF proteins was about to finish when the replication was carried out.

6.4 Immunofluorescence with microbeads

Further investigation and analysis using nano-particles as bio-markers were conducted as it was essential to prove that the pores found on the membrane surfaces were actually the granules from the exocytosis mechanism. In this research, an indirect immunofluorescence staining method was deployed in which a secondary antibody labelled with fluorochrome was used to recognize a primary antibody. The secondary antibody, conjugated with Goat anti-rabbit lgG MicroBeads 1 ml with the diameter of 50 nm for each bead were used to identify and isolate granules with possible exocytosis pores on the plasma membrane of the cancer cells.

The Ishikawa endometrial cancer cells were induced with $CoCl_2$ stimulation to monitor whether there was any up-regulation or not of the vascular endothelial growth factor (VEGF) expression. For the experiment, four cell samples were prepared. The first sample consists of control cells that were stained only with primary antibody, while the second sample consists of control cells that were stained only with secondary antibody.

Third sample were prepared for cells induced with $CoCl_2$ and stained with both primary and secondary antibodies, and in the fourth sample, the cells were incubated under normal condition but with staining from both the primary and secondary antibodies. Once they were ready, the culture media was removed and the cells were chemically fixed with 4% paraformaldehyde and dried at room temperature overnight.

Based on the results from this experiment, the anti-VEGF-coated microbeads were observed in the AFM images taken from the fixed cells, and most of the microbeads were found to be attracted to the areas of the pores. The results are demonstrated in Figure 6.6 (a), (b), (c), and (d). In Figure 6.6 (a), AFM image showing cells with low visibility of the nano-particles. Even though the cells were stained with the fluorochrome (microbeads), but because the level of VEGF expression was low, the numbers of exocytosis pores were also insignificant. Figure 6.6 (b) shows higher magnification image without any visible nano-particles near to the cell's nucleus, as compared to later image in (d). In Figure 6.6 (c), the image exhibits the microbeads (*Goat anti-rabbit lgG*) 50 nm in diameter conjugated with secondary antibody which can be distinguished by the bright white colour that surrounds the cell's nuclei. The cells were induced with $CoCl_2$ and stained with primary and secondary antibodies. $CoCl_2$ induced more secretion of VEGF, which then resulted in more pores being formed on the

surface membranes.

Figure 6.6(d) clearly displays the AFM image at higher magnification, showing the microbeads clustering in small protuberances/lumps at certain areas near to the nucleus of the cell (bright colour). The secondary antibody, labelled with fluorochrome (microbeads) was used to recognize the primary antibody. Higher numbers of visible beads would confirmed that there was an up-regulation of the VEGF expression in cells induced with $CoCl_2$, compared to the cells incubated under normal condition (as shown in Figure 6.6 (a) and (b)).

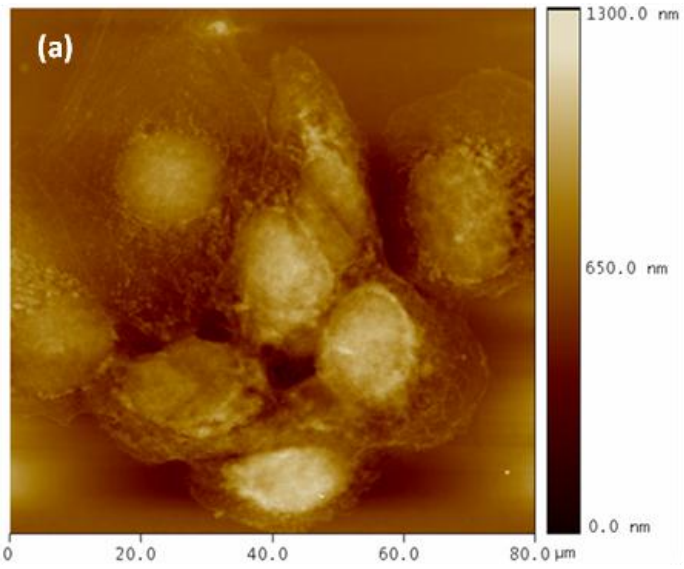

(a)

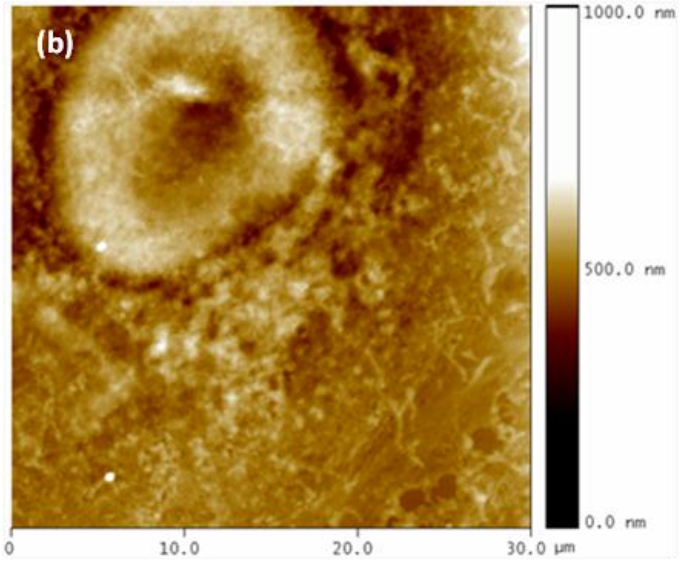
(b)
1000.0 nm
500.0 nm
0.0 nm
0
10.0
20.0
30.0 µm

(b)

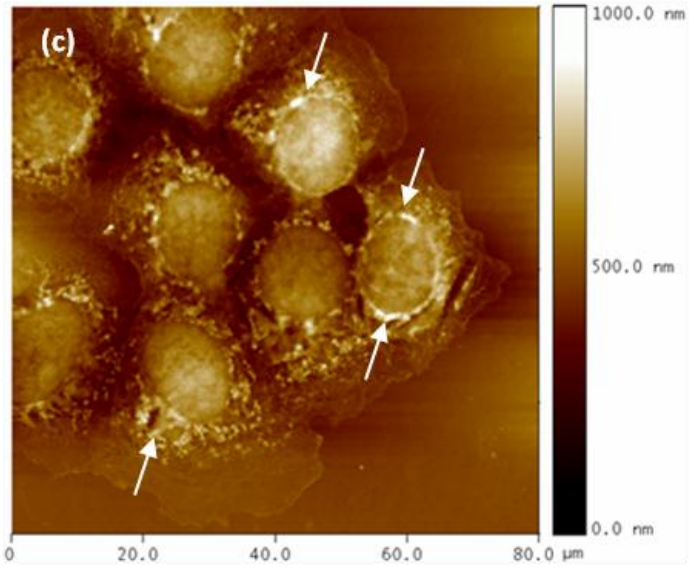
(c)
1000.0 nm
500.0 nm
0.0 nm
0
20.0
40.0
60.0
80.0 µm

(c)

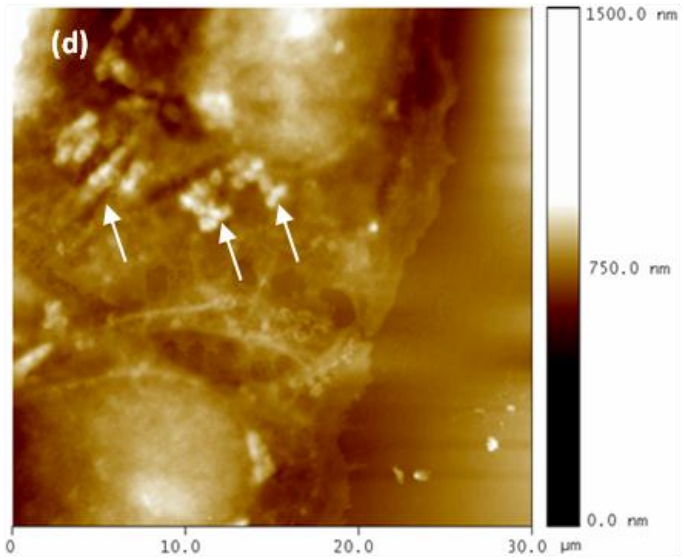

(d)

Figure 6.6: AFM images showing Ishikawa endometrial cancer cells after chemical fixation. Images of (a) and (b) represent cells that were incubated under normal condition (without any stimulation) but with staining from both the primary and secondary antibodies. Images of (c) and (d) represent cells that were induced with cobalt chloride ($CoCl_2$) and stained with primary and secondary antibodies. The cells were stimulated with $CoCl_2$ that induced more secretion of human Vascular Endothelial Growth Factor (VEGF), which then resulted in more pores being formed on the surface membranes.

6.5 Conclusions

The use of a simple UV-initiated coating of a methacrylic acid / ethylene glycol dimethacrylate copolymer allows the formation of an accurate imprint of endometrial cancer cells with features resolved to the nanoscale by use of AFM imaging. There was no evidence of any damage to the imprint from the tip of the AFM probe such as tears or scratches in the imprint. This indicates that the polymer is firm enough to resist abrasion during the microscopic imaging process and thus is suitable for use in imaging cells and their membrane topographies on the nanoscale. Nanoscopic imaging suggests that cellular structures have apparently been retained. This technique that has been developed has further benefits of fast curing, thus minimizing any morphological changes to the cells, ease of use and sufficiently low cytotoxicity. However at present total aspiration of liquid from the immobilized cells is a requirement of imprinting and this may cause some stress to the cells.

The ideal condition for replication is to have the replication material the ability to penetrate into membrane details, pores, depressions and other features, so as to fill out the finest details of the surface to be depicted in the replication. MAA/EDGMA allows this to happen as the imprints permit the

visualization of nanoscale features such as various sizes of intrusions and pores on the surface of the cells.

Minuscule delicate extrusions of molecular fibres can also be seen branching from the cell membrane. These results would suggest that the polymer has succeeded in replicating the intricate and nanoscale cellular structures of the endometrial cells and provides a viable alternative to harsher chemical fixative techniques.

There were some suggestions to take the work further, such as performing quantitative analyses to determine the number of pores in the cells with and without any stimulation, the comparison of AFM images of the cells after fixation and the imprint of the fixed cells and then compare all three quantitatively. Though the idea was good, the suggested experiments can be implemented in future research as it is beyond the scope of this work. Much of this work was intended to demonstrate that the new biopolymer has succeeded in proving the concept.

There are still a lot to learn and explore in relation to secretory vesicle mechanism of cells especially the exocytosis process, which explains how the cells secrete the contents of the vesicle to the extracellular matrix. The hypothesis is that these intrusions are steps on a transitional series of sequential structures that represent either an endocytotic or exocytotic

process. On the other hand, the possibility that these structures have other functions or they are cell permeation artifacts resulting from the polymerization process cannot be ruled out. All these can contribute to expanding the knowledge about exocytosis and fundamental physiology of cells, and also assist in understanding diseases especially cancer.

Chapter 7

Summary remarks & conclusions

In this work, the atomic force microscopy (AFM) was chosen as the main tool for cancer cell investigation as it is one of the most powerful tools for determining the surface topography of biological molecules at nanometer resolution. Unfortunately *in situ* soft cellular structures imaging still remains extremely difficult. To achieve greater results when dealing with soft samples, tapping mode was selected as the image scanning mode to work with. Tapping mode allows high resolution topographic imaging of sample surfaces that are easily damaged, loosely hold to their substrate, or difficult to image by other AFM techniques. Tapping mode overcomes problems associated with friction, adhesion, electrostatic forces, and other difficulties that can plague conventional AFM scanning methods by alternately placing the tip in contact with the surface to provide high resolution and then lifting the tip off the surface to avoid dragging the tip across the surface. Tapping mode imaging is implemented in ambient air by oscillating the cantilever

assembly at or near the cantilever's resonant frequency using a piezoelectric crystal.

AFM offers numerous advantages over other technology such as electron microscopy which include the ability to generate true, 3-D surface images, it does not require special sample treatments that can result in the sample's destruction or alteration, and it does not require a vacuum environment in order to operate (it can operate in both air and liquid). However, AFM does has its own limitations, such as the image size that it provides is much smaller than what the electron microscopes can create, and it is slow in scanning an image, unlike an electron microscopy which does it in almost real-time. Dynamic events of cells such as the exocytosis or endocytosis mechanism that occurs within a few seconds will not be captured in AFM images due to its slow rate of scanning. Furthermore, there are also other problems when operating the AFM which include damaged or contaminated tips (caused by parts of samples of liquid media that stick to them) and lost of resolution such as blurring and undefined edges, due to contamination or the presence of artifacts during the sample scanning.

To solve these issues, a novel method based on a semiconductor fabrication nanoimprint lithography technology was developed, called the Bioimprint^{TM} by our research group in the Electrical and Computer

Department, University of Canterbury, New Zealand. The idea was to replicate the soft biological cells in order to lock their active dynamic events for AFM image scanning. Bioimprint cannot work by itself. It needed a mixture of liquid resist that is biologically inert, with low viscosity that can penetrate deep into the structures and features of the biological samples. In this work, a polymer mixture that is biocompatible and can be cured by UV-light exposure with very fast curing time was developed and tested. The Biopolymer was produced by our group in collaboration with The New Zealand Institute for Plant and Food Research Limited. With Bioimprint technique, the Biopolymer mixture was used to 'freeze' the cells so that snapshots of the biological events could be imaged in real-time. Tests and experimentations have been done to optimise the Bioimprint technique using this Biopolymer. Not only the Biopolymer was able to capture faithful replicas of the living cells, but it also succeeded in forming and producing the first platform of 3-D scaffolds for tissue culture and growth.

Previous work on Bioimprint was implemented using two different elastomeric polymers known as poly (dimethylsiloxane) or PDMS and UV-cured siloxane copolymer to replicate the cells. However due to problems such as prolong curing time, cell deformation and dehydration caused by high temperature exposures, introduction of artifacts resulting from long

UV-irradiation time, and a large number of curing steps that were required to complete the process have initiated the motivation to develop a new polymer to replace the previous ones. Therefore, we have created a new polymer mixture that is biocompatible, has very fast curing time, able to replicate soft cell samples without causing any artifacts, shrinking or expansion of cell structure and has a very simple straight-forward fabrication steps.

In this thesis, the author would like to explain the development of a new Bioimprint technique that utilizes methacrylic acid / ethylene glycol dimethacrylate copolymer to achieve rapid imprinting of nanoscale features of cells. The main chemical compounds of the polymer mixture are triglyme, ethylene glycol dimethacrylate and methacrylic acid. A photo-initiator is used at later stage to promote polymerization reactions in the mixture. The use of methacrylic acid / ethylene glycol dimethacrylate copolymer has the advantages that the polymer will set under UV irradiation within seconds if applied at appropriate volumes and polymerize smoothly around surface features making it potentially useful for application in Bio-imprinting of nanoscale features. Furthermore, it can be spin-coated onto immobilized cells to produce polymer layers of various thicknesses.

Several types of living cells were investigated in this research, such as the L6 rat muscle cell line and the Ishikawa endometrial cancer cell line. These two types of cells were chosen for most of the experiments as they are very strong and tough cell lines, able to proliferate in conditions that may not be suitable for other types of cells. They have higher chances of survival during culturing and incubation, with faster growth and differentiation rates. Other than that, these cells can provide high profiles of topography and morphology features of the cellular membranes compared to other type of cells, such as the anterior pituitary gland cells that regulate several physiological processes including stress, growth and reproduction but cannot divide and multiply themselves. Different periods of cell culture and incubation were tried with various methods and techniques used to get the perfect condition of the cells suitable for the Bioimprint replication process. Longer time was taken to establish the optimum process parameters for applying the Biopolymer to the cells and later to cure it under the UV-light without introducing artifacts or free radicals and destroying the cells by dehydration or shrinkage. Only the best results were presented in this thesis and they can be found in chapters 5 and 6.

Nanoscopic AFM images of the replicated cells suggest that cellular structures have evidently been preserved without showing any effects of

dehydration, shrinking, or structural deformation of the cells topographies and morphologies. Extra-cellular structures like extrusions and fibres demonstrating the existence of ribosome on the cell's membrane. Visible fine micro-fibres on the cell membrane and polysaccharide material that form thin collagen fibrils were able to be reproduced with great accuracy and demonstrated the ability of Bioimprint to fabricate a true and faithful replication of the biological cells. Other forms of cell's topography that were able to replicate are the imprint of membranous structures of a functional single cell surrounding its nucleus. The presence of intrusions on the surface of these membranous structures may suggest they were the results of fusion pores forming on the membranes by under-laying granules during the exocytosis or endocytosis processes. At higher magnifications, structures of craters that resemble granules were visible with a high possibility of finding nano pores formed in these granules.

Exocytosis / endocytosis refer to a process of cellular secretion or excretion in which substances contained in vesicles are discharged from the cell by fusion of the vesicular membrane with the outer cell membrane. It is the active transport of material from the cell's vesicle out into the extra-cellular environment. Many researchers now believe that exocytosis and tumour growth might be linked [120, 121]. There is ample evidence in the

past demonstrating that increased production and resulting secretion of certain growth factors such as VEGF and others can result in oncogenic transformation. VEGF proteins can confer to tumour growth by triggering vessel growth which is a vital part in nutrients supplies to a growing tumour. VEGF expression can be exaggerated with the introduction of cobalt chloride ($CoCl_2$), a chemical compound that will induce higher activity level of growth factor expression, which in turn will increase the number of visible pores on the membrane surface. In this work, further analyses have been done to establish the connection between the VEGF expression and the number of pores formed on the surface membrane. Based on the results (please refer to chapter 6: Bioimprint of cancer cells – Cell structure during VEGF regulation), it is proven that the imprints of the cells showed the number of pores increased significantly on the stimulated cells when compared to those on the un-stimulated or controlled condition cells.

In this work, another unconventional step of experiment was carried out that can have huge impact in the biological study field. The experiment was designed to investigate and determine the nanopores formed on the surface membrane of the cells and their connection to the exocytosis process. To achieve this, functionalized microbeads were used to tag the pores. AFM images of these cells clearly show the microbeads were clustered in small

protuberances / lumps at certain areas near to the nucleus of the cell. Higher numbers of visible beads would confirm that there was an up-regulation of the VEGF expression in cells induced with $CoCl_2$, compared to the cells incubated under normal condition.

VEGF expression by the cells can induce numerous reactions, for example, it may cause a cell to stay alive, shift places, or further differentiate to form other types of tissues. However, over expression of VEGF can cause cardiovascular disease, primarily affecting the blood vessels. When there is an insufficient blood supply to the cell, cell growth will be affected, causing the cell to start the apoptosis process and then eventually dies. The success of proving this hypothesis will lead to the development of drugs or other type of medications that are capable of treating the cancer in this manner. Hence, VEGF growth factor has emerged as one of the promising therapeutic target in the treatment of cancer in patients around the world.

Other aspect of this project that was being pursued during the early stage of the development work was the design and fabrication of the Biochip platform. Initially, the intention of the research scope was to develop a Biochip that can work to manipulate cells movement and trapping them at certain locations with easy identifiable markings. The idea was to

have a platform that can be used for AFM image analyses of biological cells with better handling and ease of use. After the development and fabrication of numerous Biochip design schemes, it was decided not to pursue this aspect of research further, but to concentrate on developing the Bioimprint technique and try to get better results from the replications of the muscle and cancer cells. The design and fabrication of the Biochip was passed on to another postgraduate student who would concentrate on developing and solving the problems related to the manipulation and trapping of cells using the electrodes platform.

7.1 Recommendation for future work

Pre-patterned 3-D scaffolds for cell-culture with imprinted cell footprints is one of the area that looks promising and can offer a lot of interesting ideas and innovations, especially the ones that have significant impacts in medical and clinical laboratory fields. The fabrication of 3-D scaffolds for tissue implants in the biomedical engineering will lead to better addressing the cell adhesion problem that has been going on for sometimes now.

There is also another possibility of developing further the Biopolymer to become a biologically inspired material that can imitate the embryonic microenvironment, which then can be used to induce cancer cells

to revert into normal tissues. This is similar to try to ‘reset’ the cells to their original conditions before they became cancerous.

The integration of Bioimprint and microfluidics system is also another area of interest that can be explored further. To adopt the microfluidics system for the Biopolymer delivery is very useful especially for the formation of cell-culture scaffolds. The integrated system can significantly simplifies sample handling and further reduces the time-span between application and polymer curing, hence enabling the chance to better replicate the momentaneous dynamic events of cells biological mechanisms and processes. This work will help in the investigation and to further understand the effects of various cancer drugs on the cellular topography, as well as that of imprinted surface features on cell development.

7.2 Conclusions

The use of the Biopolymer in the Bioimprint technique has shown tremendous results in replicating the minuscule structures of cells like the rat muscle cells and the Ishikawa endometrial cancer cells. The imprints were able to faithfully capture the true features of topography and morphology of these cells without destroying their structures during the polymerization

process. Furthermore, with its fast curing time of less than 15 seconds, snapshots of the dynamic exocytosis events were able to be captured in these replicas. With this Biopolymer, artifacts and free radicals were able to be eliminated from the imprints as the polymer was cured within seconds and the polymer mixture cross-linked each other under the UV-light at least 15 minutes after the polymerization has started.

Using Bioimprint, the relationship between exocytosis mechanism and VEGF expression were able to be proven. It is now understood that the up-regulation of the expression of VEGF proteins will lead to the increase of the exocytosis activity in the cell, which resulted in the increase number of visible pores on the cell's membrane. The VEGF expression can be induced by applying certain compound such as cobalt chloride ($CoCl_2$) to the targeted cells. It was also proven that these pores are actually the exocytosis pores by using functionalized microbeads conjugated with different types of antibodies that were attracted to certain areas of the cell's membrane based on the attraction of the antibody to the hormones released by the cell during the exocytosis process. These results and findings were backed by the AFM image analyses obtained through the scanning of the cells' imprints and from cells acquired using the chemical fixation technique.

Appendix A

Appendix

A.1 Rat Cell Culture Protocol

The following details the protocols, reagents, culture medium, and rules used for the preparation, dispersion and incubation of rat pituitary gland cells before the start of each laboratory session.

A.1.1 Laboratory Rules

1. Cells from other laboratories are not allowed to be brought into the department's facility.
2. Work should be conducted in designated hood and only use department's own incubator. If a shared hood is occupied by another user, the booking list should be checked for the availability of another hood.
3. UV light must be turned on at least 15 minutes prior to using the hood and before commencing any work; the hood should be wiped down with 70% ethanol.

4. Reagents, medium, plastic ware or other laboratory equipment used inside the hood must be sprayed with 70% ethanol, especially reagents or medium which are being removed from the water bath, centrifuge and the refrigerator.
5. Only use self-prepared reagents, medium and Pasteur pipettes. Aliquot small amount of medium in a separate smaller container each time before use to prevent any contamination to the main medium.
6. After the experiment has finished, the hood must be cleaned and wiped down with 70% ethanol, and any glass pipettes and other disposable plastic ware must be thrown away in designated biological waste bins.
7. Temperature, water and carbon dioxide (CO_2) levels in the incubator must always be checked and monitored.

A.1.2 Reagents

Dispersion medium for cell culture and incubation.

1. 50 ml DMEM (Gibco cat. No. 10569-010) which includes 0.11 g Na pyruvate, 4500 mg/L glucose and GlutaMAX.
2. 0.18 g HEPES (Sigma H9136)
3. 0.15 g BSA (Bovine Serum Albumin)
4. 0.4 ml Penicillin/Streptomycin (Gibco cat. No. 15140-148)

5. 0.4 ml Fungizone

Everything was mixed and shaken well inside a 100 ml sterilized container. A syringe (60 cc) and Mullex GP 0.22 µm filter were used to filter out the medium and placed inside a new sterilized container. pH was adjusted to meet the range of 7.2 - 7.4 (red or slightly orange in colour).

Solution A – Digestion solution

1 pituitary	***15 – 20 pituitary***	***Type of media***
1 ml	15 ml	Dispersion medium
120 µl (3 mg)	1.8 ml (45 mg)	Trypsin [a]
20 µl (1 mg)	300 µl (15 mg)	DNase [b]

Table A.1.1: Digestion solution for different volume of cell concentration

[a] (GIBCO cat.No.15090;2.5 mg/100ul)
[b] (Sigma cat. No. DN-25 from bovine Pancreas; 10 mg/200µl PBS-phosphate buffer solution)

Pepsol

The following were mixed and refrigerated:

0.1 ml Pepsol, 0.1 M HCl, 99.9 ml DIW, 0.1 g BSA (Gibco cat. No. 30063-572).

DNase preparation

For 10 mg of DNase, 200 µl of Pepsol was needed, and for 1 mg, 20 µl of Pepsol need to be used, which was for 20 tubes. To prepare the 20 tubes, 20 mg of DNase and 400 µl of Pepsol were needed. Small Eppendoft tubes (0.5 µl) with colour coding were used and the following information was written on the tubes.

1. Solution labels (ex: DNase, Tripsin, Tripsin Inhibitor etc)
2. Weight (mg, g etc)
3. Volume of diluted solution (20 ul, 40 ul etc)
4. Date (ex: 130310)

Weight scale was used to get the right amount of powder etc. Then, the solution was diluted with Pepsol inside a larger Eppendoft tube (this was done in the hood). A small amount of the DNase was taken (ex: 20 µl) using a micro pipette and stored in a smaller Eppendoft tube (100 µl).

Solution B – Trituration solution

1 pituitary	*15 – 20 pituitary*	*Type of media*
5 ml	75 ml	Dispersion medium
10 mg	150 mg	Trypsin inhibitor [a]
20 µl (1 mg)	300 µl (15 mg)	DNase [b]

Table A.1.2: Trituration solution for different volume of cell concentration

[a] (Sigma T9128; Type II-S – *Solid form*)
[b] (Sigma cat. No. DN-25 from bovine Pancreas; 10 mg/200µl PBS-phosphate buffer solution)

A.1.3 Culture Medium

M199 Culture medium

Volume (ml)		*Type of reagents*
2.2 g	$NaHCO_3$	Sodium Bicarbonate
5.95 g	HEPES	N-2-Hydroxyethylpiperazine-N'-2-Ethanesulfonic Acid
1 g	BSA	Bovine Serum Albumin
10 ml	Pen/Strep	Penicillin/Streptomycin (Gibco)
990 ml		Distilled water

Table A.1.3: M199 culture medium

1 packet powdered medium M199 (Invitrogen, contains Earle's salts with L-glutamine but not sodium bicarbonate) was used and everything except BSA was mixed in a beaker. BSA was sprinkled on the surface and let dissolved slowly. pH was then adjusted to be between 7.2 – 7.4. Later it was sterilized using Millipore Steritop disposable bottle top filter with 0.22 uM GP Express PLUS membrane and stored 4º C for further use.

Oestradiol (Sigma Cat. No. E2758)

A stock solution of 100 µg/ml in absolute ethanol was made up and stored at 4ºC. Final concentration of 300 pg/ml of M199 was then diluted directly prior to use (333 x dilutions). Whenever 'spiking' M199 was visible in wells (600 µl), 30 µl of 6.3 µg/ml estradiol was added to each well.

GnRH (Gonadotropin-Releasing Hormone) (Peninsula Labs LH-RH no. 7201)

10^{-4} mol/L of stock solution was made up by dissolving 1 mg in 10 ml distilled water and later stored frozen and aliquotted. It was then diluted in M199 to final dilution of 10^{-8} mol/L. Whenever 'spiking' M199 was visible in wells (600 µl), 30 µl of 2 x 10^{-7} mol/L GnRH was added to each well.

(*Note: could try 10^{-9} M final concentration...4 x 10^{-9} M gave LH levels of 50–100 ng/ml*).

A.1.4 Protocols

Surgical Operation (on rats) Procedure.

1. The small theatre room must be booked for the operation before use and the rats were available for the experiment.
2. The halothane gas was turned on and the pressure was set within 3 to 4 (on the scale bar). The oxygen valve was turned to the value of 3-4. The gas container and the guillotine were placed at the right place.
3. The desirable rat was then chosen and brought to the gas container. It was anesthetised with halothane + oxygen gas. When the rat was already unconscious, it was put under the guillotine and its head was decapitated around the neck.
4. The neck muscle was then removed and the upper part of the skull was cut. The brain was slowly lifted up and removed from the skull. Anything underneath the brain must not be touched.

5. Membrane that covers the pituitary glands was pulled carefully, while maintaining the pituitary glands intact. The posterior pituitary gland was removed slowly and then the anterior pituitary gland was taken away. It was put inside a mini-tube that contained 1 ml of suspension medium.

Dispersion Procedure.

1. Pituitary gland was removed using Kahn tubes and tops. It was then placed in dispersion medium (approx 1 ml) in an Eppendorf tube.

2. The pituitaries were later placed in a small (~7 cm diam) sterile petri dish in ~1 ml dispersion medium and cut into small (~0.5 mm) pieces with No. 24 scalpel blade. Sterile Pasteur pipette was used to transfer pituitaries and moisture was maintained using dispersion medium while cutting. The cells were then centrifuged at 2000 rpm at 4ºC for 5 minutes (in Eppendorf minifuge).

3. The cells were resuspended in digestion solution[1] (Solution A) (2 ml/~2 pituitaries; 5 ml/~7 pituitaries; 8 ml/~15 pituitaries).

4. The tube with the cells was shaken (manually) at 37ºC in the water bath for 20 minutes until pieces looked broken up.

5. They were then centrifuged 2000 rpm at 4ºC for 5 mins.

6. The supernatant was then taken out from the suspension.

7. Next, the cells and pieces were resuspended in 1 ml of the Trituration solution[1] (Solution B) (10 ml/~2 pituitaries; 5 ml/~7 pituitaries; 8 ml/~15 pituitaries).

8. A 1 mol syringe and gauge needle size 18 was used to triturate the cells repeatedly for 2 minutes*.

9. The pieces were allowed to settle and the supernatant was collected afterwards.

10. Trituration was repeated once more with 1 – 2 ml, then approx twice with 0.5 – 1 ml volumes of solution until all the cells were collected without any tissue remained in the tube.

11. The pieces were filtered with Falcon 40 µm cell strainer and centrifuged at 2000 rpm at 4 ºC for 5 min. Then the supernatant was taken away.

12. Cells were resuspended in M199 – culture medium (begun with 0.5 ml/pituitary). One drop of cells was placed on the haemocytometer.

* Trituration technique was repeated again here.

- This procedure was for 6 well plates with 6 glass cover slips. It included 2 ml of Tripsin and 2 ml of DNase. The cover slips must be dipped and cleaned in a 70% ethanol. They were leaned against the cultured dish to dry.

Counting using haemocytometer

Formula for converting counts to cells/ml:

Cells in one large corner square (contains 16 smaller squares) = $\mathbf{c^1}$

Cells in each of the other large corner squares = $\mathbf{c^2}$, $\mathbf{c^3}$, $\mathbf{c^4}$

Average = ($\mathbf{c^1}$ + $\mathbf{c^2}$ + $\mathbf{c^3}$ + $\mathbf{c^4}$) / 4 = **c**

Cells /ml = **c** x 10^4

Viability count was done by adding equal volumes of cell suspension and Trypan blue solution, and then the percentage of dead cells was counted.

Cell preparation for 6 well plates

The cells were resuspended in 7 ml M199 (culture medium) and the dilution was then doubled. 2 ml per well were added, followed by adding 3 ml of M199, to double the dilution. 2 ml per well were added to the suspension and

then followed by adding another 3 ml of M199 for double dilution. To finish up the medium, another 2 ml per well were added. Lastly, after 1 hour, FBS 10% solution was added inside each well.

Culturing to study LH release

(All at 37 ºC in incubator)

Day 1*:* Cell concentration was adjusted to 0.3 – 0.5 million cells/ ml in M199. 500 µl/well was added to Falcon 48-well tissue culture coated plates *(Note: this could be scaled down to 96-well plates)*. 1 hour was given for cells to settle and attach, then 50 µl fetal calf serum was added (i.e. 10%).

Day 3*:* Estradiol treatment was started as required (spike wells or renew M199/FCS).

Day 5*:* Media was removed and fresh serum-free M199 was added for 1 hour, maintaining estradiol treatments. Meanwhile, GnRH etc. solutions were prepared for next steps so that they can be added quickly. New serum-free M199 spiked was added with GnRH or other test compounds for 3 hour. The supernatant was collected and frozen at -20 ºC for LH radioimmunoassay. Cells must not let to dry during these procedures. It is sometimes useful to pipette off less than nominally in the supernatant (e.g. if the supernatant is 600 µl then take the supernatant with a pipette set at 550

µl). Also do not remove supernatants from all the wells in one set; rather collect, for example, 3 supernatants, add the next media, then take another 3, and add, and continue.

A.2 Protocol for cancer cell culture and cloning

The following details the protocols, reagents, and culture medium used for the preparation, dispersion and incubation of Ishikawa endometrial cancer cells before the start of each laboratory session.

A.2.1 Reagents

Phosphate Buffered Saline (PBS) 10x

The following reagents were mixed:

80.0 g NaCl, 11.5 g Na_2HPO_4, 2.0 g KCl, and 2.0 g KH_2PO_4 were all dissolved together in 1 l miliQ H_2O with concentration of 10x. When all reagents were finally dissolved, the pH was adjusted to 7.4 using concentrated NaOH or HCl and later kept at room temperature.

A.2.2 Culture medium

Minimum Essential medium alpha Medium (α-MEM)

950 ml of distilled water was measured out into a 1 l Schott bottle that had been washed and autoclaved. To this, the powdered medium was added. Distilled water was then used to rinse the packet, and remove any remaining

traces of medium powder. $NaHCO_3$ was then added, followed by Penicillin Streptomycin and fungizone. Solution was next made to 1 l with distilled water. Solution was then stirred with a magnetic stirring bar. pH of the solution was adjusted to 7.4 using concentrated NaOH or HCl which were added slowly while stirring. Solution was then filtered into another sterile, autoclaved 1 l Schott bottle using a vacuum filter Vacucap 0.2 µm. This was done under aseptic conditions in the cell culture hood. α-MEM was stored at 4 ºC until required.

α-MEM culture medium

Volume (ml)		***Type of reagents***
1 packet		Minimum Essential Medium alpha Medium [a]
2.2 g	$NaHCO_3$	Sodium Bicarbonate [b]
4 ml		Fungizone
10 ml	Pen/Strep	Penicillin/Streptomycin (Gibco)
950 ml		Distilled water

Table A.2.1: α-MEM culture medium

[a] (Gibco cat. No.11900-024 with Glutamine, ribonucleosides , and deoxyribonucleosides)
[b] (Sigma 500 g S-5761)

A.2.3 Protocol

Ishikawa cancer cell line preparation for cell culture in flask

Cells were obtained from the Cyrovial (stored in the freezer cabinet with plastic coloured boxes). The cells must be kept in -80ºC freezer or in Liquid Nitrogen. Cell dispersion was carried out under aseptic conditions. They were prepared in a laminar flow cell culture hood (EMAIL Air Handling Biological Safety Cabinet Class II). All glassware used for cell preparation was autoclaved before use and together with all the solutions were sterilized with ethanol.

All cells (in the cyrovial) and solutions were first pre-warmed to 37ºC before use. The culture medium used is called Minimum Essential Medium α Medium (α-MEM) that has been added with a 10% of Fetal Bovine Serum Medium. Once the cells were ready, they were transferred into culture flasks (50 ml with carted neck) and 10 ml of the α-MEM was added in each flask. Then they were stored in the incubator (37 ºC, 0.5 % CO_2) for at least 1 – 2 days (to allow the cells to adhere to the surface). The medium should be changed after 1 - 2 days and thus, was replaced with another 10 ml of (α-MEM + FBS 10%).

Ishikawa Cells Separation

When cells reached a confluent state, they were split in preparation for further use. Cultures that had become confluent were then placed in the cell culture hood, where the cell culture media was removed by aspiration. 10 ml of Phosphate Buffered Saline (10x PBS pH 7.4) that had been pre-warmed to 37 ºC was then used to wash the cells. The PBS was then removed and the wash step was repeated twice more. Following the final aspiration of the PBS from the flask, 2.5 % trypsin♦ in PBS was added to the cells (2 ml for big flask, less volume for smaller ones < 1 ml or less). The trypsin was checked to cover the whole cells area. The flask was then put inside the incubator and was observed for every 10 minutes to see whether the cells had already detached from the surface. Cells were dislodged by light tapping on the side of the flask.

The spilt cells then were transferred into a larger multi-welled or culturing plate for different experiments. 10 ml of α-MEM was added to the cell suspension in the flask, and the cells and the media were then transferred into a 15 ml Falcon tube. Cells were evenly dispersed through the media by light tapping on the outside of the tube. A small sample of the cell suspension was then removed, and used to perform a cell count with a haemocytometer. Next, the cells were centrifuged at 1500 rpm for 5 minutes

at room temperature. After that, the supernatant was aspirated and the media (α-MEM + FBS 10%) was then added at a volume dependent on the cell count performed earlier, the size of the plate and the concentration of cells required. The plate was then stored in the incubator for 2 – 6 days depending on the type of experiments the cells were going to be used.

- Trypsin was used to chew the proteins that hold the cell to the surface. This helped to detach the cell but it was not a "happy situation" for them. The cells had sphere formation.

A.3 Protocol for cancer cell culture and regulation using cobalt chloride/ cyclohexamide

The following details the protocols for the preparation, dispersion and incubation of Ishikawa and RL95-2 endometrial cancer cell lines for regulation using cobalt chloride and cyclohexamide. Reagents and culture medium used were the same as those described in section A.2: Protocol for cancer cell culture and cloning.

A.3.1 Reagents

Cyclohexamide

Cyclohexamide was prepared from the stock solution (could only be used after at least 10 minutes it was prepared). Work was done using autoclave Eppendoft tube and in the culture hood. Cyclohexamide concentration used was 0.01 $m\mathcal{M}$.

$$c_1 v_1 = c_2 v_2$$

$$0.5\ m\mathcal{M}.\ v_1 = 0.01\ m\mathcal{M}.\ 500\ \mu l$$

$$v_1 = \frac{c_2 v_2}{c_1} = \frac{0.01\ m\mathcal{M}.\ 500\ \mu l}{0.5\ m\mathcal{M}} = \mathbf{10\ \mu l}$$

$\therefore$ 10 $\mu l\ of\ cyclohexamide\ was\ taken\ and\ added\ to$ 490 $\mu l\ of$ αMEM (**1**)

0.5 $m\boldsymbol{\mathcal{M}}\ was\ the\ stock\ solution\ concentration$

0.01 $m\boldsymbol{\mathcal{M}}\ was\ the\ concentration\ used\ for\ cell\ regulation$

500 $\mu l\ was\ the\ volume\ of\ suspension\ for\ each\ chamber$

Cobalt chloride

Cobalt chloride was prepared from the stock solution. Work was done using autoclave Eppendoft tube and in the culture hood. Cobalt chloride concentration used was 0.2 $m\boldsymbol{\mathcal{M}}$.

$$c_1 v_1 = c_2 v_2$$

$$8.38\ m\boldsymbol{\mathcal{M}}.\ v_1 = 0.2\ m\boldsymbol{\mathcal{M}}.\ 500\ \mu l$$

$$v_1 = \frac{c_2 v_2}{c_1} = \frac{0.2\ m\boldsymbol{\mathcal{M}}.\ 500\ \mu l}{8.38\ m\boldsymbol{\mathcal{M}}} = 11.9\ \cong \mathbf{12}\ \boldsymbol{\mu l}$$

$\therefore$ 12 $\mu l\ of\ cobalt\ chloride\ was\ taken\ and\ added\ to$ 488 $\mu l\ of$ αMEM (**2**)

8.38 $m\boldsymbol{\mathcal{M}}\ was\ the\ stock\ solution\ concentration$

0.2 $m\boldsymbol{\mathcal{M}}\ was\ the\ concentration\ used\ for\ cell\ regulation$

A.3.2 Protocol

Ishikawa cancer cell line preparation for cell culture in Lab-Tek™ Chamber Slide™ system

Cells were obtained from the flask (incubated in incubator 37 °C). Culture medium and other solutions (α-MEM, PBS pH 7.4, Trypsin) were prepared before use. The medium was aspirated from the flask using sterilized Pasteur pipette. The cells were washed with PBS solution (± 20 ml), while making sure the cells were covered all over. This was done for about 30 – 40 sec (repeated for 3 times).

2 ml of Trypsin was added (for big flask, less volume for smaller ones < 1 ml or less) by making sure all the cells area were covered. It was put inside the incubator and checked for every 10 minutes to see whether the cells has already detached from the surface. 3 ml of culture medium was added to the flask and the suspension was aspirated before being put into a 15 ml Falcon tube. The suspension was diluted by adding another 5 ml of culture medium to make up the volume to 10 ml. The tube was spun for 15 minutes with 3000 rpm. 100 µl of the cells were taken (with slight tap on the tube to dislodge the cells) and put into an Eppendoft tube. 25 µl of the cells were taken for cell counting using hemocytometer technique.

For cell culturing, at least 2 x 10^5 cell/well (200 000 cells) were needed. From the cell concentration, the volume of cell medium needed for each slide chamber was calculated. An example on how to obtain the cell volume is shown below:

$$Cell/ml = \frac{No.of\ cells\ .\ 25\ x\ 10^4.\ DF}{25\ (No.of\ boxes)}$$

$$Cell/ml\ = \frac{64\ .\ 25\ x\ 10^4.\ 2}{25}$$

$$= \mathbf{1.28\ x\ 10^6\ cell/ml}$$

At least 2 x 10^5 cell/well, and 1.28 x 10^6 cells per 1 ml were needed. The cell volume for each chamber was, *x* and calculated by:

$$x = \frac{2\ x\ 10^5.1\ ml}{1.28\ x\ 10^6}$$

$$x = \mathbf{160\ \mu l\ for\ each\ chamber}$$

For each chamber, 160 µl from the cell suspension was mixed with 340 µl of α-MEM medium. Then the cells were stored in the incubator (37 ºC, 0.5 % CO_2) for at least 1 – 2 days to allow the cells to attach to the surface and grow until the confluent reached at least 70% confluent.

Cell regulation using cobalt chloride and cyclohexamide

Once the cells had reached the suitable confluent, the chamber slides were taken out from the incubator and put inside the culture hood ready for cell washing. The medium from each chamber was aspirated and the cells were washed using 1x PBS buffer solution and repeated at least 3 times. Then, the exact amount of cyclohexamide (**1**) and cobalt chloride (**2**) were added together with α-MEM (without FBS) into each chamber. Chambers designated for control cells were excluded from any addition of either cyclohexamide or cobalt chloride reagent.

Cells were then stored in the incubator (37 ºC, 0.5 % CO_2) for 24 hours before the supernatants were collected and stored in -4 ºC for ELISA test later on. The cells were washed once using 1x PBS and was then aspirated with Pasteur pipette tips at the extreme edges of the chambers (with the intention not to destroy any cells on the surface). Once the surface of the slides was dry enough, the cells were ready to be replicated by the means of the Bioimprint replication process.

A.4 Protocol for DuoSet® ELISA development system to measure human Vascular Endothelial Growth Factor (VEGF)

The following details the protocols, reagents, and antibodies used for the preparation and experimentation using ELISA development system.

A.4.1 Reagents

Solution provided

The ELISA development kit contains *Capture Antibody*, *Detection Antibody*, *Standard* (human VEGF), and *Streptavidin-HRP*.

Capture Antibody (Part 841495)

- Reconstituted in 1.0 ml of PBS to make up a final concentration of 180 µg/ml mouse anti-human VEGF. Stored at 2 – 8 ºC.
- The antibody was diluted to working concentration of 1.0 µg/ml in PBS, without carrier protein. Made up in a 10 ml aliquot which contained 10 µg total ***Capture Antibody*** (final: 1.0 µg/ml) and stored in freezer.

Detection Antibody (Part 840163)

- Reconstituted in 1.0 ml of ***Reagent Diluent*** (PBS with 1% BSA) to make up a final concentration of 18 µg/ml biotinylated goat anti-human VEGF. Stored at 2 – 8 ºC.
- The antibody was diluted to working concentration of 100 ng/ml in ***Reagent Diluent***. Made up in a 10 ml aliquot which contained 1 µg total ***Detection Antibody*** (final: 100 ng/ml) and stored in freezer.

Standard (Part 840164)

- Reconstituted in 0.5 ml of ***Reagent Diluent*** (PBS with 1% BSA) to make up a final concentration of 120 ng/ml recombinant human VEGF. Stored at 2 – 8 ºC.
- Aliquot in freezer (110 µl) to get 10,000 pg/ when reconstituted in 1 ml ***Reagent Diluent***.

Streptavidin – HRP (Part 890803)

- 1.0 ml of streptavidin conjugated to horseradish-peroxidase and stored at 2 – 8 ºC.

Solution required

Phosphate Buffered Saline (PBS) 10x

The following reagents were mixed:

80.0 g NaCl, 11.5 g Na_2HPO_4, 2.0 g KCl, and 2.0 g KH_2PO_4 were all dissolved together in 1 l miliQ H_2O with concentration of 10x. When all reagents were finally dissolved, the pH was adjusted to 7.4 using concentrated NaOH or HCl and later kept at room temperature.

Wash Buffer (R&D Systems cat. No. WA126)

The solution contained 0.05% Tween in PBS. It was prepared by mixing 100 ml 10x PBS, 500 µl TWEEN® 20, and 1 l distilled water. pH was adjusted to 7.4.

Reagent Diluent (R&D Systems cat. No. DY995)

The solution was made up from 1% BSA in PBS, which was filtered through 0.2 µm filter. pH was adjusted to 7.4.

Substrate Solution (R&D Systems cat. No. DY999)

1:1 mixture between Colour Reagent A (H_2O_2) and Colour Reagent B (Tetramethylbenzidine). Stored in brown bottle in freezer and must not be exposed to light.

Stop Solution (R&D Systems cat. No. DY994)

2 N H_2SO_4 – Stored in bottle on bench.

A.4.2 Protocol

Day 1

1. One aliquot of ***Capture Antibody*** was diluted to the working concentration in 10 ml of PBS.
2. Each well of a 96 well microtitre plate was immediately coated with 100 µl of ***Capture Antibody***.
3. The plate was sealed with tin foil and incubated overnight at room temperature.

Day 2

1. Contents of plate were flicked into sink, and then were washed with ***Wash Buffer*** and the flicking/washing step was repeated twice for a

total of three washes. After the last wash, the remaining ***Wash Buffer*** was removed by aspirating or inverting the plate and blotting it against clean paper towels.

2. Plates were blocked by adding 300 µl of ***Reagent Diluent*** to each well. The plates were sealed with tin foil and incubated for 1 hour at room temperature.
3. Flicking/washing step was repeated again here (three washes). The plates were ready for sample addition at this stage.

Assay Procedure

1. 100 µl of sample or standards in ***Reagent Diluent*** was added to each well, then sealed with tin foil and incubated for two hours at room temperature.
2. Flicking/washing step was repeated again here (three washes).
3. 100 µl of ***Detection Antibody***, diluted in ***Reagent Diluent*** was added to each well. The plates were sealed with tin foil and incubated for 2 hours at room temperature.
4. Flicking/washing step was repeated again here (three washes).
5. 100 µl of ***Streptavidin – HRP***, diluted to working concentration ($1/200$ dilution rate factor in $\boldsymbol{Reagent\ Diluent}$) was added to

each well. The plates were sealed with tin foil and incubated for 20 minutes at room temperature.

6. Flicking/washing step was repeated here (three washes).
7. 100 µl of ***Substrate Solution*** was added to each well and the plates were sealed with tin foil and incubated for 20 minutes at room temperature.
8. 50 µl of ***Stop Solution*** was added to each well. The optical density of each well was determined immediately using a microplate reader. The reading was set at 450 nm. If wavelength correction was available at that time, the optical density should be set to 540 nm or 570 nm (should be done as part of the plate reader template).

Reference

[1] Y. F. Dufrene, *Properties of microbial cell surfaces examined by atomic force microscopy*. New Jersey: John Wiley & Sons, 2006.

[2] T. H. F. Papanicolaou G.N., *Am.J.Obstet.Gynecol.,* vol. 42, p. 193, 1941.

[3] L. Hamby, *Cancer Genetics News,* vol. 4, 2002.

[4] E. D. Lewis BA, "Lipid bilayer thickness varies linearly with acyl chain length in fluid phosphatidylcholine vesicles," *J.Mol.Biol,* vol. 166, pp. 211-217, May 1983.

[5] B. J. Zaccai G, Schoenborn BP, "Neutron diffraction studies on the location of water in lecithin bilayer model membranes," *Proc.Natl.Acad.Sci. U.S.A,* vol. 72, pp. 376-380, January 1975.

[6] T. J. Beveridge, Graham, L.L., "Surface layers of bacteria," *Microbiol Rev,* vol. 55, pp. 684-705, 1991.

[7] N. Mozes, Handley, P.S., Busscher, H.J., Rouxhet, P.G., *Microbial Cell Surface Analysis: Structural and physicochemical methods*. New York: VCH Publishers, 1991.

[8] G. Binnig, Quate,C.F., Gerber, C., "Atomic Force Microscope," *Phys.Rev.Lett.,* vol. 56, pp. 930-933, 1986.

[9] H. X. You and L. Yu, "Atomic force microscopy imaging of living cells: progress, problems and prospects," *Methods in Cell Science*, vol. 21, pp. 1-17, 1999.

[10] W. Haberle, J. K. H. Horber, and G. Binnig, "Force microscopy on living cells," in *Fifth international conference on scanning tunneling microscopy/spectroscopy*, Boston, Massachusetts (USA), 1991, pp. 1210-1213.

[11] S. Kasas, Ikai,A., "A method for anchoring round shaped cells for atomic force nicroscope imaging," *Biophys.J.*, vol. 68, pp. 1678-1680, 1995.

[12] Y. F. Dufrene, Boonaert,C.J.P.,Gerin,P.A.,Asther,M.,Rouxhet,P.G., "Direct probing of the surface ultrastructure and molecular interactionsof dormant and germinating spores of Phanerochaete chrysosporium," *J.Bacteriol*, vol. 181, pp. 5350-5354, 1999.

[13] A. Garg and E. Kokkoli, "Characterizing particulate drug-delivery carriers with atomic force microscopy," *Engineering in Medicine and Biology Magazine, IEEE*, vol. 24, pp. 87-95, 2005.

[14] J. Dubochet, M. Adrian, J. Lepault, and A. W. McDowall, "Emerging techniques: Cryo-electron microscopy of vitrified biological specimens," *Trends in Biochemical Sciences*, vol. 10, pp. 143-146, 1985.

[15] Y. Fujiyoshi, "The structural study of membrane proteins by electron crystallography," *Advances in Biophysics*, vol. 35, pp. 25-80, 1998.

[16] K. Mohamed and M. M. Alkaisi, "Three-dimensional pattern transfer on quartz substrates," *Microelectronic Engineering*, vol. 87, pp. 1463-1466, 2010/8// 2010.

[17] S. V. Sreenivasan, C. G. Willson, N. E. Schumaker, and D. J. Resnick, "Cost of ownership analysis for patterning using step and flash imprint lithography," in *Emerging Lithographic Technologies Vi, Pts 1 and 2*. vol. 4688, R. L. Englestad, Ed., ed Bellingham: Spie-Int Soc Optical Engineering, 2002, pp. 903-909.

[18] S. Murthy, M. Falcon, S. V. Sreenivasan, and D. Dance, "S-FIL (TM) technology: Cost of ownership case study," in *Emerging Lithographic Technologies IX, Pts 1 and 2*. vol. 5751, R. S. Mackay, Ed., ed Bellingham: Spie-Int Soc Optical Engineering, 2005, pp. 964-975.

[19] R. Allan. (2005). *Nano-inprint lithography to the rescue*. Available: http://www.elecdesign.com/Articles/Index.cfm?AD=1&ArticleID=10816

[20] V. N. Truskett and M. P. C. Watts, "Trends in imprint lithography for biological applications," *Trends in Biotechnology*, vol. 24, pp. 312-317, 2006.

[21] Y. Xia and G. M. Whitesides, "Soft Lithography," *Annual Review of Materials Science,* vol. 28, pp. 153-184, 1998.

[22] F. M. Veronese and A. Mero, "The impact of PEGylation on biological therapies.(Drug Development)," *BioDrugs,* vol. 22, p. 315(15), 2008.

[23] R. H. Schmidt, K. Mosbach, and K. Haupt, "A Simple Method for Spin-Coating Molecularly Imprinted Polymer Films of Controlled Thickness and Porosity," *Advanced Materials,* vol. 16, pp. 719-722, 2004.

[24] Y. F. David, W. Zhang, M. Palard, C. W. Patrick Jr., and S. Chen, "Flash imprint lithography using a mask aligner: a method for printing nanostructures in photosensitive hydrogels," *Nanotechnology,* vol. 19, p. 215303, 2008.

[25] M. M. Alkaisi, J. J. Muys, and J. J. Evans, "Bioimprint replication of single cells on a biochip," in *BioMEMS and Nanotechnology III*, Canberra, ACT, Australia, 2007, pp. 67990V-10.

[26] J. J. Muys, M. M. Alkaisi, and J. J. Evans, "Bioimprint: Nanoscale Analysis by Replication of Cellular Topography Using Soft Lithography," *Journal of Biomedical Nanotechnology,* vol. 2, pp. 11-15, Apr 2006.

[27] J. J. Muys, M. M. Alkaisi, and J. J. Evans, "Cellular replication and atomic force microscope imaging using a UV-Bioimprint technique," *Nanomedicine: Nanotechnology, Biology and Medicine,* vol. 2, pp. 169-176, 2006.

[28] G. M. Whitesides, E. Ostuni, S. Takayama, X. Y. Jiang, and D. E. Ingber, "Soft lithography in biology and biochemistry," *Annual Review of Biomedical Engineering,* vol. 3, pp. 335-373, 2001.

[29] J. J. Muys, M. M. Alkaisi, D. O. S. Melville, J. Nagase, P. Sykes, G. M. Parguez, and J. J. Evans, "Cellular transfer and AFM imaging of cancer cells using Bioimprint," *Journal of Nanobiotechnology,* vol. 4, p. 1, 2006.

[30] J. S. M. F. Samsuri, M.M. Alkaisi, J.J. Evans, "Formation of Nanoscale Bioimprints of Muscle Cells Using UV-Cured Spin-Coated Polymers," *Journal of Nanotechnology*, vol. 2009, 2009.

[31] F. Samsuri, M. M. Alkaisi, J. S. Mitchell, and J. J. Evans, "Replication of cancer cells using soft lithography bioimprint technique," *Microelectronic Engineering*, vol. 87, pp. 699-703, May-Aug 2010.

[32] M. K. a. L. M. Franks, *Introduction to the Cellular and Molecular Biology of Cancer*, Fourth ed. New York: Oxford University Press, 2005.

[33] M. K. a. P. Selby, *Introduction to the Cellular and Molecular Biology of Cancer*, Fourth ed. New York: Oxford University Press, 2005.

[34] http://mwcs.neric.org/faculty/wroome/powerpoints/Presentation1.ppt.

[35] B. Alberts, D. Bray, J. Lewis, M. Raff, K. Roberts, and J. D. Watson, *Molecular Biology of the Cell*, Third ed. New York: Garland Science, 1994.

[36] E. S. a. V. Lupashin, "Role of thethering factors in secretory membrane traffic," *Am.J.Physiol. Cell Physiol.*, pp. C11-C26, 2006.

[37] B. H. Jena, S. J. Cho, A. Jeremic, M. H. Stromer, and R. Abu-Hamdah, "Structure and Composition of the Fusion Pore," *Biophys J*, vol. 84, pp. 1337 - 1343, 2003.

[38] S. W. Schneider, "Kiss and Run Mechanism in Exocytosis," *Journal of Membrane Biology*, vol. 181, pp. 67-76, 2001.

[39] E. Ales, L. Tabares, J. M. Poyato, V. Valero, M. Lindau, and T. Alvarez de, "High calcium concentrations shift the mode of exocytosis to the kiss-and-run mechanism," *Nat Cell Biol*, vol. 1, pp. 40-44, 1999.

[40] J. Klingauf, E. T. Kavalali, and R. W. Tsien, "Kinetics and regulation of fast endocytosis at hippocampal synapses," *Nature*, vol. 394, pp. 581-585, 1998.

[41] S. W. Schneider, K. C. Sritharan, J. P. Geibel, H. Oberleithner, and B. P. Jena, "Surface dynamics in living acinar cells imaged by atomic

force microscopy: Identification of plasma membrane structures involved inâ€‰exocytosis," *Proceedings of the National Academy of Sciences of the United States of America,* vol. 94, pp. 316-321, January 7, 1997 1997.

[42] T. Nemoto, R. Kimura, K. Ito, A. Tachikawa, Y. Miyashita, M. Iino, and H. Kasai, "Sequential-replenishment mechanism of exocytosis in pancreatic acini," *Nat Cell Biol,* vol. 3, pp. 253-258, 2001.

[43] M. S. Guo, L. P.; Jiang, Y.; Liu, W.; Yu, Y.; Chen, G. Q., *Apoptosis* vol. 11: Springer, 2006.

[44] C. E. Griguer, Oliva, C.R., Kelley, E.E., Giles, G.I., Lancaster, J.R., Gillespie, G.Y., "Xanthine oxidase-dependent regulation of hypoxia-inducible factor in cancer cells," *Cancer Res.*, 2006.

[45] A. Vengellur and J. J. LaPres, "The Role of Hypoxia Inducible Factor 1{alpha} in Cobalt Chloride Induced Cell Death in Mouse Embryonic Fibroblasts," *Toxicol. Sci.*, vol. 82, pp. 638-646, December 1, 2004 2004.

[46] Saunders, *Saunders Comprehensive Veterinary Dictionary*

Elsevier Inc., 2007.

[47] V. Instruments. Dektak 150 Surface Profiler [Online].

[48] D. Way, D. Grosso, J. Davis, E. Surwit, and C. Christian, "Characterization of a new human endometrial carcinoma (RL95-2) established in tissue culture," *In Vitro Cellular & Developmental Biology - Plant,* vol. 19, pp. 147-158, 1983.

[49] B. a. Gentaur. (2005). *Cell attachment factors*. Available: http://www.bioxys.com/i_Biochrom/cell_attachment_factors.htm

[50] B. a. G. BVBA. (2005). *Cell attachment factors*. Available: http://www.bioxys.com/i_Biochrom/cell_attachment_factors.htm

[51] E. M. Sciences. (2010). *Cell Culture, Petri, and Permanox Dishes and Seals*. Available: http://www.emsdiasum.com/microscopy/products/preparation/dish.aspx

[52] J. M. S. Leng, J. Walston, D. Xie, N. Fedarko, G. Kuchel, "Elisa and Multiplex Technologies for Cytokine Measurement in Inflammation and Aging Research," *J Gerontol A Biol Sci Med Sci,* pp. 879–884, October 2008.

[53] S. S. M. Adler, M. Spengler "Cytokine Quantification in Drug Development: A comparison of sensitive immunoassay platforms," Chimera Biotec GmbH, Dortmund - Germany, ReportRetrieved on 01/26/2010 2009.

[54] G. Binnig, C. Gerber, E. Stoll, T. R. Albrecht, and C. F. Quate, "Atomic resolution with atomic force microscope," *Europhys Lett,* vol. 3, p. 1281, 1987.

[55] M. Gerhard and M. A. Nabil, "Novel optical approach to atomic force microscopy," *Applied Physics Letters,* vol. 53, pp. 1045-1047, 1988.

[56] Nanoscience. Atomic Force Microscopy [Online]. Available: http://www.nanoscience.com/education/afm.html

[57] I. Brevik, V. N. Marachevsky, and K. A. Milton, "Identity of the van der Waals Force and the Casimir Effect and the Irrelevance of These Phenomena to Sonoluminescence," *Phys. Rev. Lett.,* vol. 82, pp. 3948-3951, 17/05/1999 1999.

[58] I. Revenko and C. Tolksdorf, "Choosing AFM probes for Biological Applications," Veeco Metrology Group, Method paper2004.

[59] Q. Zhong, D. Inniss, K. Kjoller, and V. B. Elings, "Fractured polymer/silica fiber surface studied by tapping mode atomic force microscopy," *Surface Science Letters,* vol. 290, pp. 688-692, 10 June 1993 1993.

[60] C. A. J. Putman, K. O. van der Werf, B. G. De Grooth, N. F. Van Hulst, and J. Greve, "Tapping mode atomic force microscopy in liquid " *Applied Physics Letters,* vol. 64, pp. 2454-2456, 1994.

[61] Y. Roiter and S. Minko, "AFM Single Molecule Experiments at the Solid-Liquid Interface: In Situ Conformation of Adsorbed Flexible Polyelectrolyte Chains," *Journal of the American Chemical Society,* vol. 127, pp. 15688-15689, 2005.

[62] S. Magonov, *Applied Scanning Probe Methods*: Springer, 2004.

[63] S. I. Hajdu, "A Note from History: The First Use of the Microscope in Medicine," *Annals of Clinical & Laboratory Science,* vol. 32, pp. 309-310, 2002.

[64] M. Micic, D. Hu, Y. D. Suh, G. Newton, M. Romine, and H. P. Lu, "Correlated atomic force microscopy and fluorescence lifetime imaging of live bacterial cells," *Colloids and Surfaces B: Biointerfaces,* vol. 34, pp. 205-212, 2004.

[65] J. A. Dvorak, "The application of atomic force microscopy to the study of living vertebrate cells in culture," *Methods,* vol. 29, pp. 86-96, 2003.

[66] G. Zuccheri, B. Samorì, and H. J. K. H. Bhanu P. Jena, "Chapter 17 Scanning force microscopy studies on the structure and dynamics of single DNA molecules," in *Methods in Cell Biology*. vol. Volume 68, ed: Academic Press, 2002, pp. 357-395.

[67] W. R. Bowen, N. Hilal, R. W. Lovitt, and P. M. Williams, "Atomic force microscope studies of membranes: Surface pore structures of Cyclopore and Anopore membranes," *Journal of Membrane Science,* vol. 110, pp. 233-238, 1996.

[68] H. Wang and D. E. Clapham, "Conformational changes of the in situ nuclear pore complex," *Biophysical Journal,* vol. 77, pp. 241-247, 1 July 1999 1999.

[69] M. Benoit and H. J. K. H. Bhanu P. Jena, "Chapter 5 Cell adhesion measured by force spectroscopy on living cells," in *Methods in Cell Biology*. vol. Volume 68, ed: Academic Press, 2002, pp. 91-114.

[70] I. Revenko and M. Wright, "Tapping Mode Atomic Force Microscopy Operation in Fluid," Veeco Metrology Group, Method paper2004.

[71] C. B. Prater, P. G. Maivald, K. J. Kjoller, and M. G. Heaton, "Tapping Mode Imaging: Applications and technology," Veeco Instruments Inc., Method paper2004.

[72] C. A. Johnson, "Tapping Mode AFM Imaging in Fluids for the Study of Colloidal Particle Adsorption," Veeco Instruments Inc., Application note2004.

[73] S. J. Cho, K. Jeftinija, A. Glavaski, S. Jeftinija, B. P. Jena, and L. L. Anderson, "Structure and dynamics of the fusion pores in live GH-secreting cells revealed using atomic force microscopy," *Endocrin,* vol. 143, pp. 1144 - 1148, 1997.

[74] N. Blow, "Cell culture: building a better matrix," *Nat Meth,* vol. 6, pp. 619-622, 2009.

[75] C. Le Grimellec, E. Lesniewska, C. Cachia, J. P. Schreiber, F. de Fornel, and J. P. Goudonnet, "Imaging of the membrane surface of MDCK cells by atomic force microscopy," *Biophysical Journal,* vol. 67, pp. 36-41, 1 July 1994 1994.

[76] S. S. Schaus and E. R. Henderson, "Cell viability and probe-cell membrane interactions of XR1 glial cells imaged by atomic force microscopy," *Biophysical Journal,* vol. 73, pp. 1205-1214, 1 September 1997 1997.

[77] S. Ferrero, A. s. Piednoir, and C. R. Henry, "Atomic Scale Imaging by UHV-AFM of Nanosized Gold Particles on Mica," *Nano Letters,* vol. 1, pp. 227-230, 2001.

[78] F. Takeshi and et al., "Revealing molecular-level surface structure of amyloid fibrils in liquid by means of frequency modulation atomic force microscopy," *Nanotechnology,* vol. 19, p. 384010, 2008.

[79] R. V. Lapshin, "Feature-oriented scanning methodology for probe microscopy and nanotechnology," *Nanotechnology,* vol. 15, pp. 1135-1151, September 2004 2004.

[80] R. V. Lapshin, "Automatic drift elimination in probe microscope images based on techniques of counter-scanning and topography feature recognition," *Measurement Science and Technology,* vol. 18, pp. 907-927, March 2007 2007.

[81] S. Belikov and S. Magonov, "True Molecular-Scale Imaging in Atomic Force Microscopy: Experiment and Modeling," *Jpn. J. Appl. Phys,* vol. 45, pp. 2158-2165, March 27, 2006 2006.

[82] Mikromasch. (2010, High resolution (Atomic Force Microscopy). Available: http://www.spmtips.com/howto/res/hr

[83] Wikipedia. (2010). *Wikipedia Encyclopedia*. Available: http://en.wikipedia.org/wiki/Main_Page

[84] U.-B. T. Giang, D. Lee, M. R. King, and L. A. DeLouise, "Microfabrication of cavities in polydimethylsiloxane using DRIE silicon molds," *Lab on a Chip*, vol. 7, pp. 1660-1662, 2007.

[85] U.-B. T. Giang, M. R. King, and L. A. DeLouise, "Microfabrication of Bubbular Cavities in PDMS for Cell Sorting and Microcell Culture Applications," *Journal of Bionic Engineering*, vol. 5, pp. 308-316, 2008.

[86] D. Lee, K. Rana, K. Lee, L. A. DeLouise, and M. R. King, "Microfabricated Cavities for Adhesive Capture of Stem Cells Under Flow," *ASME Conference Proceedings*, vol. 2007, pp. 1-5, 2007.

[87] H. Morgan, M. P. Hughes, and N. G. Green, "Separation of submicron bioparticles by dielectrophoresis," *Biophys J*, vol. 77, pp. 516-525, Jul 1999 1999.

[88] J. J. Muys, "Cellular analysis by atomic force microscopy," Doctor of Philosophy, Department of Electrical & Computer Engineering, University of Canterbury, Christchurch, 2006.

[89] H. A. Pohl, *Dielectrophoresis: The behavior of neutral matter in non-uniform electric fields*. Cambridge: Cambridge University Press, 1978.

[90] H. Morgan and N. G. Green, *AC electrokinetics: Colloids and nanoparticles*. Baldock, Hertfordshire, England: Research Studies Press Ltd, 2003.

[91] T. B. Jones, *Electromechanics of particles*. Cambridge: Cambridge University Press, 1995.

[92] B. J. Kirby, *Micro- and nanoscale fluid mechanics: Transport in microfluidic devices*, 2009.

[93] R. Pethig, *Properties of biological materials*, 1979.

[94] S. Bush. (2009, 7 October 2009) Micro-fluidics cut cancer test from a day to an hour - IMEC Tech Forum. *ElectronicsWeekly.com*.

[95] D. W.-G. Alexander, "Dielectrophoretic reconfiguration of nanowire interconnects," *Nanotechnology,* vol. 17, p. 4986, 2006.

[96] P. R. C. Gascoyne and et al., "Dielectrophoretic separation of mammalian cells studied by computerized image analysis," *Measurement Science and Technology,* vol. 3, p. 439, 1992.

[97] B. P. Jena, "Cell secretion machinery: Studies using the AFM," *Ultramicroscopy,* vol. 106, pp. 663-669, 2006.

[98] T. Glinsner, U. Plachetka, T. Matthias, M. Wimplinger, and P. Lindner, "Soft UV-based nanoimprint lithography for large-area imprinting applications," in *Proceeding of SPIE Advanced Lithography*, 2007.

[99] S. Bystrova, R. Luttge, and A. van den Berg, "Study of crack formation in high-aspect ratio SU-8 structures on silicon," *Microelectronic Engineering,* vol. 84, pp. 1113-1116, 2007/8// 2007.

[100] T. Müller, W. M. Arnold, T. Schnelle, R. Hegedorn, G. Fuhr, and U. Zimmermann, "A traveling-wave micropump for aqueous solutions: comparison of 1 g and microgram results.," *Electrophoresis,* vol. 14, pp. 764-772, August 1993 1993.

[101] B. Forslind, "Clinical applications of scanning electron microscopy and X-ray microanalysis in dermatology," *Scanning Electron Microscopy,* vol. I, pp. 183-206, 1984.

[102] G. Pfefferkorn and A. Boyde, "Review of replica techniques for scanning electron microscopy," *Scanning Electron Microscopy,* vol. I, 1974.

[103] J. Sampson, "A method for replicating dry or moist surfaces for examination by light microscopy," *Nature,* vol. 191, pp. 932-933, 1961.

[104] M. Madou, *Fundamentals of Microfabrication*, 2nd Edition ed. Boca Raton, Florida: CRC Press, 2002.

[105] V. K. Varadan, X. Jiang, and V. V. Varadan, *Microstereolithography and other fabrication techniques for 3D MEMS*. Chichester: Wiley, 2001.

[106] A. Jokstad and I. A. Mjor, "Assessment of marginal degradation of restorations on impressions," *Acta Odontol Scand,* vol. 49, pp. 15-25, 1991.

[107] T. F. Walsh, A. D. Waimsley, and P. V. Carrotte, "Scanning electron microscopic investigation of changes in the dentogingival area during experimental gingivitis," *Clin Reriodontol,* vol. 18, pp. 20-25, 1991.

[108] B. Forslind, "Replication techniques for dry and wet biological surfaces," *Scanning Electron Microscopy,* vol. 13, pp. 133-139, 16 November, 1998 1999.

[109] K. Kerstin and et al., "A fast, precise and low-cost replication technique for nano- and high-aspect-ratio structures of biological and artificial surfaces," *Bioinspiration & Biomimetics,* vol. 3, p. 046002, 2008.

[110] J. J. Muys, M. A. Alkaisi, and J. J. Evans, "Bioimprint: Nanoscale analysis by replication of cellular topography using soft lithography," *J Biomed Nano*.

[111] D. P. McDaniel, G. A. Shaw, J. T. Elliott, K. Bhadriraju, C. Meuse, K.-H. Chung, and A. L. Plant, "The Stiffness of Collagen Fibrils Influences Vascular Smooth Muscle Cell Phenotype," *Biophysical Journal,* vol. 92, pp. 1759-1769, 2007.

[112] S. Zhang and F. V. W. a. G. K. George, "Designer Self-Assembling Peptide Nanofiber Scaffolds for Study of 3-D Cell Biology and Beyond," in *Advances in Cancer Research*. vol. Volume 99, ed: Academic Press, 2008, pp. 335-362.

[113] A. I. Baba and C. Catoi, *Comparative Oncology*. Bucharest: The Publishing House of the Romanian Academy, 2007.

[114] M. M. Mareel and M. De Mets, "Effect of microtubule inhibitions on invasion and on related activities of tumor cells," *Internal Rev. Cytol.*, vol. 90, pp. 125-168, 1984.

[115] P. System. (2008, Non Contact In-liquid Imaging and Ion Conductance Microscopy. Available: http://www.parkafm.com/product/product_view.php?gubun=R&id=3&XE-Bio

[116] B. Wang, Y. Zou, Z.-L. Yuan, and J.-G. Xiao, "Genistein Suppressed Upregulation of Vascular Endothelial Growth Factor Expression by Cobalt Chloride and Hypoxia in Rabbit Retinal Pigment Epithelium Cells," *Journal of Ocular Pharmacology and Therapeutics*, vol. 19, pp. 457-464, 2003.

[117] J. M. Dann, P. H. Sykes, D. R. Mason, and J. J. Evans, "Regulation of Vascular Endothelial Growth Factor in endometrial tumour cells by resveratrol and EGCG," *Gynecologic Oncology*, vol. 113, pp. 374-378, 2009.

[118] P. E. Resource. (2010). *www.cancerlearning.com*. Available: http://www.cancerlearning.com/index.cfm/fuseaction/find.online_cme/activity_type/publication

[119] G. Bergers and D. Hanahan, "Modes of resistance to anti-angiogenic therapy," *Nat. Rev. Cancer*, vol. 8, pp. 592-603, 2008.

[120] A. M. Chan and T. Weber, "A putative link between exocytosis and tumor development " *Cancer Cell Journal*, vol. 2, pp. 427-428, 2002.

[121] M. V. C. Claudia Puri, Susan D. Arden, Antonina J. Kruppa, John Kendrick-Jones, Folma Buss, "Overexpression of myosin VI in prostate cancer cells enhances PSA and VEGF secretion, but has no effect on endocytosis," *Oncogene*, vol. 29, pp. 188-200, January 14 2010.